

27 **Abstract**

28 Central pattern generators are cell- or network-driven oscillators that underlie motor
29 rhythmicity. The existence and identity of *C. elegans* CPGs remain unknown. Through
30 cell ablation, electrophysiology, and calcium imaging, we identified oscillators for
31 reverse locomotion. We show that the cholinergic and excitatory class A motor neurons
32 exhibit intrinsic and oscillatory activity, and such an activity can drive reverse
33 locomotion without premotor interneurons. Regulation of their oscillatory activity, either
34 through effecting an endogenous constituent of oscillation, the P/Q/N high voltage-
35 activated calcium channel UNC-2, or, via dual regulation – inhibition and activation - by
36 the descending premotor interneurons AVA, determines the propensity, velocity, and
37 sustention of reverse locomotion. Thus, the reversal motor executors themselves serve as
38 oscillators; regulation of their intrinsic activity controls the reversal motor state. These
39 findings exemplify anatomic and functional compression: motor executors integrate the
40 role of rhythm generation in a locomotor network that is constrained by small cell
41 numbers.

42 **Introduction**

43 Central pattern generators (CPGs) are rhythm-generating neurons and neural circuits with
44 self-sustained oscillatory activities. Across the animal phyla, they underlie rhythmic
45 motor behaviors that are either continuous, such as breathing and heartbeat, or episodic,
46 such as chewing and locomotion (Grillner, 2006; Grillner and Wallen, 1985; Kiehn,
47 2016; Marder and Bucher, 2001; Marder and Calabrese, 1996; Selverston and Moulins,
48 1985). CPGs that drive locomotor behaviors intrinsically generate and sustain oscillatory
49 activity, but generally require signals from the central or peripheral nervous systems for
50 activation or reconfiguration (Pearson, 1993).

51 The concept of self-sustained locomotor CPGs originated from the observation that
52 decerebrate cats could sustain rhythmic hind limb muscle contraction (Brown, 1911,
53 1914). In deafferented locusts, flight motor neurons (MNs) exhibited rhythmic activity, in
54 response to non-rhythmic electric stimulation (Wilson, 1961). Isolated spinal or nerve
55 cords from the leech (Briggman and Kristan, 2006), lamprey (Wallen and Williams,
56 1984), rat (Juvin et al., 2007; Kiehn et al., 1992), and cat (Guertin et al., 1995) were
57 capable of generating rhythmic MN activity and/or fictive locomotion. These findings
58 suggest that locomotor systems intrinsically sustain rhythmic and patterned electric
59 activity, independent of inputs from the descending neural networks or sensory organs.

60 Locomotor CPGs have been identified in several animals. In most systems, they
61 consist of premotor interneurons (INs) that drive MN activity (Marder and Bucher, 2001).
62 In vertebrates, multiple pools of spinal premotor INs instruct and coordinate the output of
63 different MN groups (Grillner, 2006; Kiehn, 2006, 2016). MNs retrogradely regulate the
64 activity of CPG circuits, as in the crayfish and leech swimmerets (Heitler, 1978; Rela and

65 Szczupak, 2003; Szczupak, 2014), or of premotor INs, as in the *C. elegans* motor circuit
66 (Liu et al., 2017), and the zebrafish spinal cord (Song et al., 2016). In all cases,
67 manipulation of MN activity affects the activity of their input premotor INs through a
68 mixed electric and chemical synaptic configuration (More in Discussion).

69 *C. elegans* generates rhythmic and propagating body bends that propel either
70 forward or reverse movements. Synaptic wiring of its adult locomotor system has been
71 mapped by serial electron microscopy reconstruction (White et al., 1976, 1986). There
72 are five MN classes: A, B, D, AS, and VC. The A (A-MN), B (B-MN), and D (D-MN)
73 classes contribute the vast majority of neuromuscular junctions (NMJs) to body wall
74 muscles. Each class is divided into subgroups that innervate dorsal or ventral muscles.
75 Repeated motor units, each consisting of members of the A-, B- and D-MNs that make
76 tiled dorsal and ventral NMJs, reside along the ventral nerve cord.

77 The B- and A-MNs are cholinergic and excitatory, potentiating muscle contraction
78 (Gao and Zhen, 2011; Liu et al., 2011; Nagel et al., 2005; Richmond and Jorgensen,
79 1999; White et al., 1986), whereas the D-MNs are GABAergic and inhibitory, promoting
80 muscle relaxation (Gao and Zhen, 2011; Liewald et al., 2008; Liu et al., 2011; McIntire et
81 al., 1993). Most NMJs from the A- and B-MNs are dyadic, with the D-MNs that
82 innervate opposing muscles in the dorsal-ventral axis as co-recipients. Such a pattern of
83 synaptic connectivity allows contralateral inhibition, a mechanism proposed to underlie
84 alternate ventral-dorsal bending during undulation (White et al., 1986).

85 Descending and ascending premotor INs innervate excitatory MNs. Three pairs of
86 INs - AVA, AVB, and PVC - extend axons along the entire length of the ventral nerve
87 cord, and form synapses to all members of the MN classes that they partner with. They

88 contribute to two sub-circuits: a forward-promoting unit, where AVB and PVC make
89 electric and chemical synapses with the B-MNs, respectively, and a reversal-promoting
90 motor unit, where AVA innervate the A-MNs through both electric and chemical
91 synapses (Chalfie et al., 1985; White et al., 1986; illustrated in **Figure 1A**). Reciprocal
92 inhibition between the two sub-circuits underlies stabilization of and transition between
93 the forward and reverse motor states (Kato et al., 2015; Kawano et al., 2011; Roberts et
94 al., 2016).

95 However, a fundamental question remains unanswered for the motor circuit: the
96 origin of oscillation. Despite an extensive understanding of the anatomy and physiology
97 (Duerr et al., 2008; McIntire et al., 1993; Pereira et al., 2015; Rand, 2007; White et al.,
98 1986), the existence and identity of locomotor CPGs in the *C. elegans* nervous system
99 remain speculative. They have been suggested to reside in the head, based on an
100 observation that flexion angles decay from head to tail during both foraging and reverse
101 (Karbowski et al., 2008). Several INs affect bending (Bhattacharya et al., 2014; Donnelly
102 et al., 2013; Hu et al., 2011; Li et al., 2006), but none is essential for activation or
103 rhythmicity of locomotion. The remarkable biomechanical adaptability of *C. elegans*
104 locomotion (Fang-Yen et al., 2010) predicted a prominent role of proprioceptive
105 feedback, irrespective of the presence or location of CPGs (Gjorgjieva et al., 2014).
106 Indeed, the B-MNs have been modeled as a chain of reflexes to propagate body bends in
107 the absence of CPG activity during forward movements (Cohen and Sanders, 2014; Wen
108 et al., 2012). However, there has been no direct experimental evidence that determines
109 whether CPGs exist, where they are encoded, and how they contribute to motor rhythm
110 (reviewed in Zhen and Samuel, 2015).

111 Through cell ablation, electrophysiology, genetics, and calcium imaging analyses,
112 we reveal that multiple CPGs are present; distinct ones drive forward and reverse
113 movements. For reverse movement, the A-MN themselves constitute a distributed
114 network of local CPGs. Inhibition and potentiation of their CPG activity, either by
115 altering an intrinsic channel constituent for oscillation VGCC/UNC-2, or through the dual
116 regulation by the descending premotor INs AVA, determine the initiation, velocity, and
117 duration of the reverse motor state. Therefore, the *C. elegans* circuit for reverse
118 movements shares the principle of a CPG-driven locomotor network, except with the role
119 of CPGs integrated into excitatory MNs.

120 Previous studies have revealed features of *C. elegans* that placed the system at odds
121 with other animal models. While in most locomotor networks, the CPG IN neurons and
122 MNs exhibit rhythmic action potential bursts that correlate with fictive or non-fictive
123 locomotion (reviewed in Grillner, 2006; Kiehn, 2016), *C. elegans* neurons cannot fire
124 classic action potentials (Bargmann, 1998; Consortium, 1998; Goodman et al., 1998;
125 Kato et al., 2015; Liu et al., 2017; Xie et al., 2013). Results from this study, together with
126 previous findings on the *C. elegans* body wall musculature (Gao and Zhen, 2011; Liu et
127 al., 2013), unveil a simplified, but fundamentally conserved molecular and cellular
128 underpinning of rhythmic locomotion in *C. elegans*, where the ventral cord MNs assume
129 the role of CPG, and the body wall muscles the bursting property (more in Discussion).

130 These findings point to compression, where a single neuron or neuron class
131 assumes the role of multiple neuron classes or layers in more complex circuits. At the
132 lobster stomatogastric ganglion (STG), pyloric MNs, with a descending interneuron,
133 serve as the CPG for continuous gastric rhythm (Marder and Bucher, 2001; Selverston

134 and Moulins, 1985). We propose that compression is the property of animals constrained
135 by small cell numbers, and such a property allows small nervous systems to serve as
136 compact models to dissect shared organizational logic of neural circuits (see Discussion).

137 **Results**

138 *Motor neurons sustain body bends in the absence of premotor INs*

139 To address whether and where CPGs are present, we first examined the behavioral
140 consequence of systematic ablation of MNs and premotor INs. In previous studies,
141 ablation was restricted to a few neurons and in a small number of animals (Chalfie et al.,
142 1985; Kawano et al., 2011; Rakowski et al., 2013; Roberts et al., 2016; Wicks and
143 Rankin, 1995; Zheng et al., 1999). With a flavoprotein miniSOG, which induces acute
144 functional loss, subsequent death and anatomic disappearance of neurons by photo-
145 activation (Qi et al., 2012), we ablated the entire population of premotor INs or A/B/D-
146 MNs (Materials and Methods; **Figure 1A-D**).

147 Without premotor INs, animals lost motility, as represented by reduced mid-point
148 displacement (**Figure 1Dii**; **Figure 1-figure supplement 1Aiv**; **Video 1**). These animals
149 however were not paralyzed. Their body posture recapitulated that of a class of mutants
150 called *kiners* (Kawano et al., 2011): the head oscillates, but oscillation does not
151 propagate along the body; the body bends, but bending is not organized as a propagating
152 wave (**Figure 1Aii-Cii**; **Figure 1-figure supplement 1Ai-Aiii**). In *inker* mutants,
153 instead of a lack of motor activity, the stalled mid-point displacement is due to a lack of
154 coordination between the antagonistic, forward- and reverse-driving motor activity
155 (Kawano et al., 2011). The *inker*-like posture indicates that animals without premotor
156 INs retain locomotor activity. Calcium imaging confirmed that bending in these animals
157 coordinated with persistent muscle activity (**Video 1**).

158 Persistent locomotor activity requires MNs. Upon removal of all A-, B- and D-
159 MNs, animals lost motility (**Figure 1Diii**). Similar to animals without premotor INs, head

160 oscillation persisted in A/B/D-MN-ablated animals. Unlike the premotor IN-less animals,
161 however, their body bending was attenuated, resulting in an oscillating head pulling a
162 non-bending body (**Figure 1Biii**). Attenuation of body bends concurs with the anatomy –
163 the A-, B- and D-MNs contribute the majority of NMJs along the body.

164 The persistence of head oscillations upon ablation of all premotor INs, or most
165 ventral cord MNs, indicates a separation of putative CPGs that control the head and body
166 movement. CPGs for head oscillation may promote foraging (Karbowski et al., 2008;
167 Pirri et al., 2009). The persistence of body bends in animals without premotor INs
168 suggests that some ventral cord MN themselves sustain activity.

169 *A-MNs generate rhythmic reverse movement without premotor INs*

170 To identify the MN groups with such autonomous activity, we next ablated premotor INs
171 in conjunction with the A-, B-, or D-MNs, respectively, to compare changes in their
172 locomotor pattern.

173 Ablation of each MN class resulted in drastically different motor outputs. Upon the
174 combined ablation of premotor INs and A-MNs, animals exhibited sluggish forward
175 movements (**Figure 2A-D; Video 2** part 3-4): an oscillating head slowly pulled a body
176 with shallow bends, reminiscent of animals in which all A-, B- and D-MNs were
177 removed (**Figure 1A,B**). When both premotor INs and B-MNs were removed, animals
178 exhibited reverse locomotion, with robust rhythmicity and body bends (**Figure 2A-D**).
179 Reverse movement periodically stalled when the forward-promoting head oscillation
180 interfered with body bend propagation, reducing mid-point displacement (**Video 2** part 1-
181 2). Removing the D-MNs did not alleviate premotor IN-less animals from a *kinker*-like

182 posture to either forward or reverse movements (**Figure 1–figure supplement 1; Video 2**
183 part 5-6).

184 Therefore, while B- and A-MNs generate the forward- and reversal-promoting body
185 bends, respectively, persistent body bends in premotor IN-less animals mainly originated
186 from A-MN activity. Strikingly, A-MNs drive robust reverse movements in the absence
187 of premotor INs, indicating that their endogenous activities suffice for both execution of
188 body bends and organization of their propagation. Indeed, simultaneous calcium imaging
189 of a cluster of A-MNs in premotor IN-less animals revealed phase relationships as
190 predicted from the temporal activation order of their muscle targets in wildtype animals
191 (**Figure 2E,F**).

192 *Sparse removal of A-MNs alters, but does not abolish, reverse movement*

193 Because A-MNs can organize reverse movement without premotor INs, they may form a
194 chain of either phase-locked CPGs or flexors to execute reverse locomotion. These
195 possibilities can be distinguished by examining the effect of sparse removal of A-MNs. In
196 the former case, removal of individual A-MNs should alter, but not prevent, body bend
197 propagation during reverse locomotion. In the latter case, reverse locomotion should stall
198 at body segments that are innervated by the most posteriorly ablated A-MNs.

199 Our ablation results (**Figure 3; Figure 3–figure supplement 1; Video 3**) favor the
200 first possibility. Removal of A-MNs in anterior body segments did not prevent the
201 initiation and propagation of reversal waves in mid- and posterior body segments (**Figure**
202 **3C-1i, 1ii; Figure 3–figure supplement 1B-1iii**). The head and tail exhibited
203 independent reversal bending waves upon the ablation of mid-body A-MNs. When most
204 or all mid-body A-MNs were ablated, the head exhibited either high (**Figure 3C-2i, 2ii**;

205 **Figure 3–figure supplement 1B-1i)** or low (**Figure 3–figure supplement 1B-2i)**
206 oscillations that were uncoupled in phase with slow tail-led bending. Ablation of a few
207 mid-body MNs also led to uncoupling between the anterior and posterior body bends, but
208 many tail-initiated waves propagated through to the head (**Figure 3–figure supplement**
209 **1B-2iii)**. When posterior A-MNs were removed, bending initiated and propagated from
210 body segments posterior to ablated areas (**Figure 3C-3i, 3ii; Figure 3–figure**
211 **supplement 1B-1ii, 2ii)**.

212 Quantitatively, the ablations of A-MNs from either the anterior, mid-body, or
213 posterior sections (**Figure 3A; Figure 3–figure supplement 1A)** significantly decreased
214 local reverse wave speed, but caused modest or negligible change in wave speed in other
215 body regions (**Figure 3D)**. Thus, rhythmic body bends can arise from multiple locations,
216 supporting the presence of a chain of reversal CPGs.

217 *A-MNs exhibit oscillatory activity independent of premotor IN inputs*

218 CPGs should exhibit self-sustained oscillatory activities. We sought experimental
219 evidence for such a property by electrophysiology and calcium imaging analyses.

220 First, we examined a dissected neuromuscular preparation consisting of an exposed
221 ventral nerve cord and the body wall muscles that they innervate. In adults, the majority
222 of ventral NMJs are made by ventral A- and B-MNs. Prior to ablation of premotor INs
223 and B-MNs, whole-cell voltage clamp of the ventral body wall muscles revealed ~50Hz,
224 ~ -20pA miniature postsynaptic currents (mPSCs). Upon ablation, the mPSC frequency
225 exhibited a moderate, ~30% reduction (**Figure 4–figure supplement 1A,B)**. More
226 important, however, was that in 70% of preparations ($n = 10$), we observed periodic
227 rhythmic PSC (rPSC) bursts at ~90 second intervals (**Figure 4A-C)**. These burst units

228 were distinct from high frequency mPSCs: each lasted 2-3 seconds, consisting of 5-7 Hz,
229 -100 to -300 pA depolarizing currents (**Figure 4A-C; Figure 5A**). By contrast, only in
230 10% non-ablated preparations ($n = 10$), we observed PSC bursts of similar characteristics,
231 as sporadic single unit events. These results suggest that A-MNs generate periodic
232 electric activities without premotor INs.

233 In the current clamp configuration, we observed periodic action potential bursts that
234 corresponded to rPSC bursts after both premotor IN- and B-MN were ablated (**Figure 4-**
235 **figure supplement 1C-E**). Muscle action potentials correlate with contraction (Gao and
236 Zhen, 2011), confirming the physiological relevance of the autonomous MN activity to
237 locomotion. The notion that A-MNs accounted for most periodic rPSC bursts was
238 reaffirmed by comparing with preparations in which premotor INs and A-MNs were
239 ablated: this group exhibited 60% reduction in mPSC frequency, and the rPSC bursts was
240 detected in 17% preparations ($n = 11$).

241 CPGs exhibit oscillatory activity in the presence of sustained inputs. We further
242 examined the effect of direct stimulation of excitatory MNs by a light-activated
243 rhodopsin Chrimson (Klapoetke et al., 2014). In these preparations, sustained activation
244 of the ventral muscle-innervating A- or B-MNs at high light intensity led to high
245 frequency PSCs, reflecting potentiated vesicle release (**Figure 5-figure supplement 1**).
246 Upon sequential reduction of the light intensities, however, the stimulation of A-, but not
247 B-MNs began to reveal rPSC bursts (**Figure 5-figure supplement 1A**).

248 Results from A-MN calcium imaging in intact animals further support their
249 oscillatory property. To reduce effects of proprioceptive coupling, we recorded the A-
250 MN activity from live animals with the whole body immobilized by surgical glue. While

251 sporadic calcium activities were observed for some A-MNs in some animals, robust
252 calcium oscillation was revealed in A-MNs in all animals after the co-ablation of
253 premotor INs and B-MNs (**Figure 4D-F; Video 4**). Individual A-MNs exhibited large
254 variations in amplitudes of calcium oscillation, but shared ~50s oscillation cycle (**Figure**
255 **4F-H**). The neuron DA9, which innervates the most posterior dorsal muscles (**Figure**
256 **4D**), exhibited the highest calcium activity. The ~2 fold difference between the frequency
257 of A-MN-dependent rPSC bursts and A-MN calcium oscillation may reflect the
258 difference on the CPG feedback, similar to what has been observed between the dissected
259 spinal cord preparations versus immobilized intact vertebrates (Goulding, 2009).

260 *A-MN's oscillatory activity is potentiated by optogenetically activated premotor INs*

261 A-MNs receive synaptic inputs from several premotor INs, most prominently from a pair
262 of descending INs AVA. The AVA neurons make mixed chemical and electric synapses
263 with all A-MNs (White et al., 1986). Optogenetic stimulation of AVA activates and
264 sustains reverses, and induces rPSCs in dissected preparations (Gao et al., 2015).

265 These results raise the possibility that premotor INs promote reverses through
266 potentiating A-MN's oscillatory activity. Indeed, AVA stimulation-induced rPSCs were
267 similar in amplitude and frequency to A-MN-dependent endogenous PSC bursts, albeit
268 with less variability (**Figure 5A**). Importantly, upon the removal of A-MNs, AVA-
269 evoked rPSC bursts were abolished (**Figure 5B**); no abolishment was observed when
270 either B-MNs, or AVB premotor INs were ablated (**Figure 5B-D**). Therefore, both
271 evoked and intrinsic rPSC bursts in these preparations primarily originated from the A-
272 MNs, consistent with descending premotor IN inputs potentiating A-MN's intrinsic CPG
273 activity upon stimulation.

274 ***Both evoked and intrinsic A-MN oscillation requires the P/Q/N-type VGCC UNC-2***

275 Because A-MN's oscillatory activity was robustly evoked by optogenetic stimulation of
276 premotor INs, we used this preparation to identify potential cation channels that underlie
277 locomotor CPG's intrinsic membrane oscillation (Harris-Warrick, 2002). We examined
278 three channels known to be expressed by MNs, the P/Q/N-type VGCC UNC-2 (Mathews
279 et al., 2003; Schafer and Kenyon, 1995), the L-type VGCC ELG-19 (Lee et al., 1997),
280 and the sodium leak channel NCA (Xie et al., 2013).

281 rPSC bursts were readily evoked in mutants containing a partial loss-of-function (*lf*)
282 allele for the pore-forming alpha-subunit of the L-VGCC CaV1 α EGL-19, as well as in
283 animals without the sodium leak channel's pore-forming NCA-1 and NCA-2 (Gao et al.,
284 2015), and auxiliary UNC-79 and UNC-80 subunits. By contrast, mutant animals for a
285 partial *lf* allele for the pore-forming alpha-subunit of the P/Q/N-VGCC CaV2 α UNC-2
286 failed to exhibit evoked rPSC bursts, despite an increased mPSC frequency (**Figure 6-**
287 **figure supplement 1**). In mutants that lack auxiliary subunits of the P/Q/N-VGCC,
288 UNC-36 and CALF-1 (Saheki and Bargmann, 2009), we observed similar effect (**Figure**
289 **6-figure supplement 1**). The specific loss of evoked rPSC bursts implicates a
290 requirement of the P/Q/N-type VGCC for A-MN's intrinsic oscillatory activity. Indeed,
291 endogenous rPSC bursts, which we observed upon the removal of all premotor INs and
292 B-MNs in wildtype animals, were also diminished in *unc-2(lf)* mutant preparations
293 (**Figure 6A-C**).

294 ***UNC-2 is an endogenous constituent of A-MN's oscillation***

295 UNC-2 is expressed exclusively in neurons. Like the vertebrate P/Q- and N-type VGCCs,
296 it mediates presynaptic calcium influx, subsequently activating synaptic vesicle fusion

297 and neurotransmitter release (Mathews et al., 2003). The loss of endogenous and evoked
298 rPSC bursts in *unc-2(lf)* mutants may reflect that high voltage-activated calcium channels
299 constitute A-MN's intrinsic oscillation. Alternatively, it could reflect a loss of robust
300 muscle activity due to reduced synaptic transmission between premotor INs and A-MNs,
301 and/or between A-MNs and body wall muscles.

302 We can distinguish these possibilities by directly observing the activity of the A-
303 MN soma by calcium imaging. Specifically, we compared DA9's activity in intact and
304 immobilized wildtype and *unc-2(lf)* animals, after ablating premotor INs and B-MNs.
305 Devoid of premotor IN inputs, wildtype DA9 exhibited periodic calcium oscillations
306 (**Figure 6D,F** wildtype). In *unc-2(lf)* mutants, both the amplitude and frequency of these
307 oscillations were severely reduced (**Figure 6D,F** *unc-2(e55)*). Restoring UNC-2 in A-
308 MNs, not premotor INs, in *unc-2(lf)* mutants was sufficient to restore DA9's calcium
309 signals to the wildtype level (**Figure 6-figure supplement 2**). These results argue that
310 independent of its role in exocytosis, UNC-2 constitutes an endogenous constituent of A-
311 MN's intrinsic oscillation.

312 If this is the case, A-MN's oscillatory defect should be unique for *unc-2(lf)* among
313 exocytosis mutants. UNC-13 is a conserved and essential effector of presynaptic calcium
314 influx to trigger exocytosis (Brose et al., 1995; Gao and Zhen, 2011; Richmond and
315 Jorgensen, 1999). Strikingly, in *unc-13* near null mutants, when premotor INs and B-
316 MNs were ablated, DA9 exhibited periodic calcium oscillations as in wildtype animals
317 (**Figure 6A-C**). This result not only confirms that UNC-2 has an exocytosis-independent
318 function, it reinforces the notion that A-MNs generate and sustain oscillatory activity in
319 the absence of all chemical synaptic inputs.

320 Lastly, if UNC-2 directly contributes to A-MN's membrane oscillation, it should
321 exhibit physical presence outside the presynaptic termini. We examined the subcellular
322 localization of UNC-2 by inserting GFP at the endogenous *unc-2* genomic locus
323 (Materials and Methods). Indeed, in addition to presynaptic localization along the
324 neuronal processes in both the central (nerve ring) and peripheral (VNC) nervous system
325 (Saheki and Bargmann, 2009; Xie et al., 2013), punctate signals decorate around the
326 plasma membrane of neuron soma, including those of A-MNs (soma) (**Figure 6-figure**
327 **supplement 3**).

328 *Altering A-MN's intrinsic calcium oscillation changes reversal velocity*

329 For channels that constitute membrane oscillation, mutations that alter their kinetics
330 should lead to corresponding changes in neuronal oscillatory properties and behaviors.

331 Consistent with this notion, *unc-2(lf)* mutants exhibited drastically reduced A-MN-
332 dependent rPSC bursts, and DA9's calcium oscillation was reduced in both amplitude
333 and frequency (**Figure 6A-E**, *unc-2(e55; lf)*). We further identified and examined the
334 effect of *unc-2* gain-of-function (*gf*) mutations (Materials and Methods) that reduce the
335 channel inactivation kinetics, resulting in prolonged channel opening (Huang and
336 Alkema; to be submitted; Alcaire and Zhen, unpublished). In contrast to the case of *unc-*
337 *2(lf)* mutants, upon ablation of premotor INs and B-MNs, *unc-2(gf)* exhibited endogenous
338 rPSC bursts with strikingly higher frequency and amplitude than wildtype animals
339 (**Figure 6A-C**). DA9's calcium oscillation exhibited drastically increased frequency and
340 amplitude in *unc-2(gf)* animals when compared to wildtype animals (**Figure 6D-F**).
341 Moreover, restoring UNC-2(WT) and UNC-2(*gf*) in A-MNs in *unc-2(lf)* mutants was

342 sufficient to restore the frequency and amplitude of DA9's oscillation (**Figure 6-figure**
343 **supplement 2**).

344 Altered A-MN oscillatory property corresponded with changes in reversal
345 movement. *unc-2(lf)* and *unc-2(gf)* mutants, upon the ablation of premotor INs and B
346 MNs, exhibited reverse movement at velocities that were drastically lower and higher
347 than wildtype animals, respectively (**Figure 6G; Figure 6-figure supplement 4A**). The
348 drastic increase of reverse velocity of *unc-2(gf)* animals directly correlated with a
349 significantly increased propensity (**Figure 6H**) and duration (**Figure 6-figure**
350 **supplement 4B**) for reverse movement than that of wildtype animals.

351 Therefore, not only UNC-2 constitutes A-MN membrane oscillation, modification
352 of A-MN's intrinsic oscillatory property, by either decreasing or increasing UNC-2's
353 activity is sufficient to alter the property of reverse movement.

354 ***Dual regulation of A-MN oscillation by descending premotor INs determines the***
355 ***reversal motor state***

356 When the reversal movement is driven by the intrinsic MN activity, premotor IN inputs
357 can control the reversal motor state through regulating their intrinsic activity. Descending
358 premotor INs AVA make both gap junctions and chemical synapses to all A-MNs
359 (Kawano et al., 2011; Liu et al., 2017; Starich et al., 2009; White et al., 1986). They exert
360 state-dependent dual regulation of reversal movements. At rest, AVA-A gap junctions
361 reduce reversal propensity (Kawano et al., 2011), whereas upon stimulation, AVA sustain
362 reverse movements (Gao et al., 2015; Kato et al., 2015). AVA inputs may modulate the
363 reversal motor state through dual regulation - inhibition and potentiation - of A-MN's
364 oscillatory activity.

365 To determine whether at rest, AVA reduces spontaneous reversal propensity by
366 dampening A-MN's intrinsic activity (**Figure 7J**), we examined DA9's activity in *unc-7*
367 innexin null mutants, in which gap junction coupling between AVA and A-MNs is
368 disrupted (Kawano et al., 2011; Liu et al., 2017). In the presence of premotor INs, DA9
369 exhibited low calcium activity in both *unc-13* mutants (**Figure 7A-C**) and wildtype
370 animals (**Figure 7D-F**), in which AVA-A coupling remains intact. By contrast, DA9
371 exhibited robust calcium oscillation in *unc-7* mutants, in the presence of premotor INs
372 (**Figure 7D-F**). When premotor INs were ablated, robust DA9's calcium oscillation was
373 observed across wildtype animals, *unc-13* and *unc-7* mutants (not shown). These results
374 confirm that the gap junction coupling alone is necessary for inhibiting A-MN oscillation.

375 Consistent with AVA sustaining reverse movement through potentiating A-MN's
376 oscillation, optogenetic activation of AVA evoked robust A-MN-dependent rPSC bursts
377 (**Figure 5B,C**). Moreover, stimulated AVA potentiates A-MNs mainly through chemical
378 synapses, because AVA-evoked rPSC bursts exhibited normal frequency, but with a
379 modestly reduced total discharge in *unc-7* mutants (**Figure 7G-I**). Thus, AVA's dual
380 action – attenuation and potentiation – on the reversal motor state, correlates with an
381 inhibition and stimulation of A-MN's oscillatory activity, respectively (**Figure 7J**).

382 Collectively, we show that A-MNs exhibit intrinsic and oscillatory activity that is
383 sufficient for reverse movements. Positive and negative regulation of their oscillatory
384 activity, through either manipulation of the activity of an endogenous oscillatory current,
385 or, by the descending premotor INs AVA, lead to changes in the propensity, velocity and
386 duration of the reversal motor state.

387 **Discussion**

388 We show that distinct locomotor CPGs underlie *C. elegans* forward and reversal
389 movements. For reversal movements, the excitatory A-MNs are both motor executors and
390 rhythm generators. We discuss that this functional interpretation is consistent with their
391 electrophysiology properties, and anatomic organization exhibited by other locomotor
392 networks. These and previous studies on the *C. elegans* neuromuscular system exemplify
393 succinct anatomic and functional compression: multi-functionality of neurons and
394 muscles enables the *C. elegans* motor circuit to operate with fundamental similarity to
395 large locomotor networks, through small numbers of neurons and synapses.

396 ***Separate CPGs drive forward and reverse locomotion***

397 The behavioral consequences upon premotor IN- and MN-ablation allowed us to
398 distinguish neuronal requirements for forward and reverse movements. Forward
399 movements consist of head oscillation that pulls the body forward, and body oscillation
400 that is executed by B-MNs. Reverse movement consists of body oscillation that is driven
401 by multiple A-MNs, and may be antagonized by head oscillation. Hence, *C. elegans*
402 locomotion involves orchestration of independent sets of rhythm generators that underlie
403 the head and body oscillations.

404 A separation of forward- and reversal-driving oscillators at the motor neuron level
405 provides a different strategy for directional control than that utilized by the lamprey and
406 *Drosophila* larvae. In these systems, the same spinal or ventral cord motor units underlie
407 body movements regardless of directions; a directional change is achieved through re-
408 establishment of their phase relationship that reverses the direction of propagation.

409 Is there an advantage to utilize separate motor units for directional movements? In
410 the absence of premotor INs, *C. elegans* generate deeper body bends during reverse than
411 forward movement. This suggests that A-MNs exhibit intrinsically higher activity than B-
412 MNs. In fact, establishing forward movement as the preferred motor state requires
413 premotor INs to attenuate A-MN's activity (Kawano et al., 2011). It is reasonable to
414 speculate that these motor units allow more efficient transition to reversals, the motor
415 state that is frequently incorporated in adverse stimuli-evoked behavioral responses, such
416 as escape and avoidance.

417 *A-MNs are reversal CPGs*

418 Multiple lines of evidence support the idea that A-MNs, executors for reverse movement,
419 are themselves the reversal CPGs: they exhibit intrinsic and oscillatory activity; their
420 intrinsic activity is sufficient to drive reverse movements; the level of intrinsic activity,
421 regulated by P/Q/N-VGCCs, correlates with the reversal velocity; premotor IN-mediated
422 attenuation and potentiation of their activities determine the initiation and sustention of
423 the reversal motor state.

424 These findings bear resemblance to those at the lobster STG, where MNs, with one
425 descending interneuron, constitute an oscillatory network that underlies digestive
426 behaviors (Marder and Bucher, 2001; Selverston and Moulins, 1985). In all described
427 locomotor CPG circuits, however, MNs are thought to provide feedbacks to the rhythm
428 generating premotor INs (Heitler, 1978; Song et al., 2016; Szczupak, 2014). This study
429 provides the first example of a single neuron type performing both motor and rhythm-
430 generating roles in a circuit that underlies locomotor behaviors.

431 *High-voltage-activated calcium currents are conserved constituents of oscillation*

432 We show that in addition to a role in exocytosis, the P/Q/N-type calcium conductance
433 constitutes A-MN's membrane oscillation. In *unc-2(lf)*, but not in *unc-13(lf)* mutants in
434 which synaptic transmission was abolished (Richmond and Jorgensen, 1999), A-MN
435 calcium oscillation was compromised. Restoration of UNC-2 in A-MNs was sufficient to
436 restore their oscillatory activity in *unc-2(lf)* mutants. Endogenously tagged UNC-2
437 resides at both the presynaptic termini and soma of MNs. Restoring UNC-2 in A-MNs –
438 simultaneously rescuing their oscillation and NMJ activities – restores reverse movement
439 in the absence of premotor INs.

440 An exocytosis-independent role of high-voltage activated calcium channels in
441 membrane oscillation has been noted in vertebrates. In isolated lamprey spinal neuron
442 soma, the N-type calcium currents prominently potentiate bursting, and are coupled with
443 calcium-activated potassium currents that terminate bursts (el Manira et al., 1994;
444 Wikstrom and El Manira, 1998). The intrinsic, high frequency gamma band oscillation of
445 the rat pedunclopontine nucleus (PPN) requires high-threshold N- and/or P/Q-type
446 calcium currents, a finding that coincides with the dendritic and somatic localization of
447 VGCC channels in cultured PPN neurons (Hyde et al., 2013; Kezunovic et al., 2011;
448 Luster et al., 2015). High-voltage activated calcium conductance may be a shared
449 property of neurons with oscillatory activity.

450 *Oscillators underlie rhythmicity of C. elegans' motor output*

451 In most locomotor networks, premotor INs, MNs, and muscles generate rhythmic action
452 potential bursts that correlate with fictive or non-fictive locomotion (Grillner, 2006;
453 Kiehn, 2016). *C. elegans* is superficially at odds with several fundamental features of
454 such networks: its genome does not encode voltage-activated sodium channels

455 (Bargmann, 1998; Consortium, 1998), and its nervous system does not generate sodium-
456 driven action potentials (Goodman et al., 1998; Kato et al., 2015; Liu et al., 2017; Liu et
457 al., 2014; Xie et al., 2013). Results from this and previous studies, however, reveal a
458 simplified, but fundamentally conserved cellular and molecular underpinning of
459 rhythmicity in *C. elegans* locomotion.

460 *C. elegans* MNs and premotor INs are non-spiking, exhibiting plateau potentials
461 upon stimulation (Kato et al., 2015; Liu et al., 2014). B- and A-MNs exhibit calcium
462 oscillation during forward and reverse movement (Kawano et al., 2011; Wen et al., 2012;
463 this study). Muscles alone have the ability to fire calcium-driven action potentials (Gao
464 and Zhen, 2011; Jospin et al., 2002; Liu et al., 2011; Liu et al., 2009; Raizen and Avery,
465 1994). In the circuit that drives reverse movement, activation of premotor INs or MNs
466 triggers rhythmic action potential bursts in body wall muscles, a pattern of physical
467 relevance (Gao et al., 2015). Here we further demonstrate that not only are A-MNs
468 required for these bursts, altering A-MN's oscillation leads to changes in their frequency
469 and duration.

470 We propose that the *C. elegans* locomotor network utilizes a combined oscillatory
471 and bursting property of MNs and muscles for motor rhythmicity. In the absence of
472 voltage-activated sodium channels, high voltage-activated calcium channels, specifically,
473 the P/Q/N- and L-type VGCCs that respectively drive MN oscillation and muscle
474 spiking, take deterministic roles in the rhythmicity output.

475 ***Functional and anatomic compression at the C. elegans motor circuit***

476 Upon activation, the spinal and ventral nerve cords are self-sufficient locomotor
477 networks. In the vertebrate spinal cords, distinct pools of premotor INs and MNs play

478 dedicated roles in rhythm generation, pattern coordination, proprioceptive and recurrent
479 feedback, and execution of different motor patterns (Grillner, 2006). A highly refined
480 functional specification of these circuit constituents coincides with selective recruitment
481 of sub-pools of premotor INs and MNs when rodents generate distinct and flexible motor
482 responses (Kiehn, 2016).

483 *C. elegans* locomotion operates with a remarkably small number of neurons.
484 Despite the extreme numeric simplicity, it exhibits behavioral adaptability (Fang-Yen et
485 al., 2010) and repertoire of motor outputs comparable to larger invertebrates. Such a
486 motor infrastructure has to compress multiple functions into a smaller number of cells
487 and fewer layers of neurons. The only soma that reside in the *C. elegans* ventral nerve
488 cord are of MNs, consistent with a notion that its MNs and muscles have compressed the
489 role of the entire spinal cord CPG network. Indeed, body wall muscles are the only
490 bursting cells. Excitatory MNs have absorbed the role of rhythm generators. Previous
491 (Wen et al., 2012) studies suggest that *C. elegans* MNs may have further integrated the
492 role of proprioceptive feedback.

493 Anatomical constraints may have necessitated functional compression. The small
494 lobster STG circuit, where pyloric MNs function as the CPG (Marder and Bucher, 2001;
495 Selverston and Moulins, 1985), provides another well-characterized example of such
496 compression. When a nervous system consists of a small number of neurons, instead of
497 being *simple*, it is more *compact*. The numeric complexity, reflected by both increased
498 neuronal subtypes and numbers in large circuits, is compensated by a cellular complexity
499 that endows individual neuron or neuronal class multi-functionality in a small nervous
500 system.

501 ***Revisiting the role of mixed chemical and electric synaptic connections, a conserved***
502 ***configuration of rhythm-generating circuits***

503 Locomotor circuits of the crayfish, leech, *C. elegans*, and zebrafish exhibit a conserved
504 configuration: premotor INs and MNs are connected by both gap junctions and chemical
505 synapses. A similar configuration has also been noted in other motor systems such as the
506 lobster cardiac and stomatogastric ganglia (Hartline, 1979; Marder, 1984), and the snail
507 feeding system (Staras et al., 1998). Gap junctions are prevalent at mature rodent spinal
508 cords (Kiehn and Tresch, 2002). Mixed chemical and electric synaptic connectivity may
509 be a universal feature of rhythm-generating circuits.

510 When arranged in combination with chemical synapses, gap junctions exert diverse
511 effects on circuit dynamics and flexibility (Marder et al., 2016; Rela and Szczupak,
512 2004). In the crustacean pyloric networks, the Anterior Bursting (AB) IN, the Pyloric
513 Dilator (PD) MN, and the Ventricular Dilator (VD) MN are electrically coupled. Mixed
514 electric coupling and inhibitory chemical synapses between AB and VD allows the
515 electrically coupled VD and PD MNs to fire out-of-phase (Marder, 1984). In the leech
516 swimming circuit, mixed electric coupling and hyperpolarizing chemical synapses
517 between the descending INs and MNs facilitate recurrent inhibition on the MN activity
518 (Szczupak, 2014). In the crayfish, snail, and zebrafish ventral and spinal nerve cords
519 (Heitler, 1978; Song et al., 2016; Staras et al., 1998), gap junctions allow MNs to
520 retrogradely regulate the activity of premotor INs.

521 *C. elegans* innexin mutants permit direct behavioral assessment of the role of gap
522 junctions. Genetic, electrophysiology, and optogenetic examination of innexin mutants
523 that selectively disrupt premotor IN and MN gap junctions (Starich et al., 2009) reveal

524 sophisticated roles for a mixed heterotypic and rectifying gap junction and excitatory
525 chemical synapse configuration in locomotion (Kawano et al., 2011; Liu et al., 2017). In
526 the reversal motor circuit, this configuration allows premotor INs AVA to exert state-
527 dependent regulation on reversal oscillators A-MN. At rest, AVA-A gap junctions
528 dampen the excitability of coupled premotor INs (Kawano et al., 2011) and oscillatory
529 activity of MNs to reduce propensity for reversals. Upon activation, AVA potentiate A-
530 MNs predominantly through excitatory chemical synapses, with a minor contribution
531 from gap junctions. Remarkably, the weakly rectifying gap junctions (Liu et al., 2017;
532 Starich et al., 2009) may allow activated A-MNs to antidromically amplify the excitatory
533 chemical synaptic inputs from AVA, prolonging an evoked reverse movement (Liu et al.,
534 2017). Because genetic studies for gap junctions are lacking in most studies, we may
535 continue to find us underappreciating the sophistication and diversity of such a
536 configuration in *C. elegans* and other systems.

537 ***Remaining questions and closing remarks***

538 Recent work began to dissect how the *C. elegans* motor circuit operates. Previous studies
539 suggest that the forward promoting B-MNs are strongly activated by proprioception;
540 proprioceptive coupling thus plays a critical role on bending propagation during forward
541 movement (Wen et al., 2012). Our analysis reveals another mechanism, a chain of phase-
542 coupled local CPGs to organize and execute reverse locomotion. Here, proprioception
543 may, as in other motor circuits, serve as a feedback mechanism to regulate A-MNs'
544 oscillation to organize their phasic relation. A compression model thus proposes that A-
545 MNs have integrated the role of not only rhythm-generation, but also modulatory

546 proprioceptive INs in other locomotor circuits. Several key questions remain to be
547 addressed.

548 First, understanding the molecular mechanism that underlies the functional
549 compression of excitatory MNs is crucial. Comparing the intrinsic difference between the
550 A- and B-MNs, and potentially among individual members of each class, provides a
551 starting point to evaluate this hypothesis. Second, the membrane property of CPG
552 neurons in the lampreys and other systems is mainly characterized pharmacologically: the
553 depolarization initiated by sodium and calcium conductance, potentiated and maintained
554 by voltage- or glutamate-activated calcium conductance, and terminated by calcium- and
555 voltage-activated potassium currents (Grillner et al., 2001). *C. elegans* genetics should
556 allow us to gain molecular insights, besides UNC-2, that endow oscillatory membrane
557 potentials. This pursuit may further delineate mechanisms that underlie the circuit
558 compression. Third, in the lamprey spinal cord, the fastest oscillator entrains other motor
559 CPGs and leads propagation (Grillner, 2006). DA9, the posterior unit that consistently
560 exhibits the highest activity, poises to be a leading oscillator of the *C. elegans* reverse
561 circuit. A-MNs may provide a genetic model to address molecular mechanisms that
562 endow the property of leading oscillators and underlie the entrainment of trailing CPGs.
563 Lastly, as in all other systems, A-MN oscillators must coordinate with oscillators that
564 drive other the motor states. Mechanisms that underlie their coordination may be
565 addressed in this system.

566 In closing, our studies contribute to a growing body of literature that small animals
567 can solve similar challenges in organizing locomotor behaviors faced by larger animals,
568 with a conserved molecular repertoire, and far fewer neurons. They serve as compact

569 models to dissect the organizational logic of neural circuits, where all essential functions
570 are instantiated, but compressed into fewer layers and cells of a smaller nervous system.

571 **Materials and Methods**

572 *Strains and constructs*

573 All *C. elegans* strains were cultured on standard Nematode Growth Medium (NGM)
574 plates seeded with OP50, and maintained at 15°C or 22°C. See Appendix 1 (Table 1 and
575 Table 2) for a complete list of constructs, transgenic lines, and strains generated or
576 acquired for this study.

577 *unc-2(hp647; gf)* was isolated in a suppressor screen for the motor defects of *unc-*
578 *80(e1069)* fainter mutants. Both *e1069; hp647* and *hp647* animals exhibit hyperactive
579 locomotion with high movement velocity and frequent alternation between forward and
580 reverse locomotion (Alcaire and Zhen, unpublished results). *hp647* was mapped between
581 *egl-17* and *lon-2*. Co-injected fosmids WRM0628cH07 and WRM0616dD06 rescued the
582 shuttle phenotype exhibited by *hp647* and reverted *unc-80(e1069); hp647* to *unc-*
583 *80(e1069)*-like fainter phenotypes. Subsequent exon and genomic DNA sequencing
584 revealed a causative L653F mutation in *unc-2(hp647)*. *unc-2(hp858)* is an insertion allele
585 where GFP was fused immediately in front of the ATG start codon of the *unc-2* locus by
586 CRISPR. *hp858* animals exhibit wildtype behaviors. Other genetic mutants used in this
587 study were obtained from the *Caenorhabditis Genetics Center (CGC)*; all were
588 backcrossed at least 4 times against N2 prior to analyses.

589 *Constructs and molecular biology*

590 All promoters used in this study were generated by PCR against a mixed-stage N2 *C.*
591 *elegans* genomic DNA. Promoters include the 5.1 kb *Pnmr-1*, 4.8 kb *Prig-3*, 2.8 kb *Psra-*
592 *11*, 1.8 kb *Pacr-2s*, 2.5 kb *Punc-4*, 4.2 kb *Pacr-5*, 0.9 kb *Pttr-39*, 2.8 kb *Pceh-12*, 2.7 kb
593 *Punc-129(DB)*, and 0.86 kb *Plgc-55B* genomic sequence upstream of the respective ATG

594 start codon. The *Pnmr-1* used in this study excluded a 2 kb internal fragment that encodes
595 *cex-1*, which interferes with reporter expression (Kawano et al., 2011).

596 For calcium imaging constructs, the genetic calcium sensor GCaMP3 and
597 GCaMP6s were used for muscle and neuronal calcium imaging, respectively. The
598 GCaMP6s sequence (Chen et al., 2013) was codon-optimized for expression in *C.*
599 *elegans*. The synthesized gene contained three *C. elegans* introns and contain restriction
600 enzyme sites to facilitate subsequent cloning. In all constructs, GCaMP was fused with
601 Cherry at the C-terminus to allow ratiometric measurement via simultaneous imaging of
602 GFP and RFP.

603 For neuronal ablation constructs, MiniSOG (Shu et al., 2011) fused with an outer
604 mitochondrial membrane tag TOMM20 (tomm20-miniSOG or mito-miniSOG) (Qi et al.,
605 2012) was used. An intercistronic sequence consisting of a U-rich element and Splice
606 Leader sequence (UrSL) was inserted between the coding sequence of tomm20-miniSOG
607 and Cherry or BFP to visualize neurons that express miniSOG and the efficacy of
608 ablation. Inter-cistronic region consisting of a U-rich element and Splice Leader sequence
609 (UrSL) between *gpd-2* and *gpd-3* was PCR amplified with OZM2301
610 (AAGCTAGCGAATTCGCTGTCTCATCCTACT TTCACC) and OZM2302
611 (AAGGTACCGATGCGTTGAAGCAGTTTC CC) using pBALU14 as the template.
612 Two sets of the bicistronic expression reporters used in this study, were codon-optimized
613 Cherry and BFP, gifts of Desai (UCSD) and Calarco (Harvard), respectively. They were
614 used for behavioral analyses and to be combined with calcium imaging analyses,
615 respectively.

616 ***Transgenic arrays and strains***

617 All strains were cultured on OP50 seeded NGM pates maintained at 22 °C. Unless
618 otherwise stated, the wildtype strain refers to the Bristol N2 strain. Transgenic animals
619 that carry non-integrated, extra-chromosomal arrays (*hpEx*) were generated by co-
620 injecting an injection marker with one to multiple DNA construct at 5-30 ng/μl. Animals
621 that carry transgenic arrays that were integrated into the genome (*hpIs*) were generated
622 from the *hpEx* animals by UV irradiation, followed by outcrossing against N2 at least
623 four times. L4-stage or young adults (24h post L4) hermaphrodites were used in all
624 experiments.

625 All strains that contain *hpIs166*, *hpIs270*, *hpIs569* and *hpIs578* were cultured in
626 the dark at 22 °C on NGM plates supplemented with or without ATR (Liewald et al.,
627 2008). All strains that contains miniSOG and GCaMP transgene were cultured in
628 darkness at 22 °C on standard NGM plates.

629 ***On plate, whole population neuron ablation***

630 To distinguish the role of different classes of neurons in locomotion modulation, we
631 expressed mito-miniSOG into the A-, B-, D-MNs, premotor INs (AVA, AVE, PVC,
632 AVD, AVB) and a few other unidentified neurons, respectively (Supplemental
633 Information Table 1A and B). On plate ablation of all members of MNs and premotor INs
634 was performed using a homemade LED box, where the standard NGM culture plates,
635 without lid, were exposed under a homemade 470 nm blue LED light box for 30-45
636 minutes. To monitor the specificity and efficacy of cell ablation, cytoplasmic RFP was
637 co-expressed with miniSOG (tomm-20-miniSOG-SL2-RFP) in targeted neurons by the
638 same promoter. Ablation was performed when most animals were in the L2 stage; L4
639 stage animals were recorded for behavioral or calcium imaging analyses. Afterwards,

640 they were mounted individually on agar pads to be examined for RFP signals; recordings
641 from animals where RFP signals were absent were analyzed.

642 *On plate locomotion analyses*

643 A single 12-18h post-L4 stage adult hermaphrodite, maintained on standard culture
644 conditions, was transferred to a 100 mm imaging plate seeded with a thin layer of OP50.
645 One minute after the transfer, a two-minute video of the crawling animal was recorded on
646 a modified Axioskop 2 (Zeiss) equipped with an automated tracking stage MS-2000
647 (Applied Scientific Instruments), a digital camera (Hamamatsu). Imaging plates were
648 prepared as follows: a standard NGM plate was seeded with a thin layer of OP50 12-14h
649 before the experiment. Immediately before the transfer of worms, the OP50 lawn was
650 spread evenly across the plate with a sterile bent glass rod. Movements exhibited by *C.*
651 *elegans* were recorded using an in-house developed automated tracking program. All
652 images were captured with a 10X objective, at 10 frames per second. Data recorded on
653 the same plate and on the same day, were pooled, quantified and compared.

654 Post-imaging analyses utilized an in-house developed ImageJ Plugin (Kawano et al.,
655 2011). The mid-point of the animal was used to track and calculate the velocity and
656 direction of the animal's movement between each frame. The percentage of total frames
657 exhibiting pausing, reverse or forward movement was defined by the centroid position
658 change: between -1 (- was defined as movement towards the tail) and +1 (+ was defined
659 as movement towards the head) pixel per second was defined as pause, less than -1 pixel
660 per second reverse, and more than +1 pixel per second forward movement. For the
661 curvature analysis of the animals, the angle between three joint points was defined as the

662 curvature of the middle point loci, all angles were then pooled and shown as color map
663 using in-house written MATLAB scripts.

664 *Calcium imaging of crawling animals*

665 Imaging of multiple A-MNs, VA10, VA11, and DA7 in moving animals (**Figure 2E**) was
666 performed similarly as described in previous study (Kawano et al., 2011). Animals were
667 placed on a 2% agarose pad on a slide, suspended in the M9 buffer, covered by a
668 coverslip, and imaged with a 63X objective. Neurons were identified by their stereotypic
669 anatomical organization. Multiple Regions of interest (ROI) containing the interested MN
670 soma were defined using a MATLAB script developed in-house. Videos were recorded
671 with a CCD camera (Hamamatsu C2400) at 100 ms per frame. Simultaneous velocity
672 recording at each time point was measured using an Image J plug-in developed in-house
673 (Gao et al., 2015; Kawano et al., 2011).

674 DA9 MN activity recording from immobilized intact animals (the rest of calcium
675 imaging figures) was carried out as follows: animals were glued as described for
676 electrophysiological recording (Gao et al., 2015), and imaged with a 60X water objective
677 (Nikon) and sCMOS digital camera (Hamamatsu ORCA-Flash 4.0V2) at 100 ms per
678 frame. Data were collected by MicroManager and analyzed by ImageJ.

679 In both systems, GCaMP and RFP signals were simultaneously acquired using the
680 Dual-View system (Photometrics), and the GCaMP/RFP ratios were calculated to control
681 for motion artifacts and fluorescence bleaching during recording.

682 *Region-specific photo-ablation of MNs and behavioral analyses*

683 Data in Figure 3 and Supplementary Figure 2 were collected from animals where A-type
684 MNs were ablated in three strains, where A- or A/B-MNs were labeled by RFP. For

685 miniSOG-based ablation, ZM9062 *hpIs583* (A- and B-MNs miniSOG) or YX167
686 *hpIs366/qhIs4; qhIs1* (A miniSOG) L2 larva were immobilized on a 4% agar pad with
687 5mM tetramisole. Region-specific illumination was performed by targeting a 473nm laser
688 at an arbitrary portion of the animal using a digital micromirror device (DMD) through a
689 20X objective (Leifer et al., 2011). The final irradiance at the stage was approximately 16
690 mW/mm². The DMD was set to pulse the laser with a duty cycle of 1s on, 0.8s off, for a
691 total of 300 of total ON time. Each animal was immobilized for a maximum of 30
692 minutes. Most posterior MNs (VA12-DA9) ablation was also performed in YX148 *qhIs4;*
693 *qhIs1* (A/B RFP) by a pulsed infrared laser illumination system (Churgin MA, 2013)
694 modified with increased output power. L2 animals were immobilized in the same manner.
695 A single 2ms pulse was applied to each neuron through a 60X objective visualized by
696 RFP. This procedure never affected VA11, the nearest non-targeted neuron. Following
697 ablation, each animal was transferred to an OP-50-seeded NGM plate and allowed to
698 grow to the day 1 adult stage. Controls were animals of the same genotype treated
699 identically except without blue or infrared laser illumination.

700 For behavior recording, each animal was transferred to an unseeded NGM plate,
701 and on plate crawling was recorded for at least 5 minutes under bright field illumination.
702 If the animal became sluggish or idle, the plate was agitated using the vibration motor
703 from a cell phone. After recordings, each animal was immobilized by 2 mM sodium azide
704 on an agar pad, and imaged at 40X for RFP pattern for the entire body. We manually
705 assigned present and missing neurons based on their relative positions and commissural
706 orientation (White et al., 1976, 1986). Here we included data from animals where we
707 were confident of the identity of neurons. For YX167, where A and B-MNs were labeled,

708 two researchers independently analyzed the same image, discussed, and agreed on the
709 identification.

710 Analyses of locomotion of ablated and control animals were carried out using
711 WormLab (MBF Bioscience, Williston, VT) and in-house Matlab codes. Data from all
712 three ablation methods were pooled to generate the summary statistics. Bouts of reverses
713 that lasted at least 3 seconds were analyzed for the speed of wave propagation. Curvature
714 segmentations from the behavioral recordings were constructed using WormLab (MBF
715 Bioscience, Williston, VT). Wave speed was measured as a function of body coordinate
716 and time, by taking the derivative of each curvature map with respect to time (dk/dt), and
717 to body coordinate (dk/dC). Wave speed was defined as the ratio between these gradients
718 (body coordinate/s). Wave speed was averaged over the length of each bout, and binned
719 for the anterior (5% to 25% of body length from the head), mid-body (40-60%), and
720 posterior (75-95%) region in each bout.

721 *Electrophysiology and optogenetic stimulation*

722 Dissection and recording were carried out using protocols and solutions described in
723 (Gao and Zhen, 2011), which was modified from (Mellem et al., 2008; Richmond and
724 Jorgensen, 1999). Briefly, 1- or 2-day-old hermaphrodite adults were glued (Histoacryl
725 Blue, Braun) to a sylgard-coated cover glass covered with bath solution (Sylgard 184,
726 Dowcorning) under stereoscopic microscope MS5 (Leica). After clearing the viscera by
727 suction through a glass pipette, the cuticle flap was turned and gently glued down using
728 WORMGLU (GluStitch Inc.) to expose the neuromuscular system. The integrity of the
729 anterior ventral body muscle and the ventral nerve cord were visually examined via DIC
730 microscopy (Eclipse FN1, Nikon), and muscle cells were patched using 4-6 M Ω -resistant

731 borosilicate pipettes (1B100F-4, World Precision Instruments). Pipettes were pulled by
732 micropipette puller P-1000 (Sutter), and fire-polished by microforge MF-830 (Narishige).
733 Membrane currents and action potentials were recorded in the whole-cell configuration
734 by a Digidata 1440A and a MultiClamp 700A amplifier, using the Clampex 10 and
735 processed with Clampfit 10 software (Axon Instruments, Molecular Devices). Currents
736 were recorded at holding potential of -60 mV, while action potentials were recorded at 0
737 pA. Data were digitized at 10–20 kHz and filtered at 2.6 kHz. The pipette solution
738 contains (in mM): K-gluconate 115; KCl 25; CaCl_2 0.1; MgCl_2 5; BAPTA 1; HEPES 10;
739 Na_2ATP 5; Na_2GTP 0.5; cAMP 0.5; cGMP 0.5, pH7.2 with KOH, ~ 320 mOsm. cAMP
740 and cGMP were included to maintain the activity and longevity of the preparation. The
741 bath solution consists of (in mM): NaCl 150; KCl 5; CaCl_2 5; MgCl_2 1; glucose 10;
742 sucrose 5; HEPES 15, pH7.3 with NaOH, ~ 330 mOsm. Chemicals and blockers were
743 obtained from Sigma unless stated otherwise. Experiments were performed at room
744 temperatures (20 – 22°C).

745 Optogenetic stimulation of transgenic animals was performed with an LED lamp, at
746 470 nm (from 8 mW/mm²) for *hpIs166* and *hpIs279*, and at 625 nm (from 1.1 mW/mm²),
747 for *hpIs569* and *hpIs578*, respectively, controlled by the Axon amplifier software. One-
748 second light exposure, a condition established by our previous study (Gao et al., 2015),
749 was used to evoke PSC bursts. The frequency power spectrum of rPSC bursts was
750 analyzed using Clampfit 10.

751 ***Statistical analysis***

752 The Mann-Whitney U test, two-tailed Student's *t* test, one-way ANOVA test, or the
753 Kolmogorov-Smirnov test were used to compare data sets. $P < 0.05$ was considered to be

754 statistically significant (* $P < 0.05$, ** $P < 0.01$, *** $P < 0.001$). Graphing and
755 subsequent analysis were performed using Igor Pro (WaveMetrics), Clampfit (Molecular
756 Devices), Image J (National Institutes of Health), R (<http://www.R-project.org>), Matlab
757 (MathWorks), and Excel (Microsoft). For electrophysiology and calcium imaging, unless
758 specified otherwise, each recording trace was obtained from a different animal; data were
759 presented as the Mean \pm SEM.

760 **Acknowledgements**

761 We thank Y. Wang, A. Liu, S. Teng, and J. R. Mark for technical assistance, the
762 *Caenorhabditis Genetics Center* and National Bioresource Project for strains, C.
763 Bargmann for UNC-2 cDNA, S. Takayanagi-Kiya for *juls440*. We thank Q. Wen, A.
764 Samuel and A. Chisholm for discussions and comments on the manuscript. This work
765 was supported by The National Natural Science Foundation of China (NSFC 31671052)
766 and the Junior Thousand Talents Program of China (S. Gao), the National Institute of
767 Health (C. F-Y, MA, YJ, MZ), and the Canadian Institute of Health Research and the
768 Natural Sciences and Engineering Research Council of Canada (MZ).

769 **References**

- 770 Bargmann, C.I. (1998). Neurobiology of the *Caenorhabditis elegans* genome. *Science*
771 282, 2028-2033.
- 772 Bhattacharya, R., Touroutine, D., Barbagallo, B., Climer, J., Lambert, C.M., Clark, C.M.,
773 Alkema, M.J., and Francis, M.M. (2014). A conserved dopamine-cholecystokinin
774 signaling pathway shapes context-dependent *Caenorhabditis elegans* behavior. *PLoS*
775 *Genet* 10, e1004584.
- 776 Briggman, K.L., and Kristan, W.B., Jr. (2006). Imaging dedicated and multifunctional
777 neural circuits generating distinct behaviors. *J Neurosci* 26, 10925-10933.
- 778 Brose, N., Hofmann, K., Hata, Y., and Sudhof, T.C. (1995). Mammalian homologues of
779 *Caenorhabditis elegans* unc-13 gene define novel family of C2-domain proteins. *J Biol*
780 *Chem* 270, 25273-25280.
- 781 Brown, T.G. (1911). The Intrinsic Factors in the Act of Progression in the Mammal. *roc*
782 *R Soc Lond B Biol Sci* 84 308–319.
- 783 Brown, T.G. (1914). On the nature of the fundamental activity of the nervous centres;
784 together with an analysis of the conditioning of rhythmic activity in progression, and a
785 theory of the evolution of function in the nervous system. *J Physiol* 48, 18-46.
- 786 Chalfie, M., Sulston, J.E., White, J.G., Southgate, E., Thomson, J.N., and Brenner, S.
787 (1985). The neural circuit for touch sensitivity in *Caenorhabditis elegans*. *J Neurosci* 5,
788 956-964.
- 789 Chen, T.W., Wardill, T.J., Sun, Y., Pulver, S.R., Renninger, S.L., Baohan, A., Schreiter,
790 E.R., Kerr, R.A., Orger, M.B., Jayaraman, V., *et al.* (2013). Ultrasensitive fluorescent
791 proteins for imaging neuronal activity. *Nature* 499, 295-300.
- 792 Churgin MA, H.L., Murray JI, Fang-Yen C. (2013). Efficient single-cell transgene
793 induction in *Caenorhabditis elegans* using a pulsed infrared laser. *G3 (Bethesda)* 3,
794 1827-1832.
- 795 Cohen, N., and Sanders, T. (2014). Nematode locomotion: dissecting the neuronal-
796 environmental loop. *Curr Opin Neurobiol* 25, 99-106.
- 797 Consortium, C.e.S. (1998). Genome sequence of the nematode *C. elegans*: a platform for
798 investigating biology. *Science* 282, 2012-2018.
- 799 Donnelly, J.L., Clark, C.M., Leifer, A.M., Pirri, J.K., Haburcak, M., Francis, M.M.,
800 Samuel, A.D., and Alkema, M.J. (2013). Monoaminergic orchestration of motor
801 programs in a complex *C. elegans* behavior. *PLoS biology* 11, e1001529.

- 802 Duerr, J.S., Han, H.P., Fields, S.D., and Rand, J.B. (2008). Identification of major classes
803 of cholinergic neurons in the nematode *Caenorhabditis elegans*. *J Comp Neurol* *506*, 398-
804 408.
- 805 el Manira, A., Tegner, J., and Grillner, S. (1994). Calcium-dependent potassium channels
806 play a critical role for burst termination in the locomotor network in lamprey. *J*
807 *Neurophysiol* *72*, 1852-1861.
- 808 Fang-Yen, C., Wyart, M., Xie, J., Kawai, R., Kodger, T., Chen, S., Wen, Q., and Samuel,
809 A.D. (2010). Biomechanical analysis of gait adaptation in the nematode *Caenorhabditis*
810 *elegans*. *Proc Natl Acad Sci U S A* *107*, 20323-20328.
- 811 Gao, S., Xie, L., Kawano, T., Po, M.D., Pirri, J.K., Guan, S., Alkema, M.J., and Zhen, M.
812 (2015). The NCA sodium leak channel is required for persistent motor circuit activity that
813 sustains locomotion. *Nat Commun* *6*, 6323.
- 814 Gao, S., and Zhen, M. (2011). Action potentials drive body wall muscle contractions in
815 *Caenorhabditis elegans*. *Proc Natl Acad Sci U S A* *108*, 2557-2562.
- 816 Gjorgjieva, J., Biron, D., and Haspel, G. (2014). Neurobiology of *Caenorhabditis elegans*
817 Locomotion: Where Do We Stand? *Bioscience* *64*, 476-486.
- 818 Goodman, M.B., Hall, D.H., Avery, L., and Lockery, S.R. (1998). Active currents
819 regulate sensitivity and dynamic range in *C. elegans* neurons. *Neuron* *20*, 763-772.
- 820 Goulding, M. (2009). Circuits controlling vertebrate locomotion: moving in a new
821 direction. *Nat Rev Neurosci* *10*, 507-518.
- 822 Grillner, S. (2006). Biological pattern generation: the cellular and computational logic of
823 networks in motion. *Neuron* *52*, 751-766.
- 824 Grillner, S., and Wallen, P. (1985). Central pattern generators for locomotion, with
825 special reference to vertebrates. *Annu Rev Neurosci* *8*, 233-261.
- 826 Grillner, S., Wallen, P., Hill, R., Cangiano, L., and El Manira, A. (2001). Ion channels of
827 importance for the locomotor pattern generation in the lamprey brainstem-spinal cord. *J*
828 *Physiol* *533*, 23-30.
- 829 Guertin, P., Angel, M.J., Perreault, M.C., and McCrea, D.A. (1995). Ankle extensor
830 group I afferents excite extensors throughout the hindlimb during fictive locomotion in
831 the cat. *J Physiol* *487*, 197-209.
- 832 Harris-Warrick, R.M. (2002). Voltage-sensitive ion channels in rhythmic motor systems.
833 *Curr Opin Neurobiol* *12*, 646-651.
- 834 Hartline, D.K. (1979). Integrative Neurophysiology of the Lobster Cardiac Ganglion.
835 *American Zoologist* *19*, 53-65.

- 836 Heitler, W.J. (1978). Coupled motoneurons are part of the crayfish swimmeret central
837 oscillator. *Nature* 275, 231-234.
- 838 Hu, Z., Pym, E.C., Babu, K., Vashlishan Murray, A.B., and Kaplan, J.M. (2011). A
839 neuropeptide-mediated stretch response links muscle contraction to changes in
840 neurotransmitter release. *Neuron* 71, 92-102.
- 841 Hyde, J., Kezunovic, N., Urbano, F.J., and Garcia-Rill, E. (2013). Spatiotemporal
842 properties of high-speed calcium oscillations in the pedunculopontine nucleus. *J Appl*
843 *Physiol* (1985) 115, 1402-1414.
- 844 Jospin, M., Jacquemond, V., Mariol, M.C., Segalat, L., and Allard, B. (2002). The L-type
845 voltage-dependent Ca²⁺ channel EGL-19 controls body wall muscle function in
846 *Caenorhabditis elegans*. *J Cell Biol* 159, 337-348.
- 847 Juvin, L., Simmers, J., and Morin, D. (2007). Locomotor rhythmogenesis in the isolated
848 rat spinal cord: a phase-coupled set of symmetrical flexion extension oscillators. *J*
849 *Physiol* 583, 115-128.
- 850 Karbowski, J., Schindelman, G., Cronin, C.J., Seah, A., and Sternberg, P.W. (2008).
851 Systems level circuit model of *C. elegans* undulatory locomotion: mathematical modeling
852 and molecular genetics. *J Comput Neurosci* 24, 253-276.
- 853 Kato, S., Kaplan, H.S., Schrodell, T., Skora, S., Lindsay, T.H., Yemini, E., Lockery, S.,
854 and Zimmer, M. (2015). Global brain dynamics embed the motor command sequence of
855 *Caenorhabditis elegans*. *Cell* 163, 656-669.
- 856 Kawano, T., Po, M.D., Gao, S., Leung, G., Ryu, W.S., and Zhen, M. (2011). An
857 imbalancing act: gap junctions reduce the backward motor circuit activity to bias *C.*
858 *elegans* for forward locomotion. *Neuron* 72, 572-586.
- 859 Kezunovic, N., Urbano, F.J., Simon, C., Hyde, J., Smith, K., and Garcia-Rill, E. (2011).
860 Mechanism behind gamma band activity in the pedunculopontine nucleus. *Eur J Neurosci*
861 34, 404-415.
- 862 Kiehn, O. (2006). Locomotor circuits in the mammalian spinal cord. *Annu Rev Neurosci*
863 29, 279-306.
- 864 Kiehn, O. (2016). Decoding the organization of spinal circuits that control locomotion.
865 *Nat Rev Neurosci* 17, 224-238.
- 866 Kiehn, O., Iizuka, M., and Kudo, N. (1992). Resetting from low threshold afferents of N-
867 methyl-D-aspartate-induced locomotor rhythm in the isolated spinal cord-hindlimb
868 preparation from newborn rats. *Neurosci Lett* 148, 43-46.
- 869 Kiehn, O., and Tresch, M.C. (2002). Gap junctions and motor behavior. *Trends Neurosci*
870 25, 108-115.

- 871 Klapoetke, N.C., Murata, Y., Kim, S.S., Pulver, S.R., Birdsey-Benson, A., Cho, Y.K.,
872 Morimoto, T.K., Chuong, A.S., Carpenter, E.J., Tian, Z., *et al.* (2014). Independent
873 optical excitation of distinct neural populations. *Nat Methods* *11*, 338-346.
- 874 Lee, R.Y., Lobel, L., Hengartner, M., Horvitz, H.R., and Avery, L. (1997). Mutations in
875 the alpha1 subunit of an L-type voltage-activated Ca²⁺ channel cause myotonia in
876 *Caenorhabditis elegans*. *EMBO J* *16*, 6066-6076.
- 877 Leifer, A.M., Fang-Yen, C., Gershow, M., Alkema, M.J., and Samuel, A.D. (2011).
878 Optogenetic manipulation of neural activity in freely moving *Caenorhabditis elegans*. *Nat*
879 *Methods* *8*, 147-152.
- 880 Li, W., Feng, Z., Sternberg, P.W., and Xu, X.Z. (2006). A *C. elegans* stretch receptor
881 neuron revealed by a mechanosensitive TRP channel homologue. *Nature* *440*, 684-687.
- 882 Liewald, J.F., Brauner, M., Stephens, G.J., Bouhours, M., Schultheis, C., Zhen, M., and
883 Gottschalk, A. (2008). Optogenetic analysis of synaptic function. *Nat Methods* *5*, 895-
884 902.
- 885 Liu, P., Chen, B., Mailler, R., and Wang, Z.-W. (2017). Antidromic-rectifying gap
886 junctions amplify chemical transmission at functionally mixed electrical-chemical
887 synapses. *Nat Commun* *8*:14818. doi: 10.1038/ncomms14818.
- 888 Liu, P., Chen, B., and Wang, Z.W. (2013). Postsynaptic current bursts instruct action
889 potential firing at a graded synapse. *Nat Commun* *4*, 1911.
- 890 Liu, P., Chen, B., and Wang, Z.W. (2014). SLO-2 potassium channel is an important
891 regulator of neurotransmitter release in *Caenorhabditis elegans*. *Nat Commun* *5*, 5155.
- 892 Liu, P., Ge, Q., Chen, B., Salkoff, L., Kotlikoff, M.I., and Wang, Z.W. (2011). Genetic
893 dissection of ion currents underlying all-or-none action potentials in *C. elegans* body-wall
894 muscle cells. *J Physiol* *589*, 101-117.
- 895 Liu, Q., Hollopeter, G., and Jorgensen, E.M. (2009). Graded synaptic transmission at the
896 *Caenorhabditis elegans* neuromuscular junction. *Proc Natl Acad Sci U S A* *106*, 10823-
897 10828.
- 898 Luster, B., D'Onofrio, S., Urbano, F., and Garcia-Rill, E. (2015). High-threshold Ca²⁺
899 channels behind gamma band activity in the pedunculo-pontine nucleus (PPN). *Physiol*
900 *Rep* *3*.
- 901 Marder, E. (1984). Roles for electrical coupling in neural circuits as revealed by selective
902 neuronal deletions. *J Exp Biol* *112*, 147-167.
- 903 Marder, E., and Bucher, D. (2001). Central pattern generators and the control of rhythmic
904 movements. *Curr Biol* *11*, R986-996.

- 905 Marder, E., and Calabrese, R.L. (1996). Principles of rhythmic motor pattern generation.
906 *Physiol Rev* 76, 687-717.
- 907 Marder, E., Gutierrez, G.J., and Nusbaum, M.P. (2016). Complicating connectomes:
908 Electrical coupling creates parallel pathways and degenerate circuit mechanisms. *Dev*
909 *Neurobiol.*
- 910 Mathews, E.A., Garcia, E., Santi, C.M., Mullen, G.P., Thacker, C., Moerman, D.G., and
911 Snutch, T.P. (2003). Critical residues of the *Caenorhabditis elegans* unc-2 voltage-gated
912 calcium channel that affect behavioral and physiological properties. *J Neurosci* 23, 6537-
913 6545.
- 914 McIntire, S.L., Jorgensen, E., and Horvitz, H.R. (1993). Genes required for GABA
915 function in *Caenorhabditis elegans*. *Nature* 364, 334-337.
- 916 Mellem, J.E., Brockie, P.J., Madsen, D.M., and Maricq, A.V. (2008). Action potentials
917 contribute to neuronal signaling in *C. elegans*. *Nat Neurosci* 11, 865-867.
- 918 Nagel, G., Brauner, M., Liewald, J.F., Adeishvili, N., Bamberg, E., and Gottschalk, A.
919 (2005). Light activation of channelrhodopsin-2 in excitable cells of *Caenorhabditis*
920 *elegans* triggers rapid behavioral responses. *Curr Biol* 15, 2279-2284.
- 921 Pearson, K.G. (1993). Common principles of motor control in vertebrates and
922 invertebrates. *Annu Rev Neurosci* 16, 265-297.
- 923 Pereira, L., Kratsios, P., Serrano-Saiz, E., Sheftel, H., Mayo, A.E., Hall, D.H., White,
924 J.G., LeBoeuf, B., Garcia, L.R., Alon, U., *et al.* (2015). A cellular and regulatory map of
925 the cholinergic nervous system of *C. elegans*. *Elife* 4.
- 926 Pirri, J.K., McPherson, A.D., Donnelly, J.L., Francis, M.M., and Alkema, M.J. (2009). A
927 tyramine-gated chloride channel coordinates distinct motor programs of a *Caenorhabditis*
928 *elegans* escape response. *Neuron* 62, 526-538.
- 929 Qi, Y.B., Garren, E.J., Shu, X., Tsien, R.Y., and Jin, Y. (2012). Photo-inducible cell
930 ablation in *Caenorhabditis elegans* using the genetically encoded singlet oxygen
931 generating protein miniSOG. *Proc Natl Acad Sci U S A* 109, 7499-7504.
- 932 Raizen, D.M., and Avery, L. (1994). Electrical activity and behavior in the pharynx of
933 *Caenorhabditis elegans*. *Neuron* 12, 483-495.
- 934 Rakowski, F., Srinivasan, J., Sternberg, P.W., and Karbowski, J. (2013). Synaptic
935 polarity of the interneuron circuit controlling *C. elegans* locomotion. *Front Comput*
936 *Neurosci* 7, 128.
- 937 Rand, J.B. (2007). Acetylcholine. *WormBook*, 1-21.
- 938 Rela, L., and Szczupak, L. (2003). Coactivation of motoneurons regulated by a network
939 combining electrical and chemical synapses. *J Neurosci* 23, 682-692.

- 940 Rela, L., and Szczupak, L. (2004). Gap junctions: their importance for the dynamics of
941 neural circuits. *Mol Neurobiol* 30, 341-357.
- 942 Richmond, J.E., and Jorgensen, E.M. (1999). One GABA and two acetylcholine receptors
943 function at the *C. elegans* neuromuscular junction. *Nat Neurosci* 2, 791-797.
- 944 Roberts, W.M., Augustine, S.B., Lawton, K.J., Lindsay, T.H., Thiele, T.R., Izquierdo,
945 E.J., Faumont, S., Lindsay, R.A., Britton, M.C., Pokala, N., *et al.* (2016). A stochastic
946 neuronal model predicts random search behaviors at multiple spatial scales in *C. elegans*.
947 *Elife* 5.
- 948 Saheki, Y., and Bargmann, C.I. (2009). Presynaptic CaV2 calcium channel traffic
949 requires CALF-1 and the alpha(2)delta subunit UNC-36. *Nat Neurosci* 12, 1257-1265.
- 950 Schafer, W.R., and Kenyon, C.J. (1995). A calcium-channel homologue required for
951 adaptation to dopamine and serotonin in *Caenorhabditis elegans*. *Nature* 375, 73-78.
- 952 Selverston, A.I., and Moulins, M. (1985). Oscillatory neural networks. *Annu Rev Physiol*
953 47, 29-48.
- 954 Shu, X., Lev-Ram, V., Deerinck, T.J., Qi, Y., Ramko, E.B., Davidson, M.W., Jin, Y.,
955 Ellisman, M.H., and Tsien, R.Y. (2011). A genetically encoded tag for correlated light
956 and electron microscopy of intact cells, tissues, and organisms. *PLoS biology* 9,
957 e1001041.
- 958 Song, J., Ampatzis, K., Bjornfors, E.R., and El Manira, A. (2016). Motor neurons control
959 locomotor circuit function retrogradely via gap junctions. *Nature* 529, 399-402.
- 960 Staras, K., Kemenes, G., and Benjamin, P.R. (1998). Pattern-generating role for
961 motoneurons in a rhythmically active neuronal network. *J Neurosci* 18, 3669-3688.
- 962 Starich, T.A., Xu, J., Skerrett, I.M., Nicholson, B.J., and Shaw, J.E. (2009). Interactions
963 between innexins UNC-7 and UNC-9 mediate electrical synapse specificity in the
964 *Caenorhabditis elegans* locomotory nervous system. *Neural Dev* 4, 16.
- 965 Szczupak, L. (2014). Recurrent inhibition in motor systems, a comparative analysis. *J*
966 *Physiol Paris* 108, 148-154.
- 967 Wallen, P., and Williams, T.L. (1984). Fictive locomotion in the lamprey spinal cord in
968 vitro compared with swimming in the intact and spinal animal. *J Physiol* 347, 225-239.
- 969 Wen, Q., Po, M.D., Hulme, E., Chen, S., Liu, X., Kwok, S.W., Gershow, M., Leifer,
970 A.M., Butler, V., Fang-Yen, C., *et al.* (2012). Proprioceptive coupling within motor
971 neurons drives *C. elegans* forward locomotion. *Neuron* 76, 750-761.
- 972 White, J.G., Southgate, E., Thomson, J.N., and Brenner, S. (1976). The structure of the
973 ventral nerve cord of *Caenorhabditis elegans*. *Philos Trans R Soc Lond B Biol Sci* 275,
974 327-348.

- 975 White, J.G., Southgate, E., Thomson, J.N., and Brenner, S. (1986). The structure of the
976 nervous system of the nematode *Caenorhabditis elegans*. *Philos Trans R Soc Lond B Biol*
977 *Sci* 314, 1-340.
- 978 Wicks, S.R., and Rankin, C.H. (1995). Integration of mechanosensory stimuli in
979 *Caenorhabditis elegans*. *J Neurosci* 15, 2434-2444.
- 980 Wikstrom, M.A., and El Manira, A. (1998). Calcium influx through N- and P/Q-type
981 channels activate apamin-sensitive calcium-dependent potassium channels generating the
982 late afterhyperpolarization in lamprey spinal neurons. *Eur J Neurosci* 10, 1528-1532.
- 983 Wilson, D.M. (1961). The central nervous control of flight in a locust. *J Exp Biol* 38,
984 471-490.
- 985 Xie, L., Gao, S., Alcaire, S.M., Aoyagi, K., Wang, Y., Griffin, J.K., Stagljar, I.,
986 Nagamatsu, S., and Zhen, M. (2013). NLF-1 delivers a sodium leak channel to regulate
987 neuronal excitability and modulate rhythmic locomotion. *Neuron* 77, 1069-1082.
- 988 Zhen, M. and Samuel, A. D. (2015). *C. elegans* locomotion: small circuits, complex
989 functions. *Curr Opin Neurobiol* 33, 117-26.
- 990 Zheng, Y., Brockie, P.J., Mellem, J.E., Madsen, D.M., and Maricq, A.V. (1999).
991 Neuronal control of locomotion in *C. elegans* is modified by a dominant mutation in the
992 GLR-1 ionotropic glutamate receptor. *Neuron* 24, 347-361.

993 **Figure Titles and Legends**

994 **Figure 1. Body bends persist upon the ablation of premotor INs.**

995 **(A)** Removal of premotor INs or MNs exerts different effects on body bends. *Upper*
996 *panel:* Schematics of the *C. elegans* motor circuit components and connectivity in (i)
997 wildtype animals (i) and upon ablation of respective neuronal populations (ii, iii).
998 Hexagons and circles represent premotor INs and ventral cord MNs, respectively. Orange
999 and blue denotes components of the forward- and reverse-promoting motor circuit,
1000 respectively. Taupe denotes neurons that participate in movements of both directions.
1001 *Lower panel:* the representative body posture of adult *C. elegans* with intact motor circuit
1002 (i), and upon premotor IN (ii) or MN (iii) ablation. **(B)** Representative curvature
1003 kymogram along the entire length of moving animals of their respective genetic
1004 background. The upper and lower panels denote animals without (Control, -LED) and
1005 with (+LED) illumination during development (Materials and Methods). i, Wildtype (N2)
1006 animals exhibit a preference for continuous forward locomotion, consisting of anterior to
1007 posterior body bend propagation, with occasional and short reverse movement, exhibited
1008 as posterior to anterior body bend propagation; ii, Ablation of all premotor INs (+LED)
1009 leads to stalling body bends that antagonize the propagation of head bending; iii,
1010 simultaneous ablation of three major MN classes largely eliminates body bend in regions
1011 posterior to head. **(C)** Distribution of body curvatures posterior to head (33-96% anterior-
1012 posterior body length) in wildtype (i), premotor IN-ablated (ii), and MN-ablated (iii)
1013 animals, with (Control) and without (Ablated) LED exposure. Premotor IN ablation leads
1014 to an increase (ii), whereas MNs ablation a decrease (iii) of curvature. **(D)** Distribution of
1015 instantaneous velocity, represented by centroid displacement, in wildtype (i), premotor
1016 IN-ablated (ii), and MN-ablated (iii) animals, with (Control) and without (Ablated)

1017 exposure to LED. Both premotor IN- and MN-ablations lead to a drastic reduction of
1018 velocity. $n = 10$ animals per group (C, D). $P > 0.05$ (not significant), $P < 0.01$, $P < 0.001$
1019 against the respective non-ablated Control group by the Kolmogorov-Smirnov test.

1020 **Figure 1- figure supplement 1. Locomotor phenotypes of animals upon (A) the ablation**
1021 **of premotor INs and (B) the co-ablation of premotor INs and D-MNs.**

1022 (A) Ablation of all premotor INs, using different miniSOG transgene combinations, also
1023 leads to the *kinker* motor defects. i: Schematics of the motor circuit components and
1024 connectivity in animals upon ablation of respective neuronal populations. As in Figure 1,
1025 the AVA, AVE, AVD and PVC INs were ablated by *hpIs321*. Different from Figure 1,
1026 AVB INs were ablated by *juIs440*. *hpIs331* and *juIs440* overlap in miniSOG expression
1027 only in AVB. ii: Representative curvature kymogram of moving animals. The upper and
1028 lower panels denote animals without (-LED) and with (+LED) neuronal ablation.
1029 Ablation of premotor INs led to antagonizing head and tail body bends, or *kink*; iii:
1030 Distribution of body curvatures (33-96% of anterior-posterior body length). Ablation of
1031 premotor INs leads to increased curvatures. iv: Distribution of instantaneous velocity,
1032 represented by the animal's midpoint displacement, without (Control) and with (Ablated)
1033 exposure to LED. Premotor INs ablation leads to a drastic reduction of velocity.

1034 (B) Ablating D-MNs does not alleviate the *kink* posture caused by premotor INs ablation.
1035 i: Schematics of the motor circuit components and connectivity in animals upon ablation.
1036 Premotor interneurons are ablated by the same transgenes as in Figure 1. ii, Co-ablation
1037 of premotor INs and D-MNs leads to *kinker* postures as in premotor INs-ablated animals.
1038 iii. Distribution of body curvatures indicates a curvature increase upon the co-ablation of
1039 premotor INs and D-MNs. iv: Distribution of instantaneous velocity showed a drastic

1040 reduction of mid-point displacement in premotor INs and D-MNs co-ablated animals. $n =$
1041 10. $P < 0.01$; $P < 0.001$ against with Control by the Kolmogorov-Smirnov test.

1042 **Figure 2. MNs execute directional, rhythmic locomotion without premotor INs.**

1043 **(A)** Schematics of the motor circuit components and connectivity of animals of respective
1044 genotypes, upon co-ablation of premotor INs and B-MNs (i), or premotor INs and A-
1045 MNs (ii). **(B)** Representative curvature kymograms along the entire length of moving
1046 animals, without (Control) and with (Ablated) exposure to LED. Animals without
1047 premotor INs and B-MNs (i, lower panel) exhibit reverse movement, as posterior to
1048 anterior propagating body bends, regardless of the propagation direction of head bending.
1049 Those without premotor INs and A-MNs (ii, lower panel) often exhibit slow forward
1050 movements, consisted of slowly propagating, anterior to posterior, shallow body bends.
1051 **(C)** Propensity of directional movement in animals of respective genotypes, quantified by
1052 the animal's midpoint displacement. The co-ablation of premotor INs and B-MNs shifts
1053 the animal's preference for reverse movement (i), whereas the co-ablation of premotor
1054 INs and A-MNs shifts their preference for forward movement (ii). Both exhibit a drastic
1055 increase propensity for the pause state. **(D)** Distribution of instantaneous velocity of
1056 animals of respective genotypes, quantified by the midpoint displacement. Forward
1057 velocity (ii) was more drastically decreased than reverse velocity (i) upon premotor IN
1058 ablation. $P < 0.001$ against non-ablated Control groups by the Kolmogorov-Smirnov test.
1059 **(E) Upper panel:** example traces of calcium activity of three A-MNs (VA10, DA7,
1060 VA11), in animals where premotor INs and B-MNs (A, i) have been ablated. VA10 and
1061 VA11 innervate adjacent ventral body wall muscles, DA7 innervates dorsal muscles
1062 opposing to those by VA10 and VA11. Periodic calcium rise and fall were observed in all

1063 their soma, represented by changes in the GCaMP6/RFP ratio (Y-axis) over time (X-
1064 axis). *Lower panel:* the animal's instantaneous velocity (Y-axis) during recoding,
1065 represented by the displacement of VA11 soma. Values above and below 0 indicate
1066 forward (displacement towards the head) and reversal (towards the tail) movements,
1067 respectively. This animal exhibited continuous reverse locomotion; the speed of calcium
1068 oscillation positively correlates with reverse velocity. **(F)** Phasic relationships among
1069 DA7, VA10 and VA11. DA7 activity change is anti-phasic to that of VA10 and V11,
1070 whereas VA10 and VA11's activity changes exhibit a small phase shift, with VA11
1071 preceding VA10. The red line denotes the mean of all recordings. $n = 10$ (C, D), $n = 7$ (F)
1072 animals per group.

1073 **Figure 3. Sparse removal of A-MNs alters, not abolishes reverse movement.**

1074 **(A)** Schematics presentation of approximate locations of all A-MNs and regions of
1075 targeted ablation. An ablation is classified as "Anterior", "Mid-body", or "Posterior"
1076 when at least one neuron from each region was ablated, and no neurons from other
1077 regions were ablated. **(B)** Missing A-MNs for each animal that was classified as Anterior
1078 ($n = 13$), Mid-body ($n = 9$), Posterior ($n = 10$), or Mock ($n = 17$) ablated. Black and white
1079 arrows denote animals whose curvature maps are shown in (C) and **Figure 3-figure**
1080 **supplement 1**, respectively. **(C)** Representative curvature maps for each ablation type
1081 (upper panels) and mock controls for three strains from which pooled ablation data were
1082 quantified (lower panels). **(D)** The rate of reversal bending wave propagation in the
1083 anterior, mid- and posterior body for each ablation class. Each dot represents one bout of
1084 reverse movement > 3 seconds. Black bars indicate the mean, and white boxes denote the
1085 95% confidence interval of the mean. Ablation decreases bending speed locally, but not

1086 in other body regions. *** $P < 0.001$ by one-way ANOVA followed by Bonferroni post-
1087 hoc comparisons.

1088 ***Figure 3- figure supplement 1. Information on all other partial A-MN-ablated animals.***

1089 (A) The ablation pattern of each animal that was examined in our study, but could not be
1090 classified into the ablation groups as defined in Figure 3. White arrows denote animals
1091 whose curvature maps were shown in Panel B. (B) Additional example curvature maps
1092 from the classified (Figure 3) and not classified (this figure) ablated animals with
1093 different phenotypes: those with independent head and tail oscillation (i), head
1094 oscillations with little tail movements (ii), and complete tail-to-head bending waves
1095 despite a few missing motor neurons (iii).

1096 ***Figure 4. A-MNs exhibit rhythmic activities upon premotor IN ablation.***

1097 (A) A representative post-synaptic PSC recording at the NMJ preparation of the same
1098 genotype, without (Control, -LED, left panel) or with (Ablated, +LED, right panel) the
1099 ablation of premotor INs and B-MNs. Rhythmic PSC burst events (arrow heads) were
1100 reliably observed upon the removal of premotor INs and B-MNs. (B) Quantification of
1101 the rPSC burst frequency, without (Ctrl) or with (Ablated) the ablation of premotor INs
1102 and B-MNs. (C) Quantification of the burst discharge, without (Ctrl) or with (Ablated)
1103 the ablation of premotor INs and B-MNs. Both the rPSC burst frequency and discharge
1104 are significantly increased in ablated animals. $n = 10$ animals each group. (D) Left panels:
1105 schematics of the morphology and trajectory of the DA9 MN soma and processes,
1106 visualized by the A-MN GCaMP6s::RFP calcium imaging reporter. Right panels:
1107 fluorescent signals during oscillatory Ca^{2+} changes in DA9 soma. (E) Examples of the
1108 DA9 soma Ca^{2+} transient traces, and raster plots of all recording from animals of the

1109 same genotype, without (Control, -LED) or with (Ablated, +LED) the ablation of
1110 premotor INs and B-MNs. $n = 10$ animals each group. **(F)** Quantification of the Ca^{2+}
1111 oscillation frequency, without (Ctrl) and with (Ablated) the ablation of premotor INs and
1112 B-MNs. **(G)** Quantification of the mean total Ca^{2+} activities, without (Ctrl) and with
1113 (Ablated) the ablation of premotor INs and B-MNs. Both the oscillation frequency and
1114 total activity of DA9 are significantly increased in ablated animals. $** P < 0.01$, $*** P <$
1115 0.001 against Control by the Mann-Whitney U test. Error bars, SEM.

1116 **Figure 4- figure supplement 1. Rhythmic rPSC bursts upon co-ablation of premotor**
1117 **INs and B-MNs at the neuromuscular preparations.**

1118 **(A)** Representative, spontaneous mini-postsynaptic currents (mPSCs) recorded at -60 mV
1119 without (Control, -LED) and with (Ablated, +LED) the ablation of premotor INs and B-
1120 MNs. **(B)** Quantification of the mPSC frequency and amplitude, without (Ctrl) and with
1121 (Ablated) the ablation of premotor INs and B-MNs. There was a moderate decrease of
1122 mPSC frequency, but no change in the amplitude upon ablation of premotor INs and B-
1123 MNs. $n = 10$ animals each group, ns, not significant, $* P < 0.05$ against Control by the
1124 Mann-Whitney U test. Error bars, SEM. **(C)** Representative spontaneous postsynaptic
1125 muscle action potentials (APs), without (Control, -LED) and with (Ablated, +LED) the
1126 ablation of premotor INs and B-MNs. Muscles were hold at 0 pA. Resting membrane
1127 potential was unchanged (not shown), but the AP pattern was altered. Without ablation,
1128 the preparation exhibits single APs; after the ablation of premotor INs and B-MNs,
1129 periodic AP bursts were observed. **(D, E)** The AP spike interval was decreased, whereas
1130 the relative power of high frequency AP firing was increased upon the ablation of
1131 premotor INs and B-MNs.

1132 **Figure 5. Activation of premotor IN AVA potentiates intrinsic and A-MN-dependent**
1133 **rPSC bursts.**

1134 (A) Evoked and spontaneous rPSC bursts share frequency spectrum characteristics. *Black*
1135 *traces*: frequency spectrum analyses (upper panel) for three rPSC traces upon the
1136 optogenetic activation of AVA premotor INs (lower panel); *Red traces*: frequency
1137 spectrum analyses (upper panel) for three spontaneous rPSC bursts exhibited by animals
1138 upon the ablation of premotor INs and B-MNs (lower panel). (B) Representative traces of
1139 AVA-evoked rPSC bursts in respective genotypic backgrounds, in the presence (Control,
1140 -LED) or absence (Ablated, +LED) of specific neuronal groups. +: *hpIs270* (AVA-
1141 specific ChR2 activation in wildtype background); - AVA: *hpIs270*; *hpIs321*, which
1142 ablates a subset of premotor INs including AVA upon exposure to LED); - AVB: *hp270*;
1143 *hpIs331*, which ablates several INs including AVB upon exposure to LED); - A: *hpIs270*;
1144 *hpIs371*, which ablates A-MN upon exposure to LED); - B (*hpIs270*; *hpIs604*, which
1145 ablates B-MNs upon exposure to LED). (C) Quantified rPSC burst frequency evoked by
1146 AVA in respective genetic backgrounds. (D) Quantification of total discharge of rPSC
1147 bursts evoked by AVA in respective genetic backgrounds. Both are diminished upon the
1148 ablation of AVA, but not affected by ablation of the AVB premotor INs. They are both
1149 significantly decreased in A-, but not B-MN ablated animals ($n \geq 5$ in each data set). ns,
1150 not significant $P > 0.05$, *** $P < 0.001$ against non-ablated respectively Control group by
1151 the students' t - test. Error bars, SEM.

1152 **Figure 5- figure supplement 1. A-MNs exhibit rhythmic PSCs upon direct optogenetic**
1153 **stimulation.**

1154 (A, B) Representative evoked postsynaptic currents by LED-mediated optogenetic
1155 (Chrimson) stimulation of the A-MNs, A MN (A) and the ventral muscle innervating B-
1156 MNs, VB MN (B). Muscles were held at -60 mV. Chrimson was expressed in A-MNs by
1157 *Punc-4* and VB-MNs by *Pceh-12*, respectively. The top panel illustrates the duration of
1158 light stimulation. The PSC frequencies were recorded upon sequential increase of the
1159 LED intensity, which exhibit corresponding increase upon stimulation. rPSCs, denoted as
1160 red stars were readily evoked upon stimulation of the A-MNs at intermediate stimulation
1161 light intensities, but were not observed with the full-range of VB-MN stimulations.

1162 **Figure 6. Endogenous UNC-2 activity regulates A-MN's rhythmic activity.**

1163 (A) Representative PSC recordings of the NMJ preparations in animals of respective
1164 genotypes, after the ablation of premotor INs and B-MNs. The amplitude and frequency
1165 of periodic rPSC bursts (arrowheads) were reduced in *unc-2(e55; lf)* and increased in
1166 *unc-2(hp647; gf)* mutant animals. (B) Quantification of the rPSC burst frequency in
1167 respective genotypes. (C) Quantification of the total discharge of rPSC burst in respective
1168 genotypes. Both were reduced in *unc-2(e55; lf)* and increased in *unc-2(hp647, gf)* mutants
1169 ($n \geq 7$ in each dataset). (D) An example DA9 soma Ca^{2+} traces (left panels), and raster
1170 plots of Ca^{2+} recordings (right panels) in wildtype animals ($n = 10$), *unc-2(e55, lf)* ($n =$
1171 12) and *unc-2(hp647, gf)* ($n = 10$) mutants upon the ablation of premotor INs and B-MNs.
1172 (E) Quantification of DA9's Ca^{2+} oscillation frequency in respective genotypes upon
1173 premotor INs and B-MNs ablation. (F) Quantification of the overall DA9 Ca^{2+} activity in
1174 respective genotypes upon premotor INs and B-MNs ablation. Compared to wildtype
1175 animals, the frequency and activity of Ca^{2+} oscillation are significantly reduced in *unc-*
1176 *2(e55, lf)* and increased in *unc-2(hp647, gf)* animals. * $P < 0.05$, ** $P < 0.01$, *** $P <$

1177 0.001 by the Mann-Whitney U test. **(G)** Locomotor behaviors of animals of respective
1178 genotypes. (i) Representative curvature kymographs of wildtype and *unc-2* mutant
1179 animals, without (Control, -LED) and with (Ablated, +LED) the ablation of premotor INs
1180 and MNs. (ii) Distribution of instantaneous velocity of respective genotypes, presented
1181 by the animal's mid-point displacement where the positive and negative values represent
1182 the forward and reverse movement, respectively. While all animals exhibit reverse
1183 movement upon premotor INs and B-MNs ablation, the bending wave propagation,
1184 representing the reverse velocity, is significantly reduced and increased in *unc-2(lf)* and
1185 *unc-2(gf)* mutants, respectively. ** $P < 0.01$, *** $P < 0.001$ against non-ablated animals
1186 of the same genotype by the Kolmogorov-Smirnov test. **(H)** Propensity of directional
1187 movement in animals of respective genotypes as in panel G, quantified by the animal's
1188 midpoint displacement. Upon the removal of premotor INs and B-MNs, all animals shift
1189 to a bias for reverse movement; Note that *unc-2(lf)* mutants exhibit a significant increase
1190 of pauses, whereas *unc-2(gf)* mutants eliminated the forward movement. Error bars,
1191 SEM.

1192 **Figure 6- figure supplement 1. The P/Q/N-type VGCC UNC-2 is required for evoked**
1193 ***rPSC bursts*.**

1194 **(A)** Representative traces for evoked rPSCs in animals of respectively genotypes. All are
1195 loss-of-function (*lf*) alleles. Wildtype refers to the optogenetic stimulation strain, *hpIs166*
1196 (*Pglr-1::ChR2*), which expresses ChR2 in multiple premotor INs. The top panel
1197 illustrates the duration of continuous light stimulation. Partial *lf* alleles for the pore-
1198 forming alpha subunit UNC-2 (*e55* and *ra612*), beta subunit UNC-36 (*e251*), and the ER
1199 delivery subunit CALF-1 (*ky867*) of the P/Q/N-type VGCC exhibited the same

1200 phenotype: optogenetic stimulation of premotor INs led to increased mPSC frequency,
1201 without rPSC bursts. The same stimulation protocol induced robust rPSC bursts in a
1202 partial *lf* mutant for the alpha subunit of L-type VGCC EGL-19 (*n582*). (B, C)
1203 Quantification of the burst frequency (B) and total charge (C) of the evoked rPSC bursts.
1204 Both were reduced in the P/Q/N-VGCC mutants (*unc-2*, *unc-36* and *calf-1*), but
1205 unaffected in L-VGCC (*egl-19*) and the NCA sodium leak channel (*unc-79* and *unc-80*)
1206 mutants. $n \geq 5$. *** $P < 0.001$ against wildtype animals by the Mann-Whitney U test.
1207 Error bars, SEM.

1208 **Figure 6- figure supplement 2. Cell-autonomous UNC-2 conductance is sufficient for**
1209 **DA9 calcium oscillation.**

1210 (A) Representative DA9 Ca²⁺ transient traces (left panels), and raster plots of all Ca²⁺
1211 recordings (right panels), when UNC-2(WT) or UNC-2(GF) were specifically restored
1212 into the A-MNs in *unc-2(e55; lf)* mutant animals. All data were recorded after the
1213 ablation of premotor INs and B-MNs. $n = 10$ per group. (B) Quantification of DA9 Ca²⁺
1214 oscillation frequency in respective genotypes. (C) Quantification of overall DA9 Ca²⁺
1215 activity in respective genotypes. Both the frequency and level of DA9 Ca²⁺ oscillation are
1216 rescued by specific restoration of either UNC-2(WT) or UNC-2(GF) to A-MNs. ** $P <$
1217 0.01 , *** $P < 0.001$ against wildtype animals by the Mann-Whitney U test. Error bars,
1218 SEM.

1219 **Figure 6- figure supplement 3. Endogenous GFP::UNC-2 localizes to both the axon**
1220 **and soma of A-MNs.**

1221 The expression pattern of UNC-2, determined by an endogenous GFP::UNC-2(*hp858*)
1222 allele, stained with antibodies against GFP. Dense, punctate signals decorate the nerve

1223 processes of the central and peripheral nervous systems, as well as the neuron soma in
1224 central nervous system (top panel) and ventral cord motor neurons (middle panel),
1225 including the DA8 and DA9 soma (bottom panel). VNC, ventral nerve cord. Scale bar: 5
1226 μm .

1227 **Figure 6- figure supplement 4. Increased UNC-2 activity leads to increased reversal**
1228 **speed and duration.**

1229 (A), Distribution of the instantaneous velocity, represented by the midpoint displacement,
1230 in wildtype, *unc-2(lf)*, and *unc-2(gf)* mutant animals, upon the removal of premotor INs
1231 and B-MNs. Decreased UNC-2 activity leads to drastic reduction of velocity, whilst
1232 increased UNC-2 activity leads to increased velocity. *** $P < 0.001$ against wildtype
1233 animals by the Kolmogorov-Smirnov test. (B) Quantification of the duration of forward
1234 and reverse locomotion in wildtype, *unc-2(lf)*, and *unc-2(gf)* animals, upon the ablation of
1235 premotor INs and B-MNs. Decreased and increased UNC-2 activities lead to drastic
1236 reduction and increase of reverse duration, respectively. $n = 10$ animals per group. * $P <$
1237 0.05 ; *** $P < 0.001$ against Control by the Mann-Whitney U test. Error bars, SEM.

1238 **Figure 7. Descending premotor INs exert dual modulation of A-MN's oscillatory**
1239 **activity to control the reversal motor state.**

1240 (A) Representative DA9 soma Ca^{2+} traces (upper panels) and raster plots of all Ca^{2+} traces
1241 (lower panels) in *unc-13(lf)* mutants, without (-LED, $n = 10$) and with ablation of
1242 premotor INs and B-MNs (+LED, $n = 11$). (B, C) Quantification of the Ca^{2+} oscillation
1243 frequency (B) and overall activities (C) in *unc-13* mutants. (D) Representative DA9 soma
1244 Ca^{2+} traces (upper panels) and raster plots of all Ca^{2+} traces (lower panels) in wildtype
1245 animals (left panels) and *unc-7(lf)* mutants (right panels), upon the ablation of premotor

1246 INs and B-MNs. $n = 10$ animals each group. **(E, F)** Quantification of the Ca^{2+} oscillation
1247 frequency (E) and overall activities (F) in respective genotypes. DA9's activity exhibits
1248 significant increase in *unc-7(lf)* mutants. **(G)** Representative rPSC recordings in wildtype,
1249 *unc-7(lf)* and *unc-13(lf)* animals upon optogenetic stimulation of premotor INs AVA. **(H,**
1250 **I)** Quantification of the frequency (H) and total discharge (I) of rPSC bursts in respective
1251 genotypes. ns, not significant $P > 0.05$, * $P < 0.05$, ** $P < 0.01$, *** $P < 0.001$ against
1252 wildtype by the Mann-Whitney U test. $n = 16, 7$ and 3 animals for wildtype, *unc-7* and
1253 *unc-13*, respectively. Error bars, SEM. **(J)** Schematics of a model for the distributed
1254 CPG-driven reverse-promoting motor circuit, and its regulation by descending premotor
1255 interneurons. The A-MNs represent distributed and phase-coordinated intrinsic oscillators
1256 to drive reverse movement. State-dependent dual regulation by the descending premotor
1257 INs determines the initiation and substation of the reversal motor state. (Left panel): at
1258 rest, their CPG activity is inhibited by premotor INs through UNC-7-dependent gap
1259 junctions. (Center panel): the ablation of premotor INs, removing their coupling with
1260 AVA release the A-MN's CPG activity, promoting initiation of reverse movement
1261 through UNC-2-dependent calcium oscillation. (Right panel): upon stimulation, AVA
1262 potentiate A-MNs' CPG activity, mainly through chemical synapses, with a minor
1263 contribution from the gap junctions, for sustained reverse movement.

1264 **Video Captions:**

1265 ***Video 1: Locomotor behaviors (Part 1 and Part 2) and calcium imaging of the body***
1266 ***wall muscles (Part 3) of C. elegans without premotor INs.***

1267 (Part 1, 2) Upon ablation of all premotor INs, animals exhibit kinked posture and
1268 uncoordinated body bends; head oscillations persist but fail to propagate down the body.

1269 (Part 3) Calcium imaging of body wall muscles was carried out in transgenic animals
1270 after the ablation of all premotor INs. Calcium activity persists in muscles, and its activity
1271 corroborates with body bending. Left panel: RFP in muscles (with extra signals in the gut
1272 from the miniSOG transgene). Right panel: GCaMP3 in muscles.

1273 ***Video 2: Co-ablation of premotor INs with the A-, B- and D-MNs leads to different***
1274 ***locomotor behaviors.***

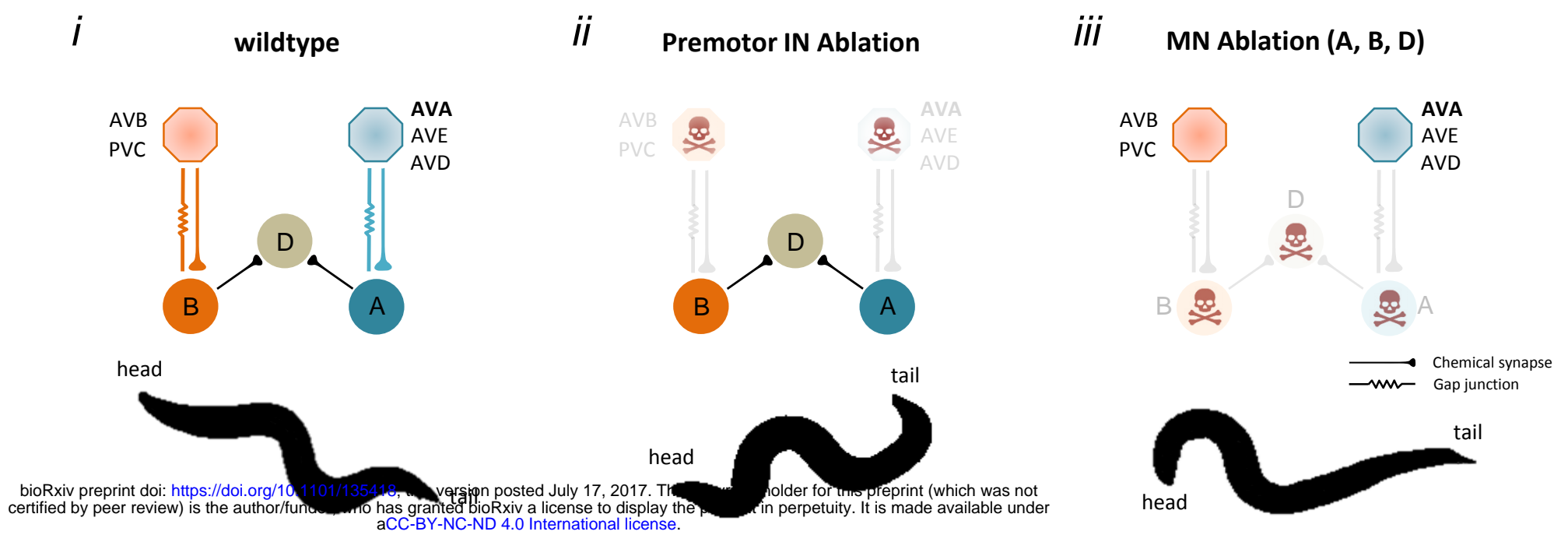
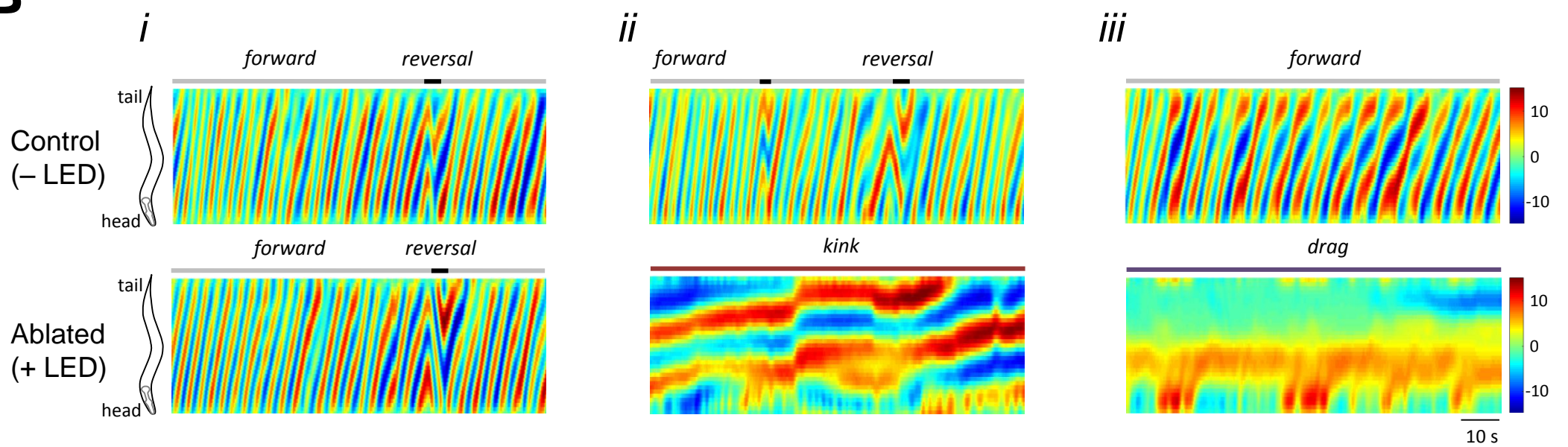
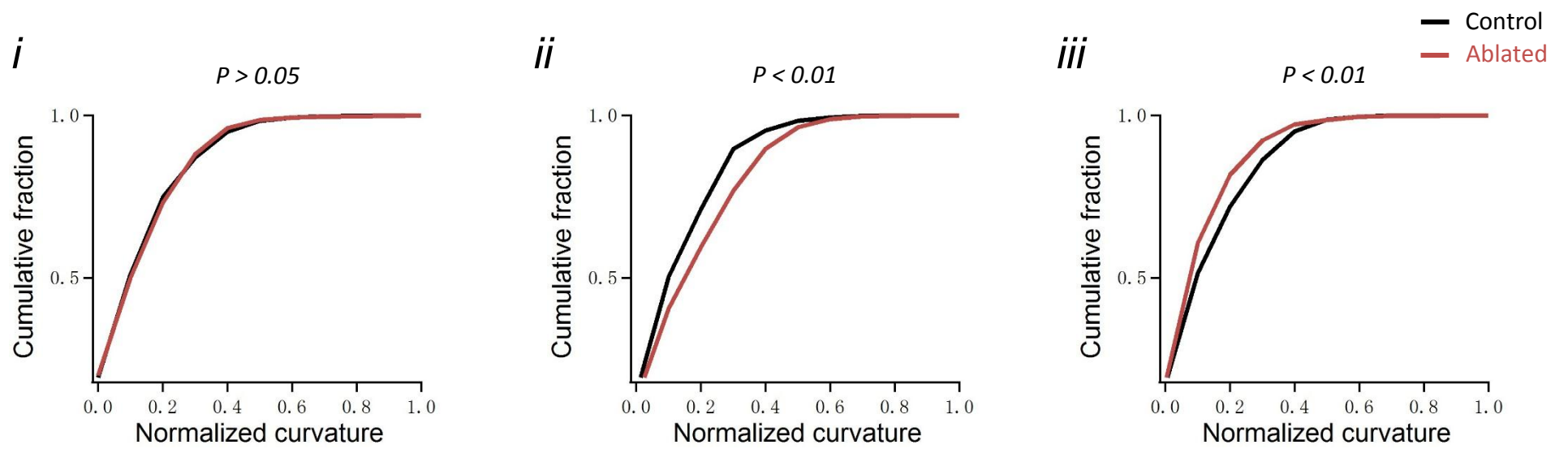
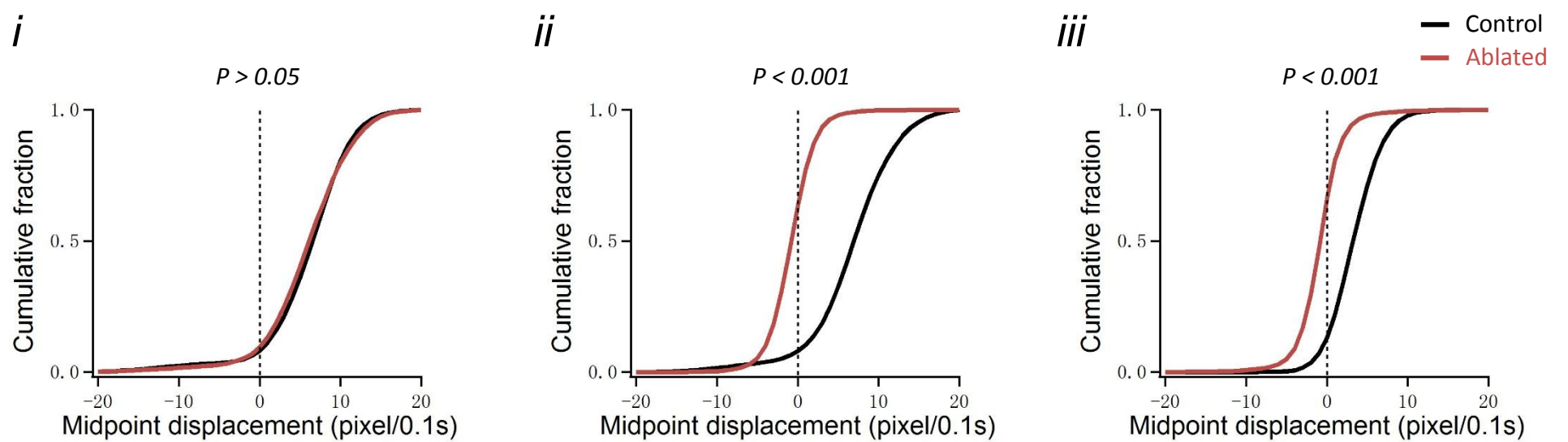
1275 (Part 1, 2) Upon co-ablation of the premotor INs and B-MNs, animals exhibit sluggish
1276 forward movement where the body passively follows head oscillation. (Part 3, 4) Upon
1277 the co-ablation of premotor INs and A-MNs, animals exhibit exclusively reverse
1278 locomotion, with active body bending, robust rhythmicity, and velocity. Periodically,
1279 reverses were interrupted, when, with exaggerated head oscillation, the anterior and
1280 posterior body segments are pulled to opposing directions. (Part 5, 6) Upon the co-
1281 ablation of premotor INs and D-MNs, animals exhibit *kinker* postures.

1282 ***Video 3: Local ablation of the A-MNs does not prevent body bends in other segments.***

1283 During reverses, localized ablations of a fraction of the A-MNs lead to defective local
1284 bends, but do not abolish bending in other segments. Example movies for the behavioral
1285 consequence of ablating anterior, mid-body, and posterior A-MNs are shown.

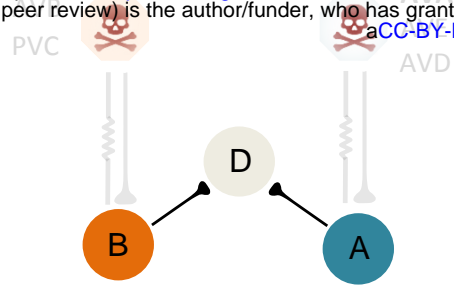
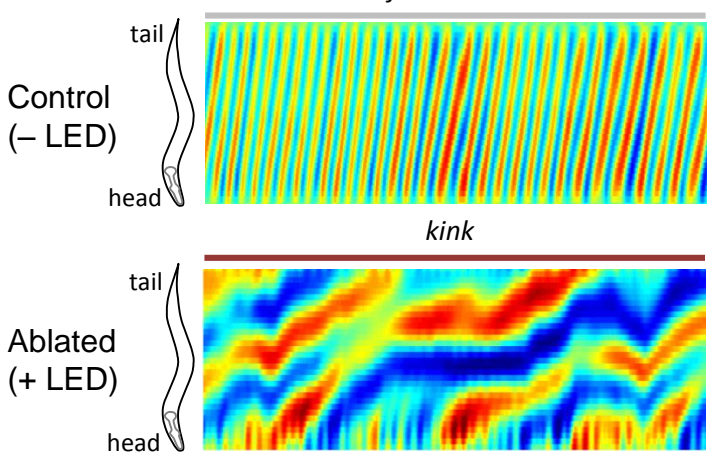
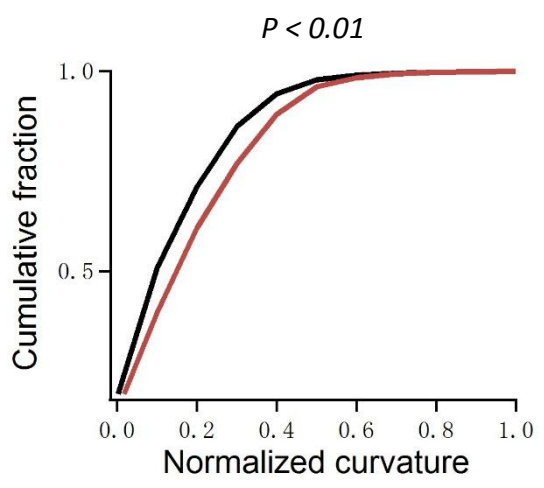
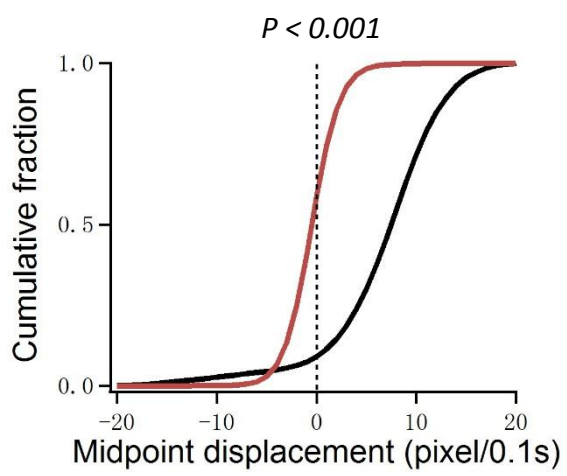
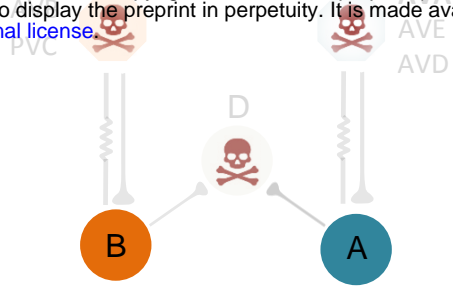
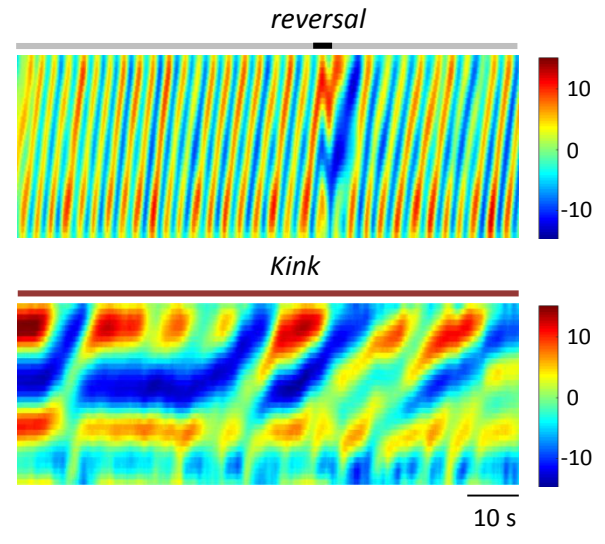
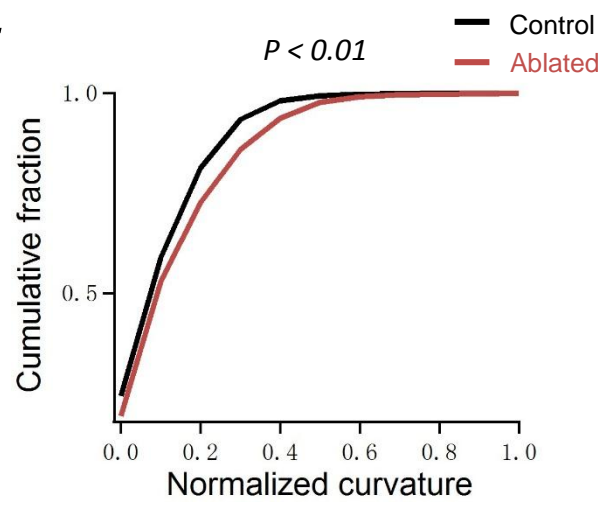
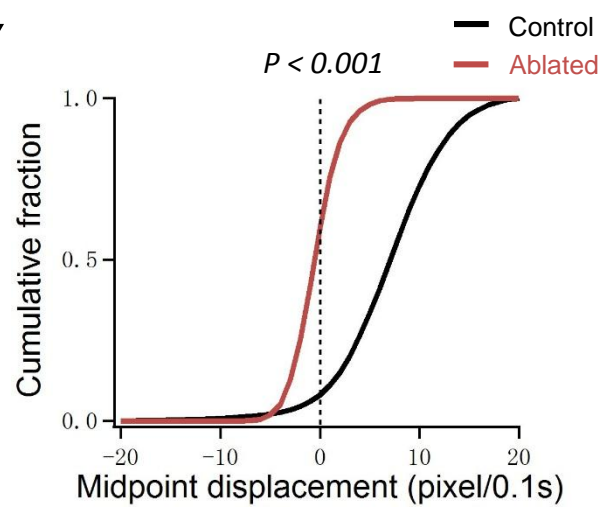
1286 ***Video 4: DA9 soma exhibits robust Ca²⁺ oscillation upon ablation of all premotor INs***
1287 ***and B-MNs.***

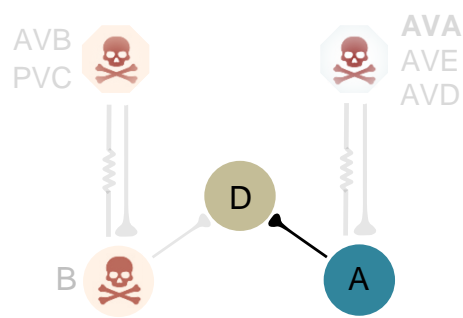
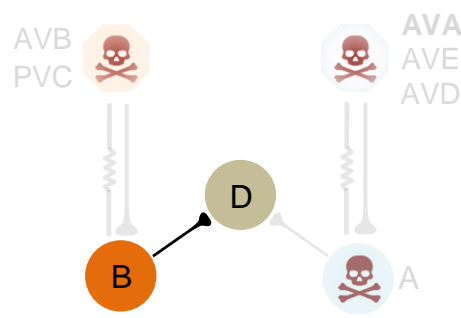
1288 An example Ca²⁺ oscillation at the DA9 motor neuron in an adult animal upon the
1289 ablation of premotor INs and B-MNs.

A**B****C****D**

A**i** Premotor IN Ablation

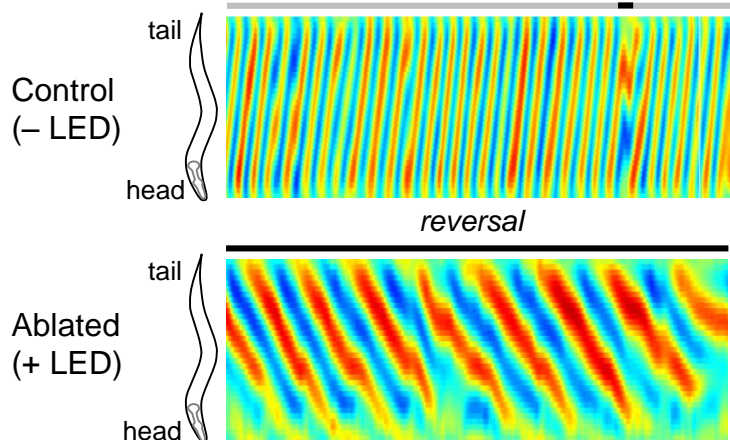
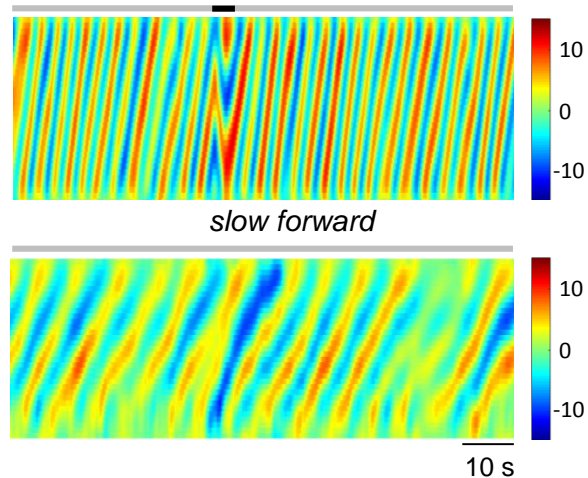
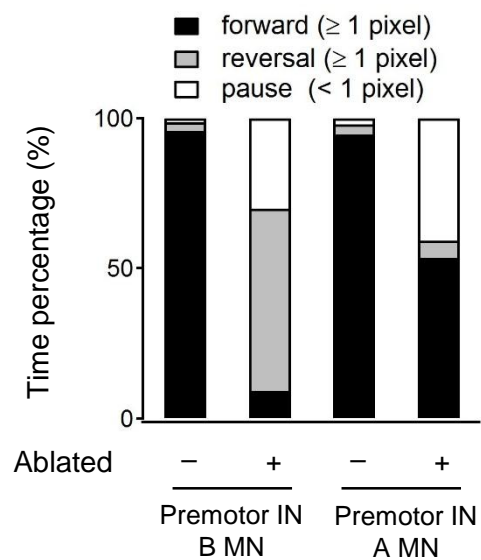
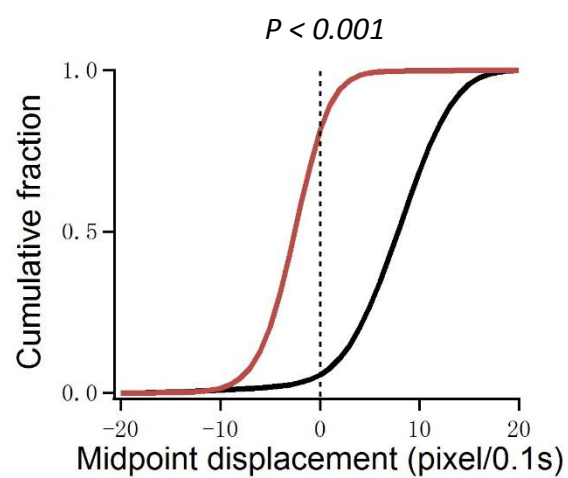
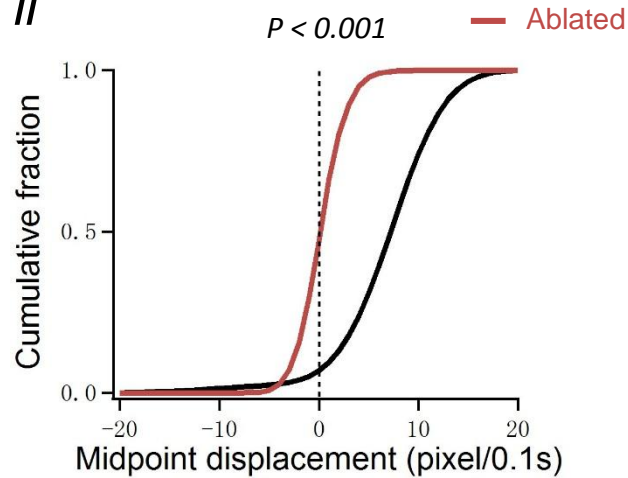
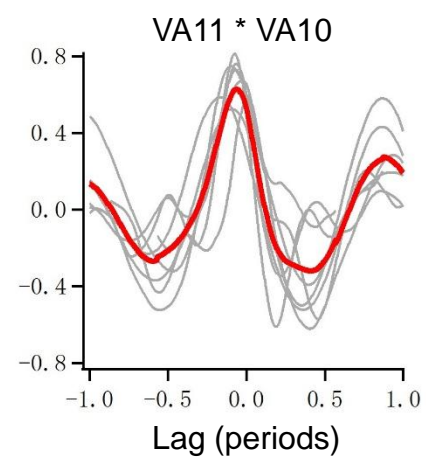
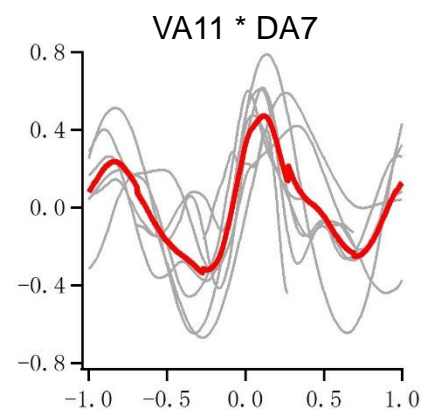
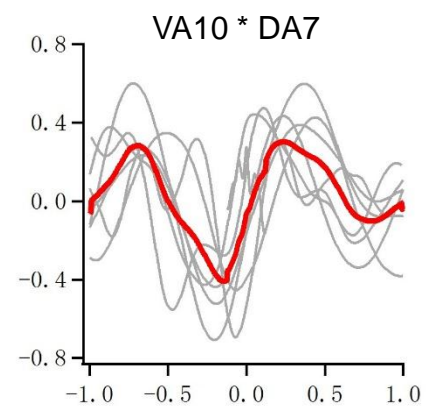
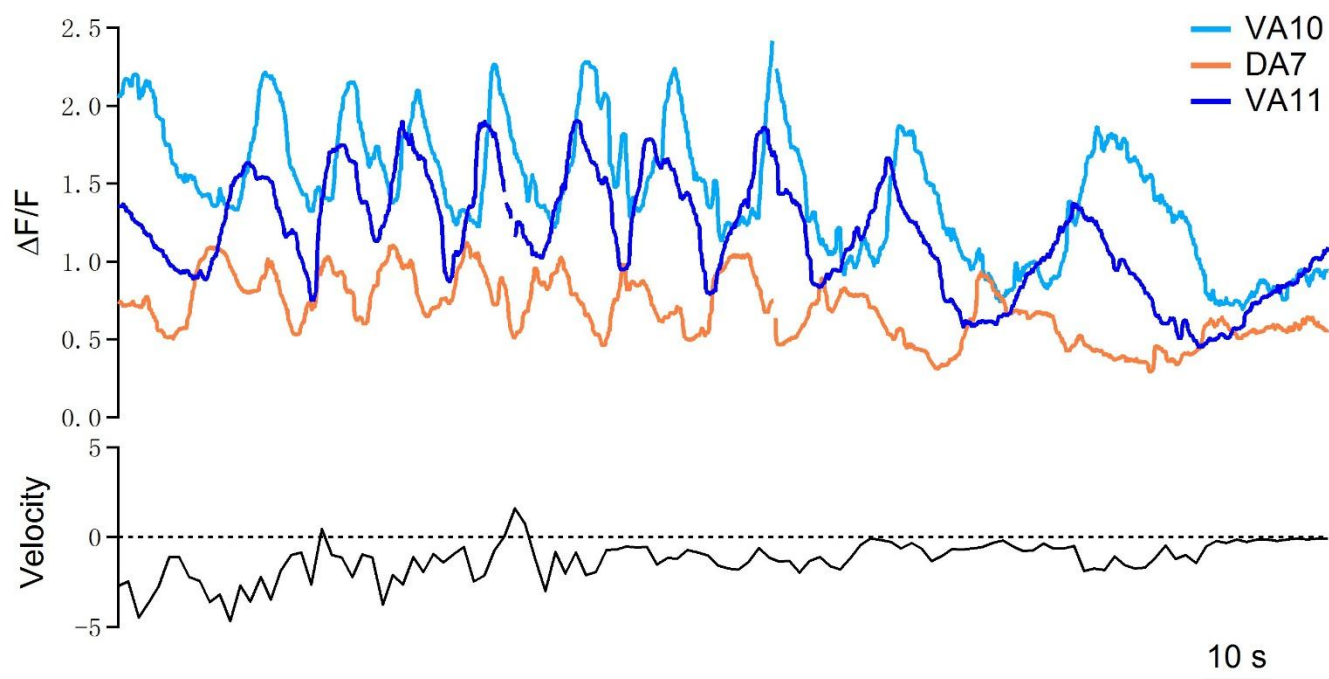
bioRxiv preprint doi: <https://doi.org/10.1101/135418>; this version posted July 17, 2017. The copyright holder for this preprint (which was not certified by peer review) is the author/funder, who has granted bioRxiv a license to display the preprint in perpetuity. It is made available under aCC-BY-NC-ND 4.0 International license.

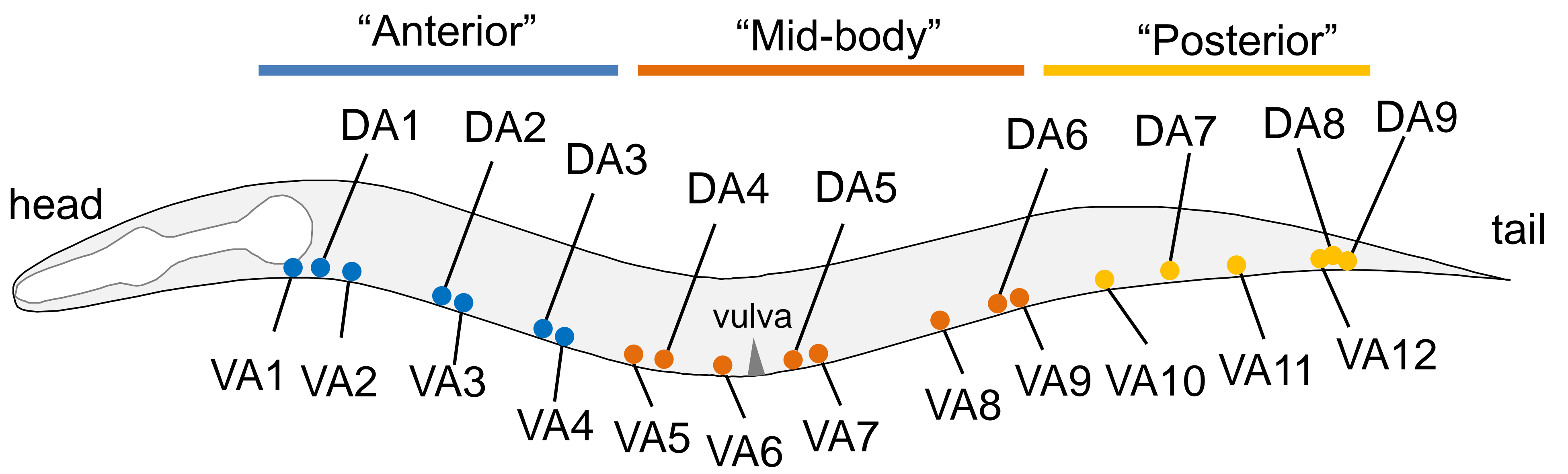
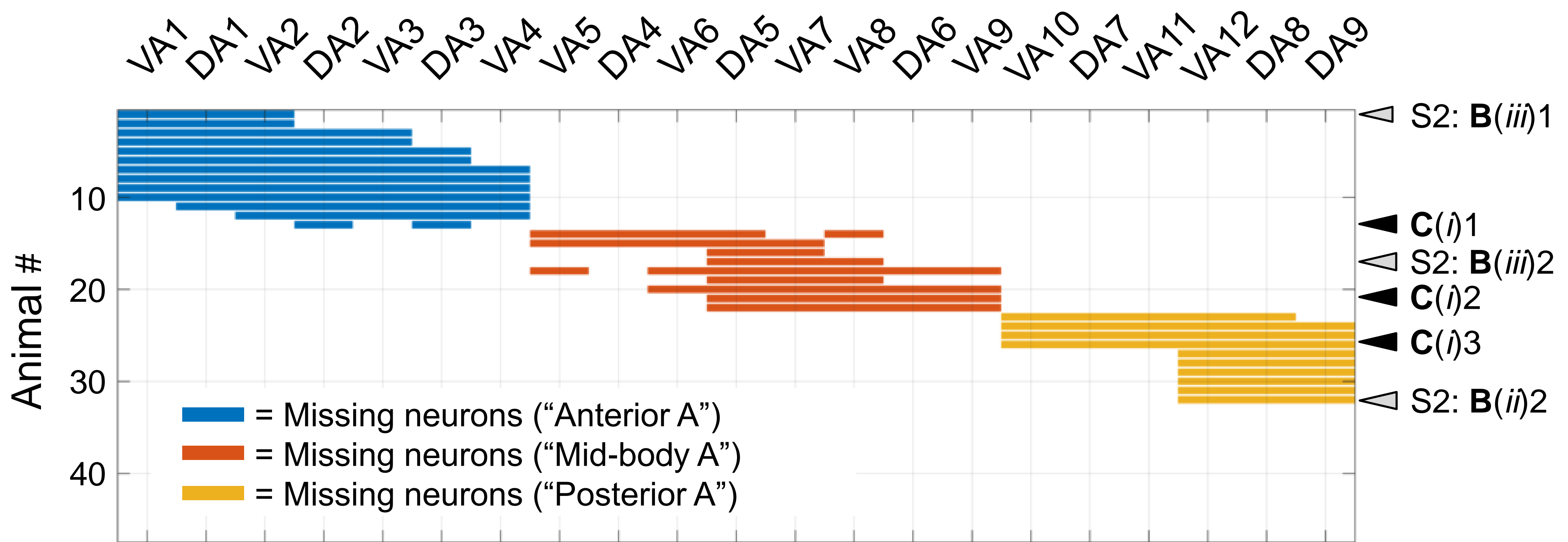
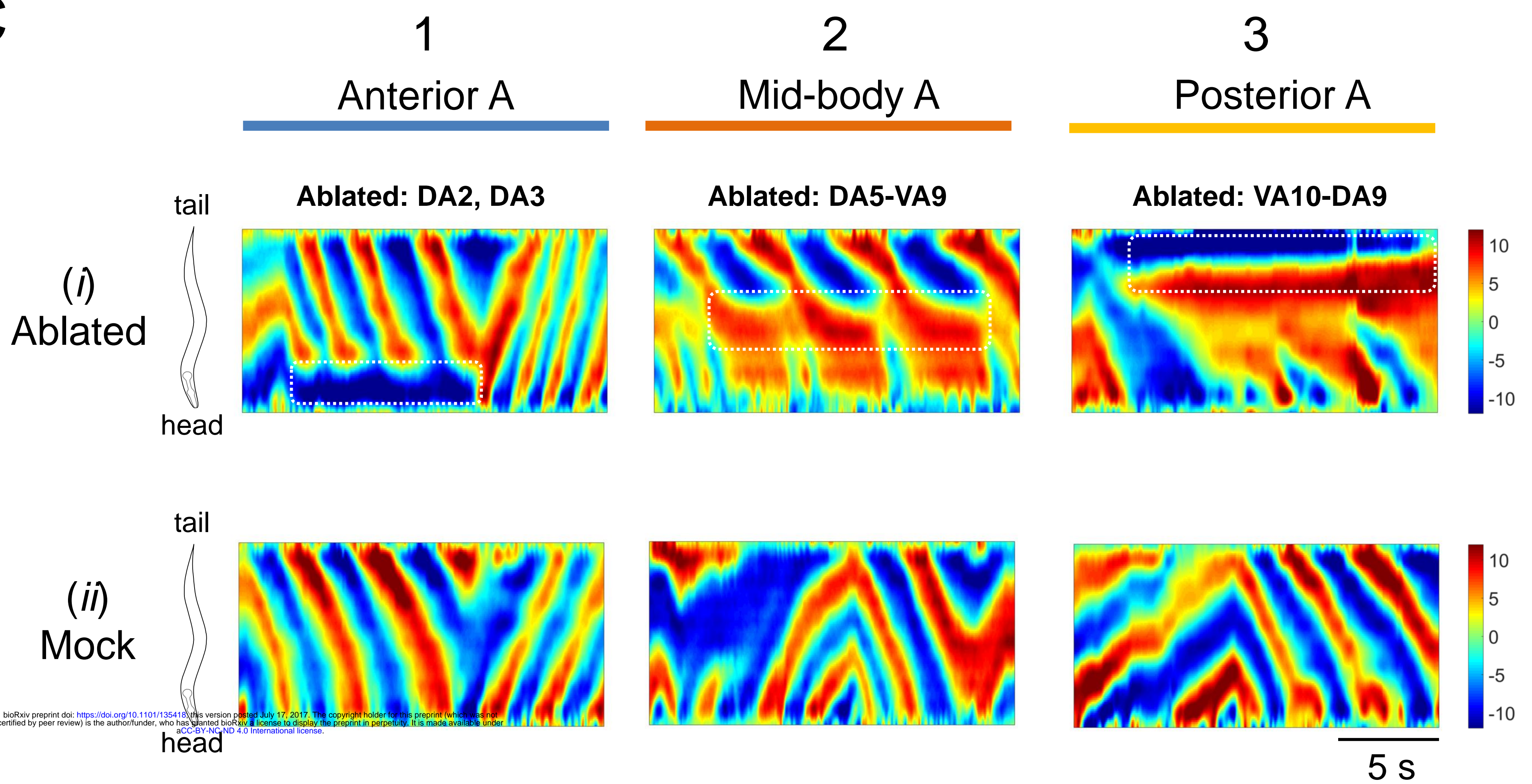
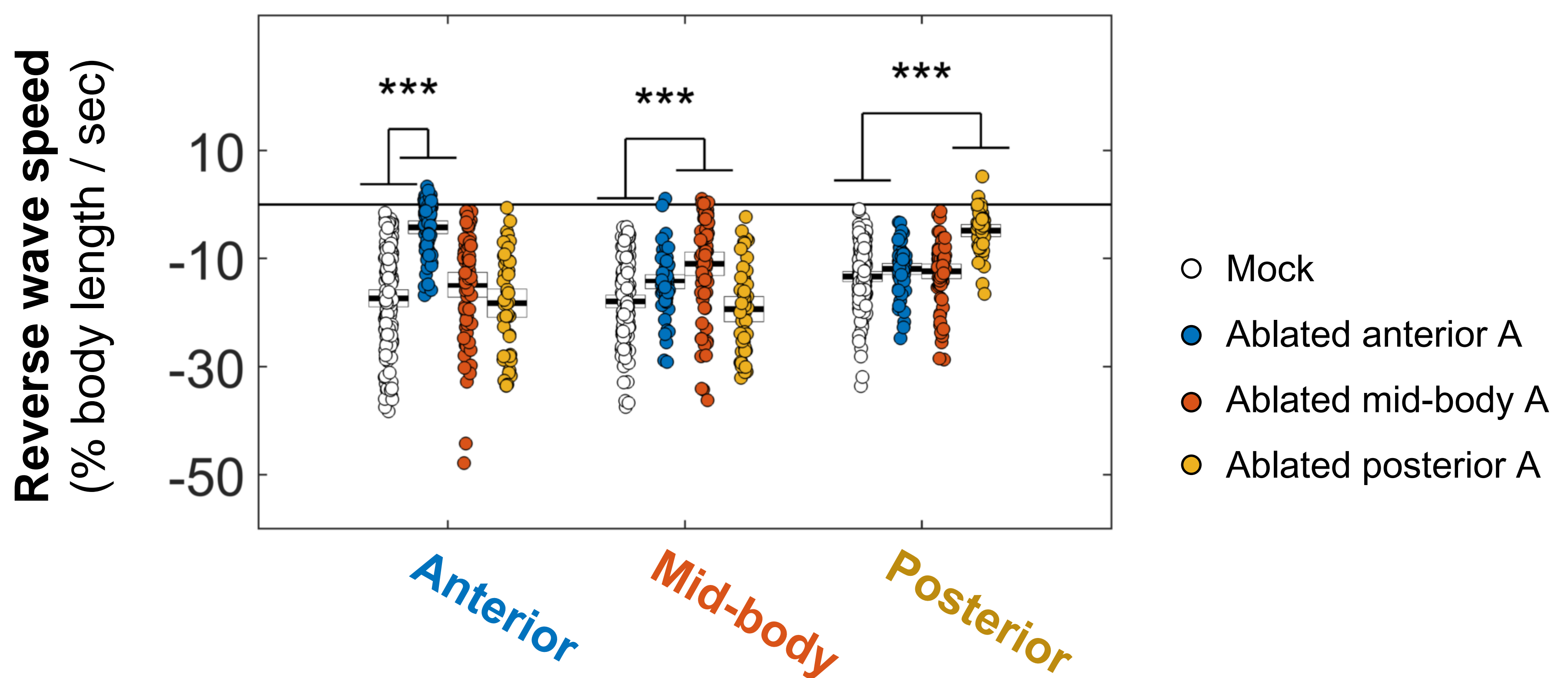
**ii****iii****iv****B****i** Premotor IN / D MN Ablation**ii****iii****iv**

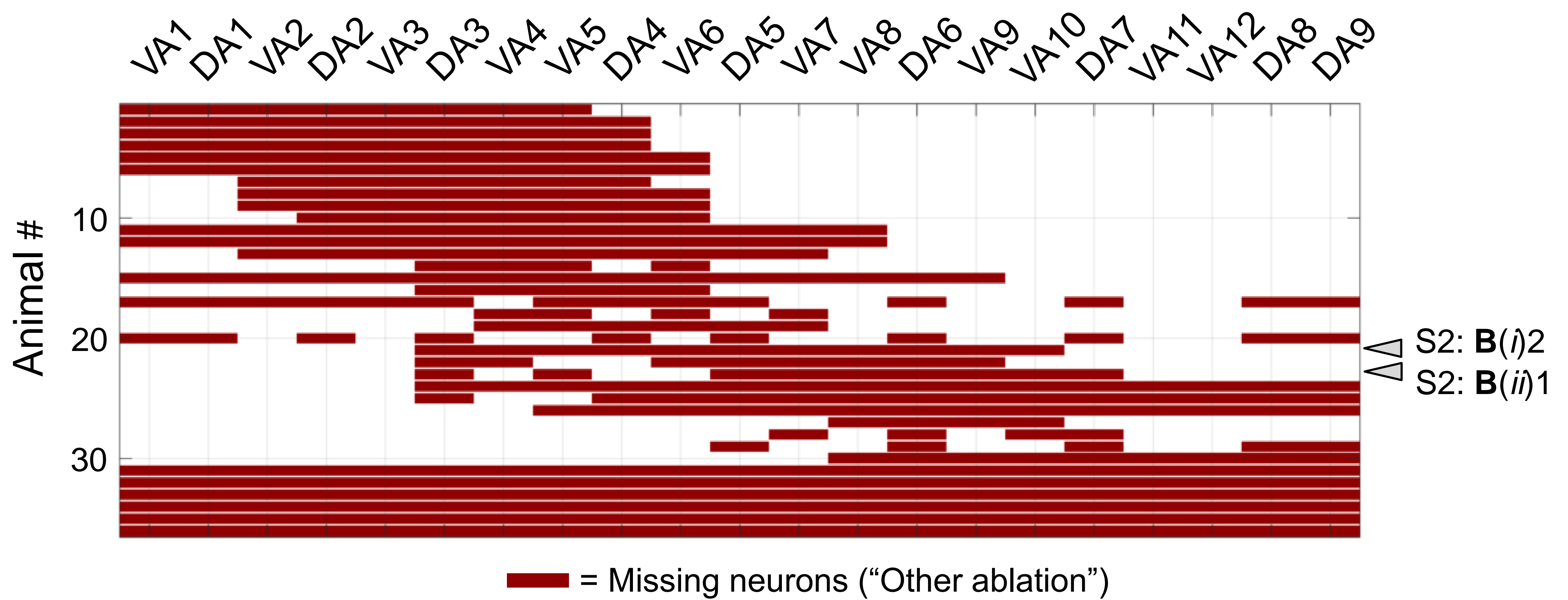
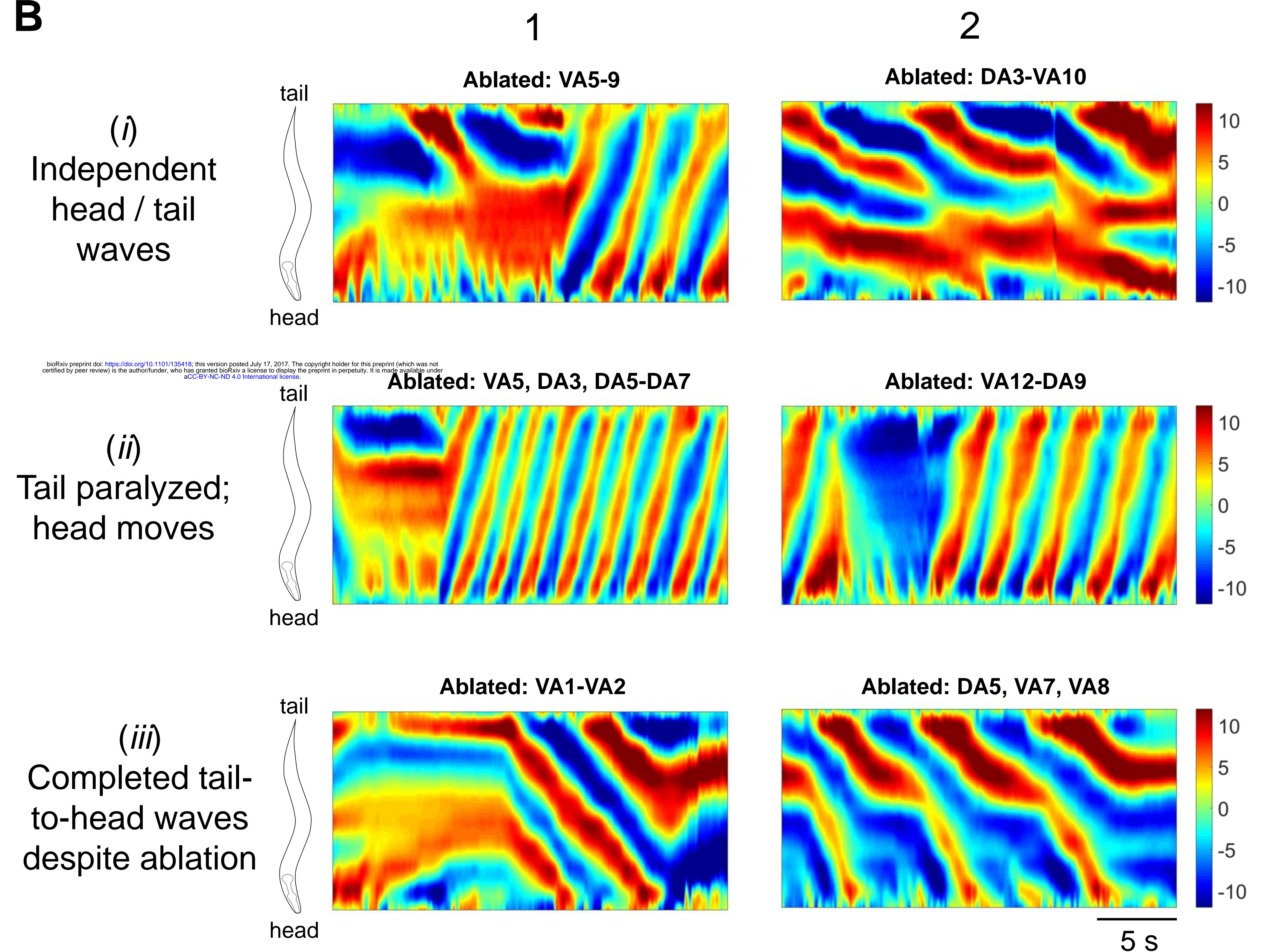
A*i***Premotor IN / B MN Ablation***ii***Premotor IN / A MN Ablation**

—●— Chemical synapse
 —〰— Gap junction

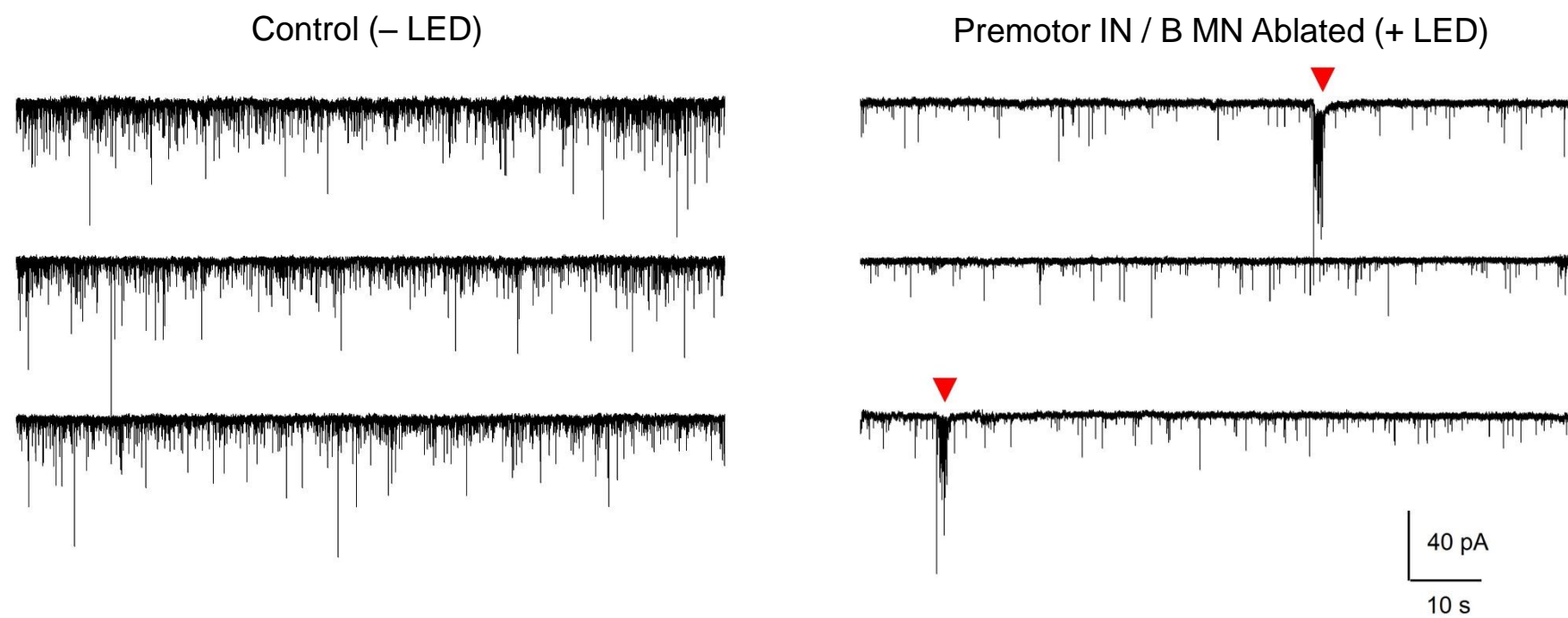
bioRxiv preprint doi: <https://doi.org/10.1101/135418>; this version posted July 17, 2017. The copyright holder for this preprint (which was not certified by peer review) is the author/funder, who has granted bioRxiv a license to display the preprint in perpetuity. It is made available under aCC-BY-NC-ND 4.0 International license.

B*i**forward* *reversal**ii**reversal***C****D***i**ii***F****E**

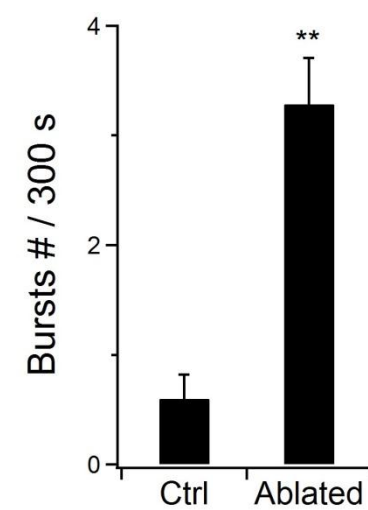
A**B****C****D**

A**B**

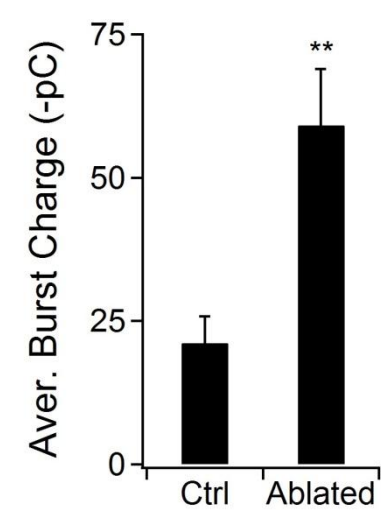
A



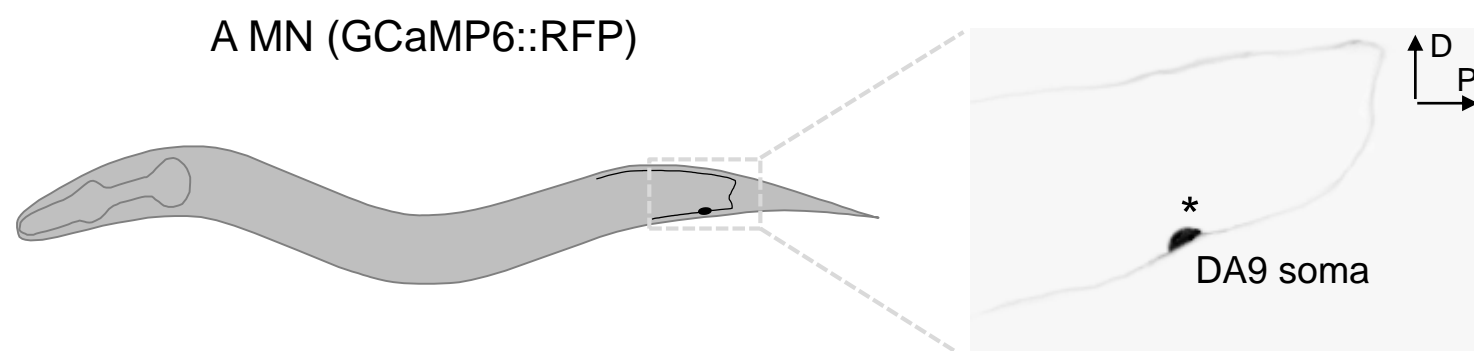
B



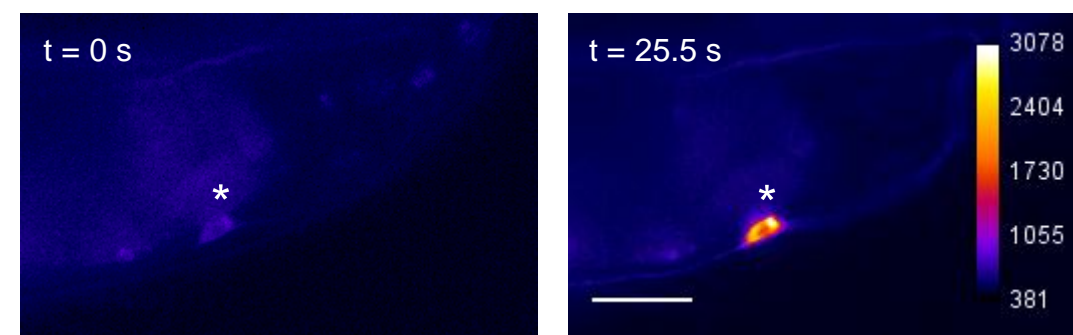
C



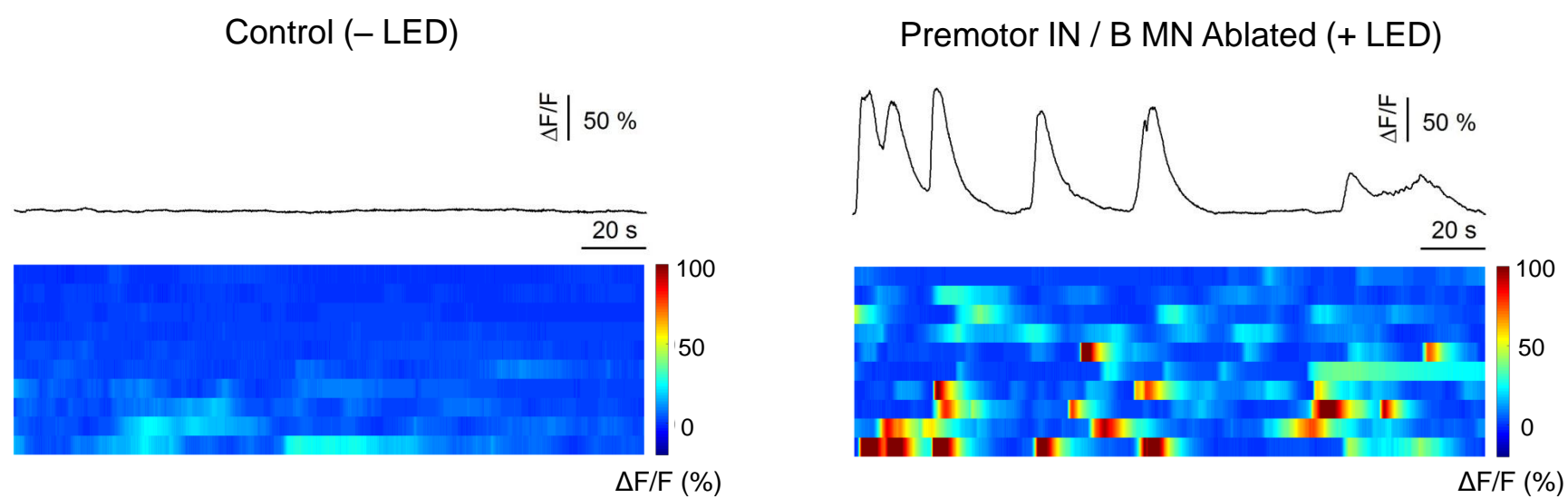
D



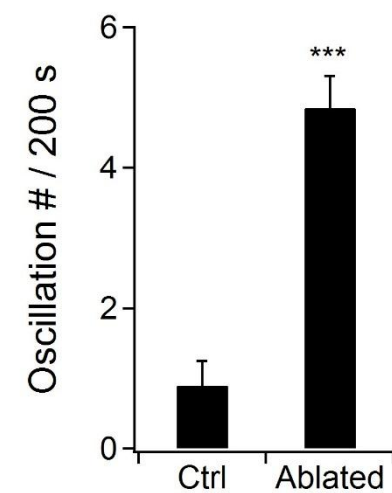
E



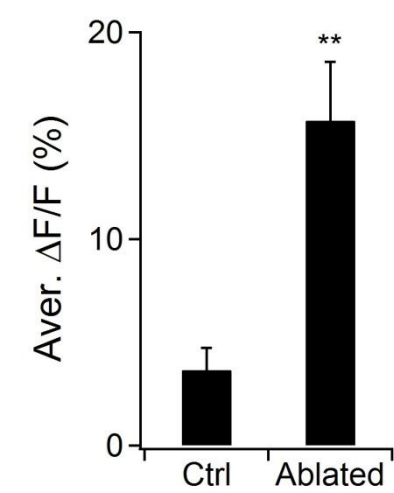
F



G

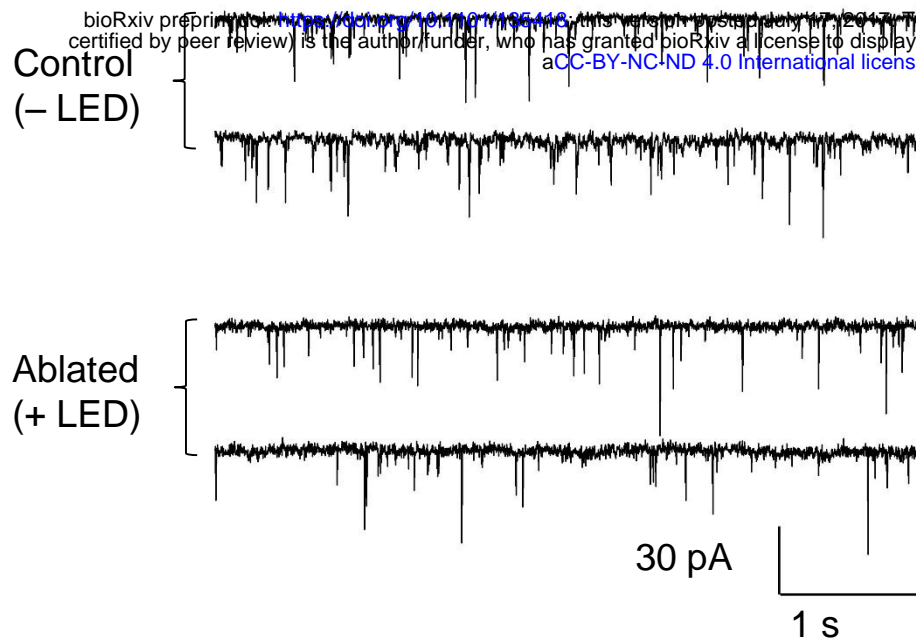
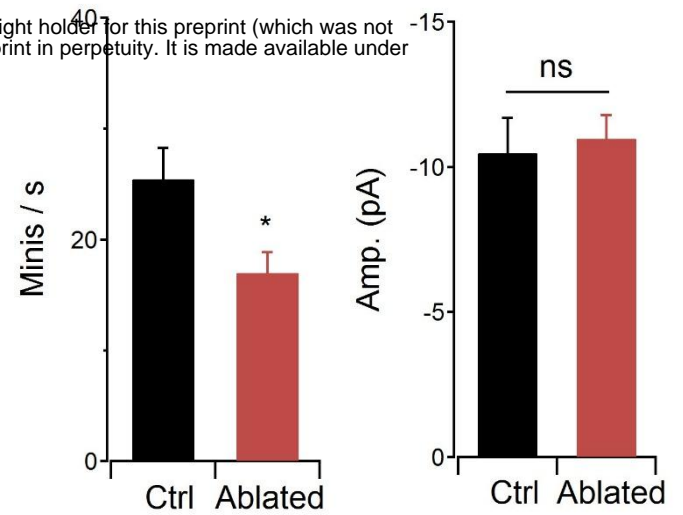


H

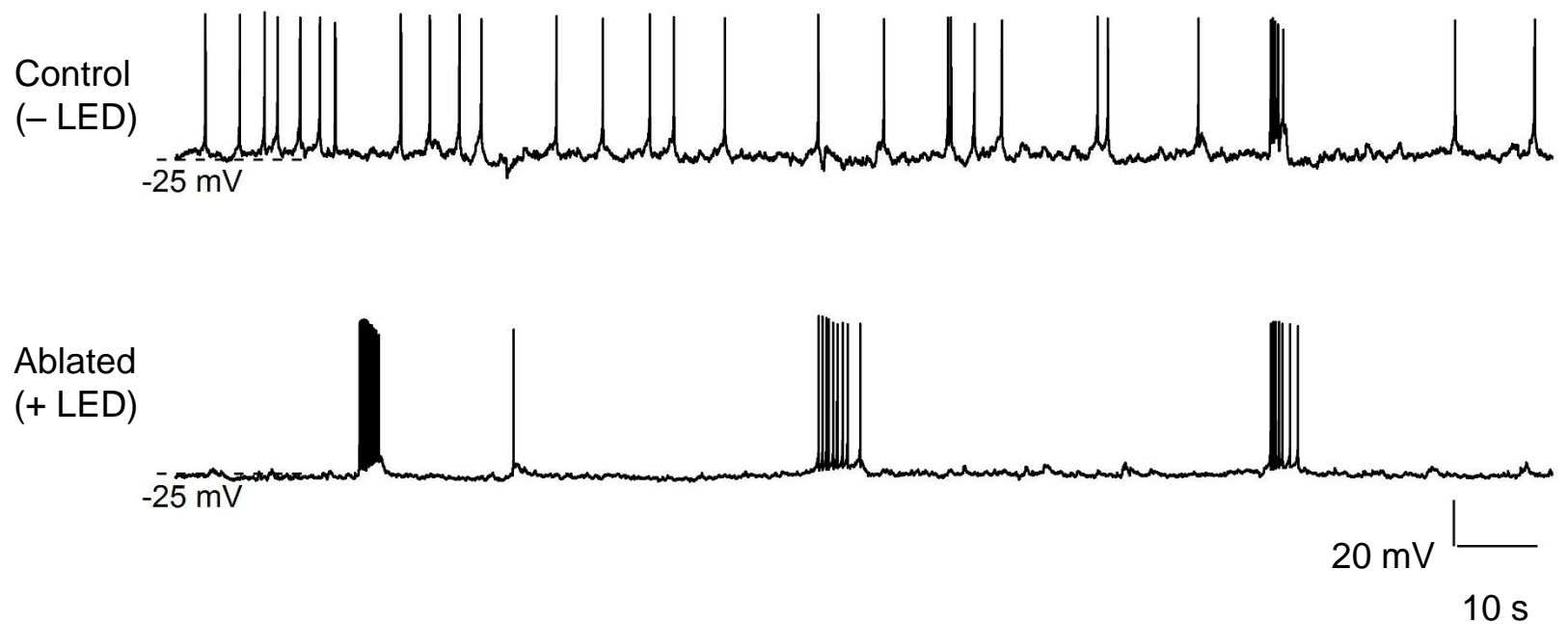
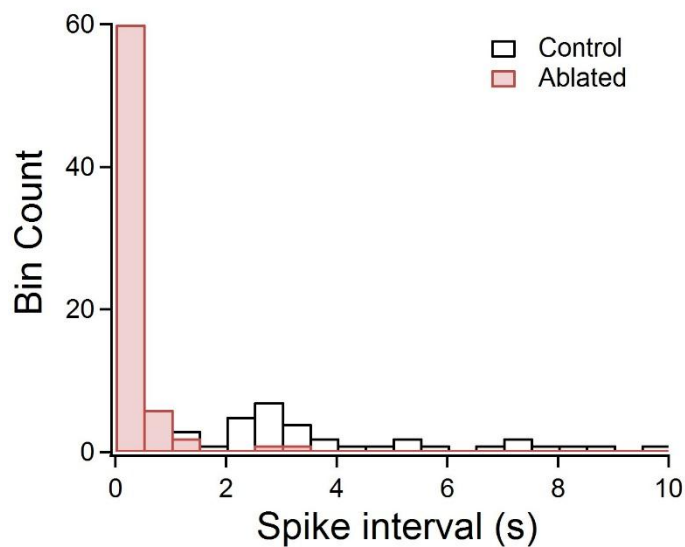
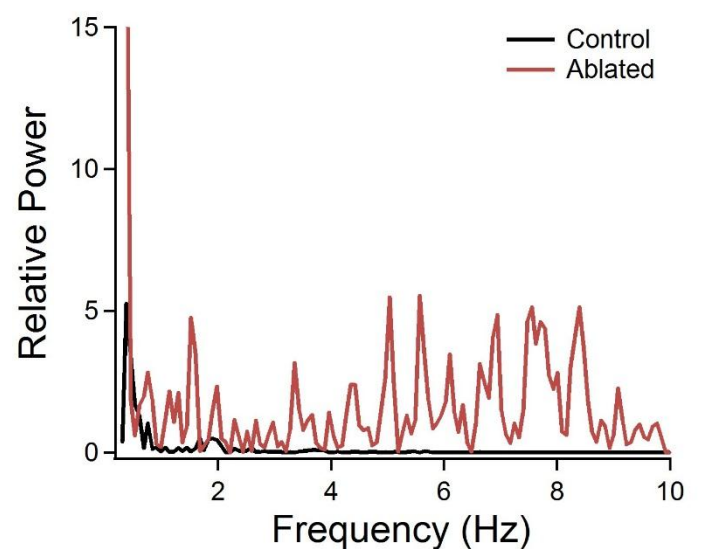


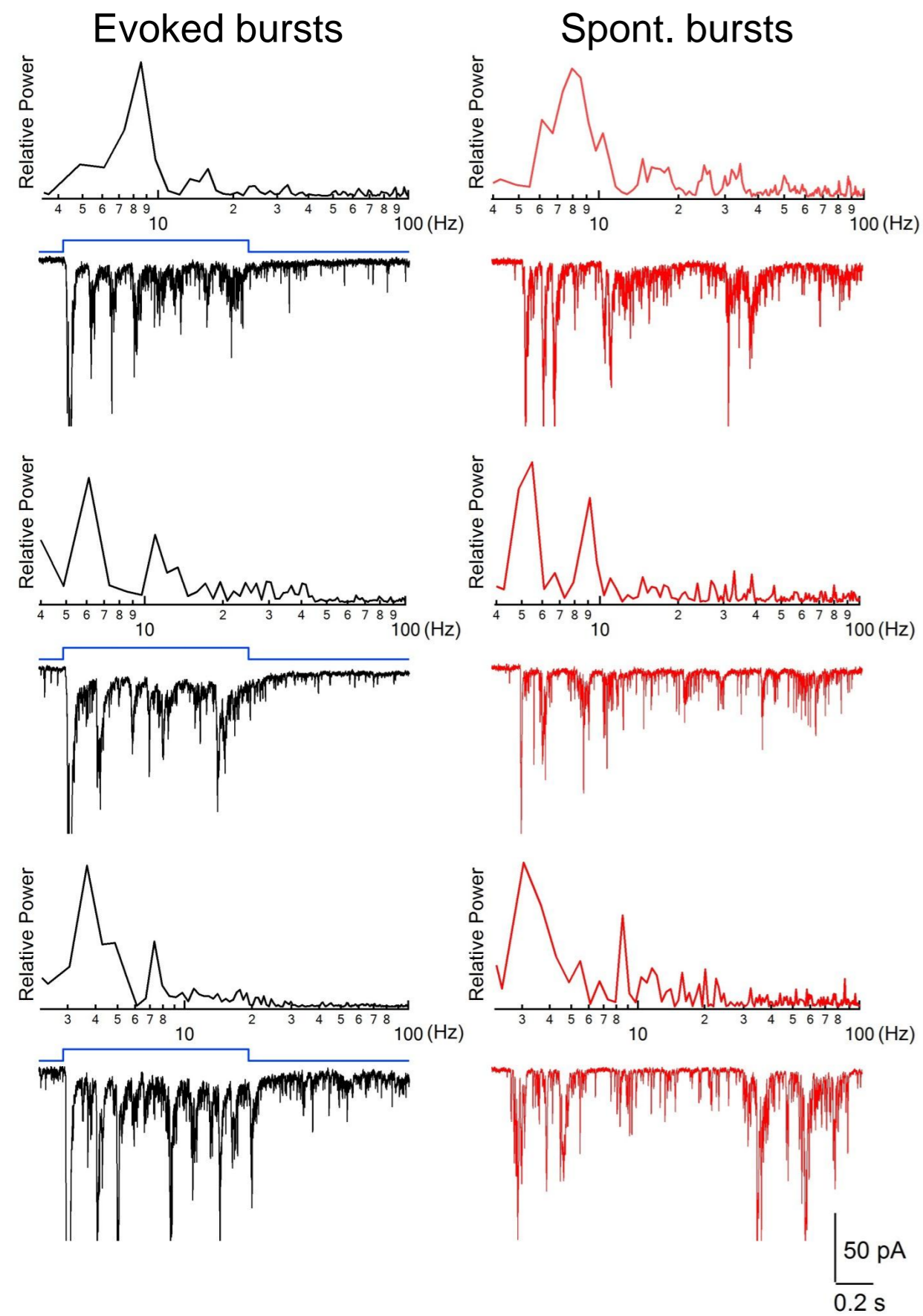
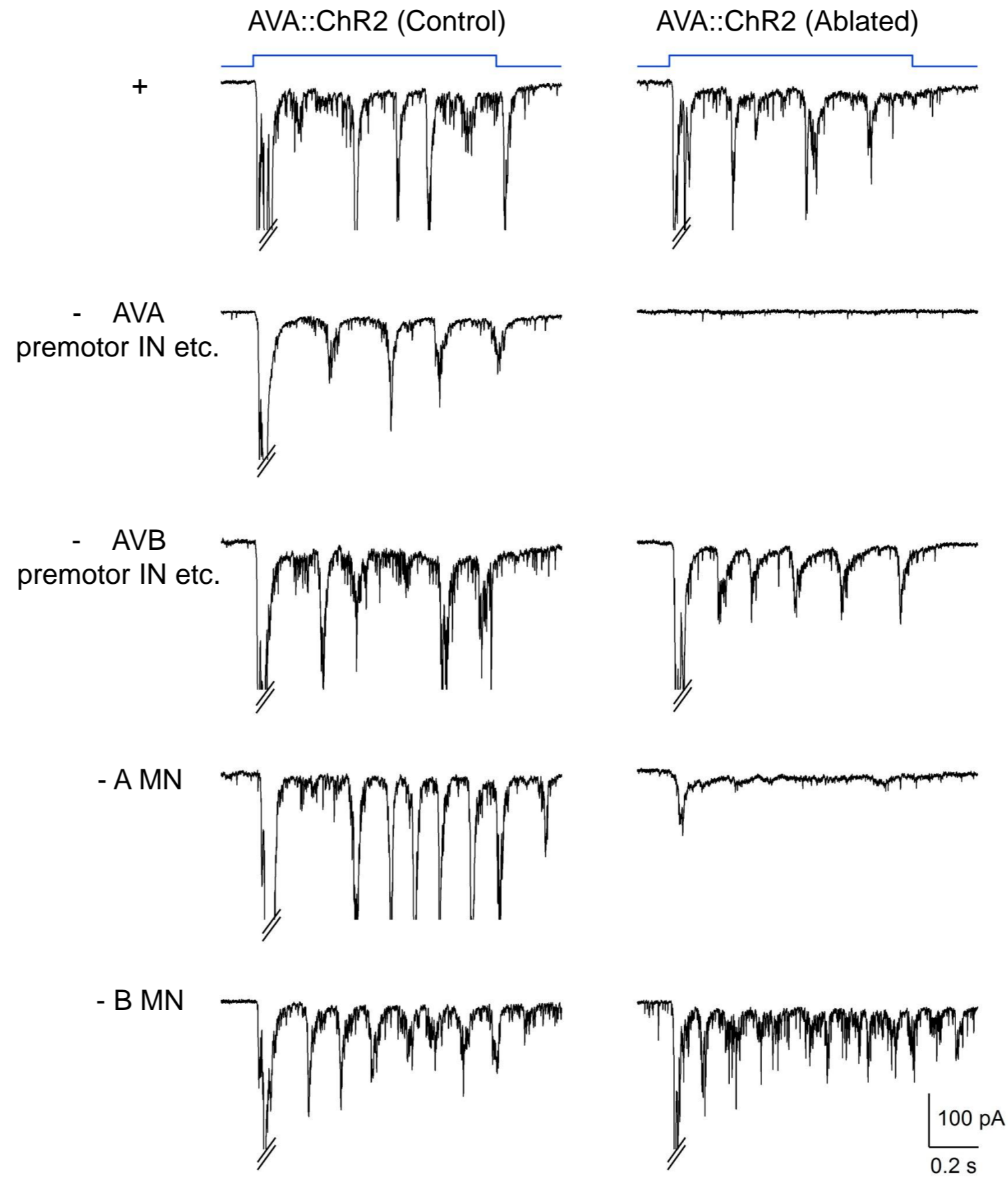
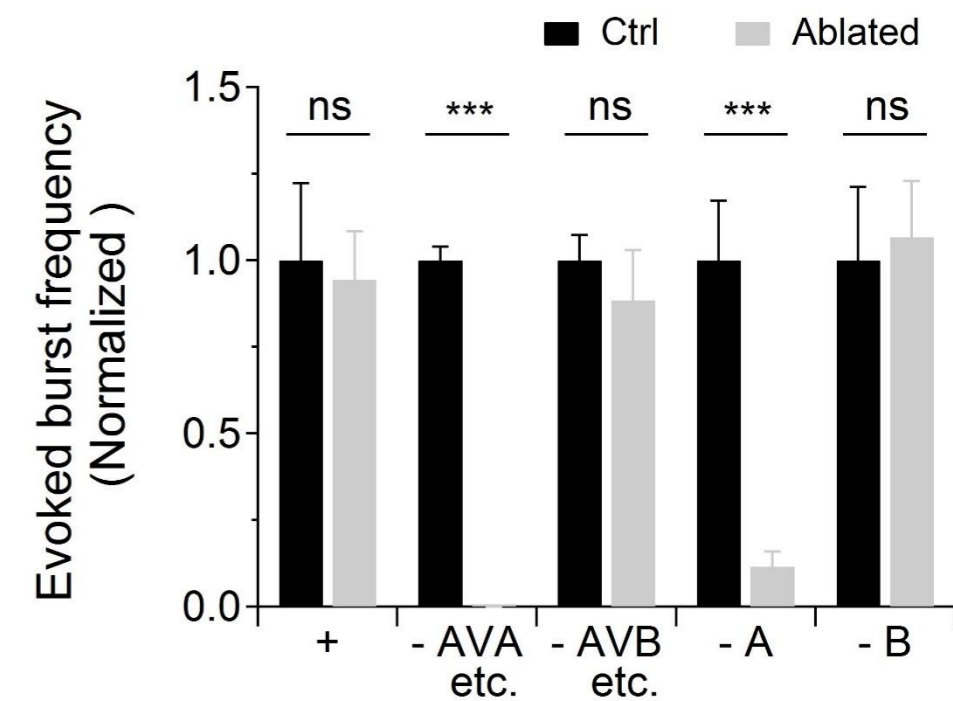
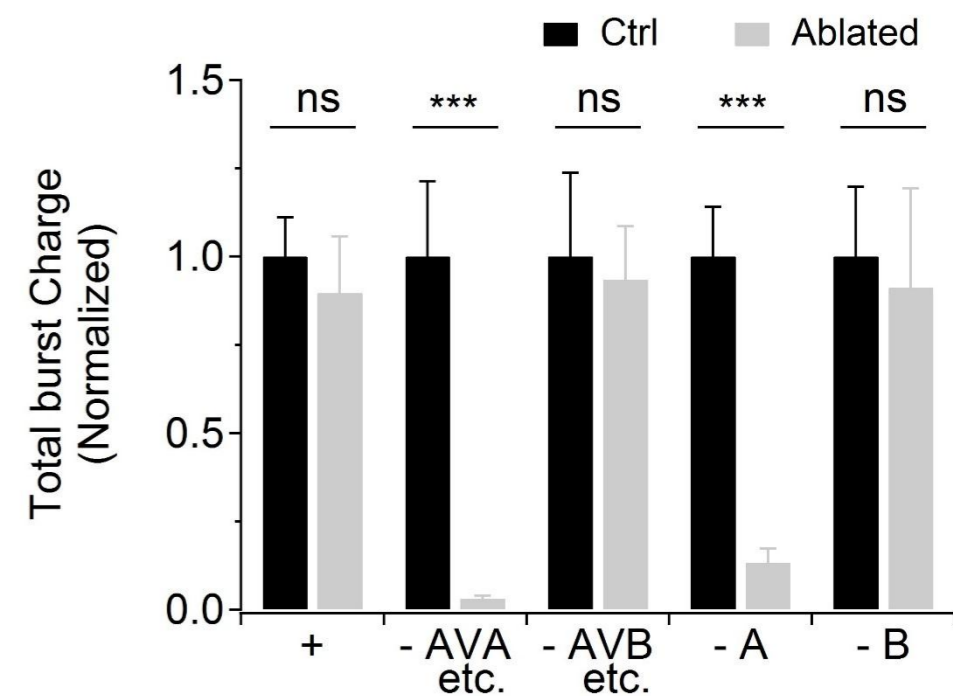
A

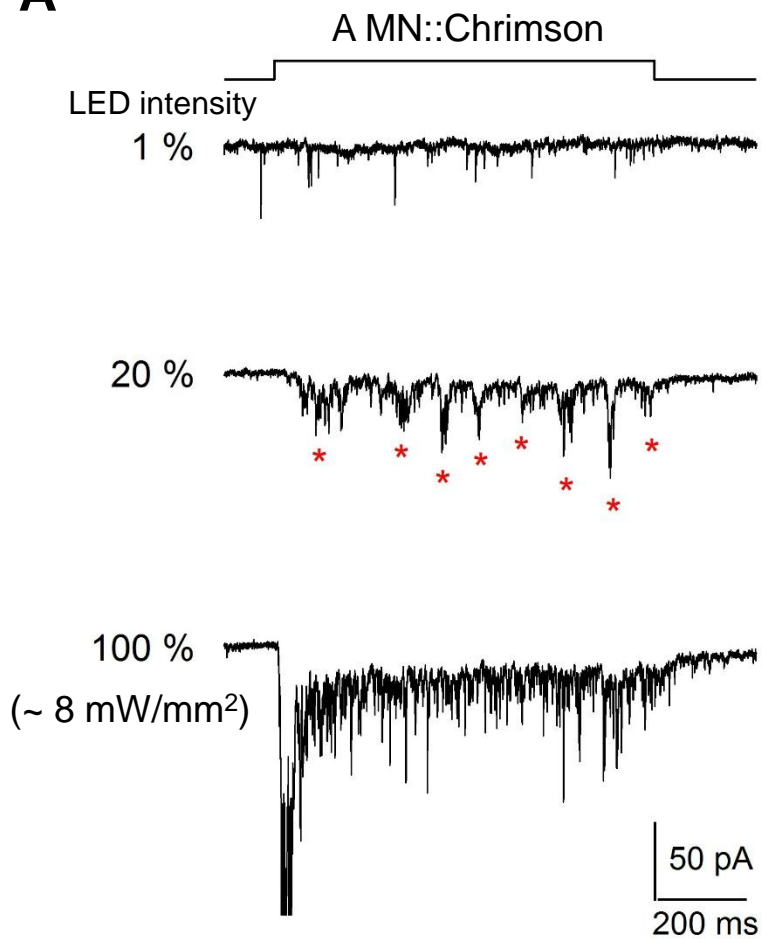
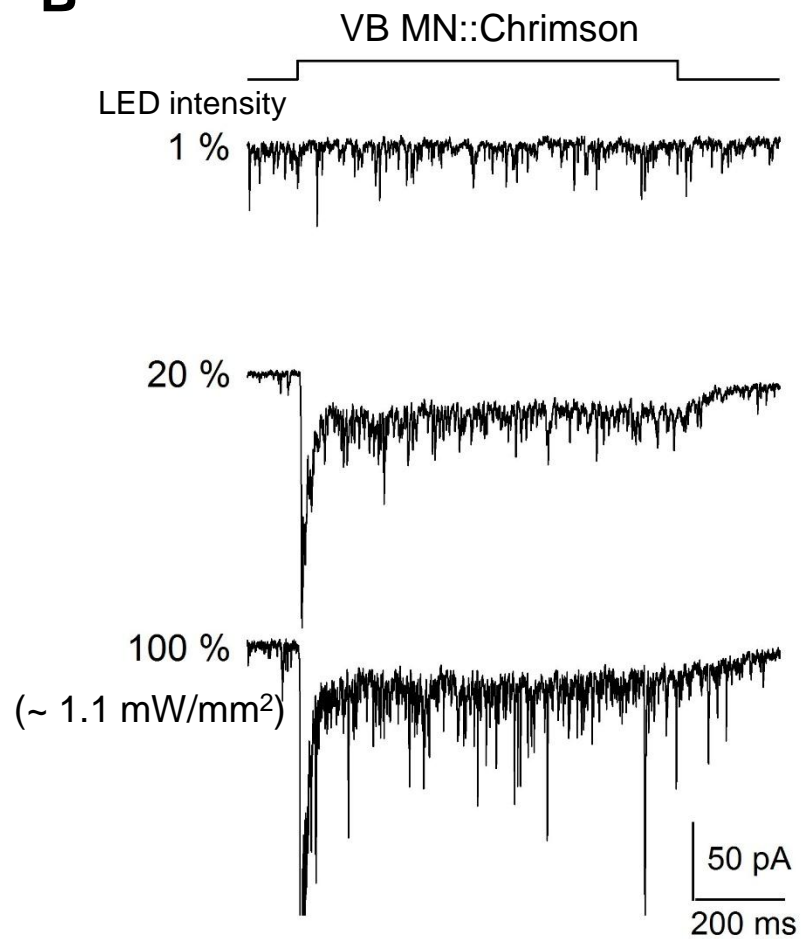
mPSCs (Premotor IN/B MN ablation)

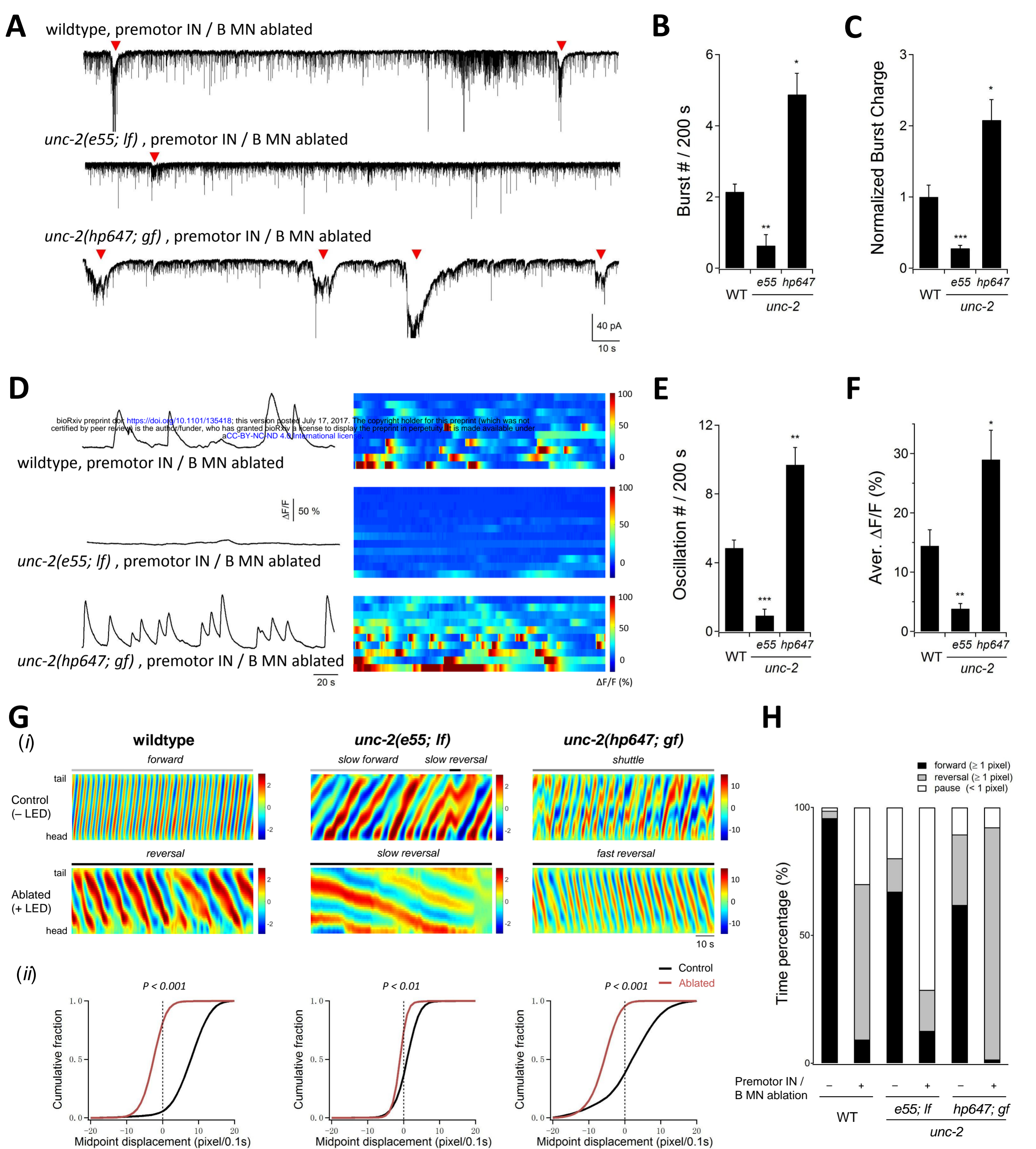
**B****C**

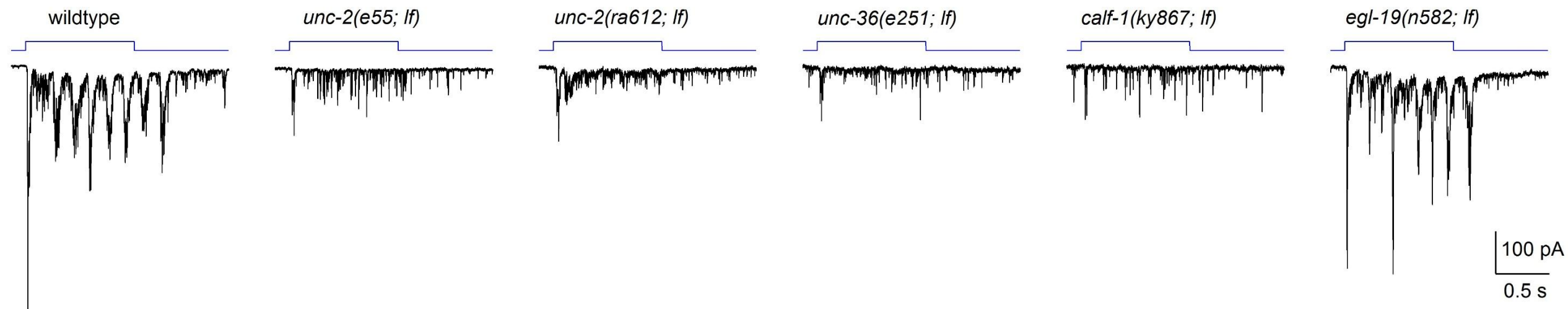
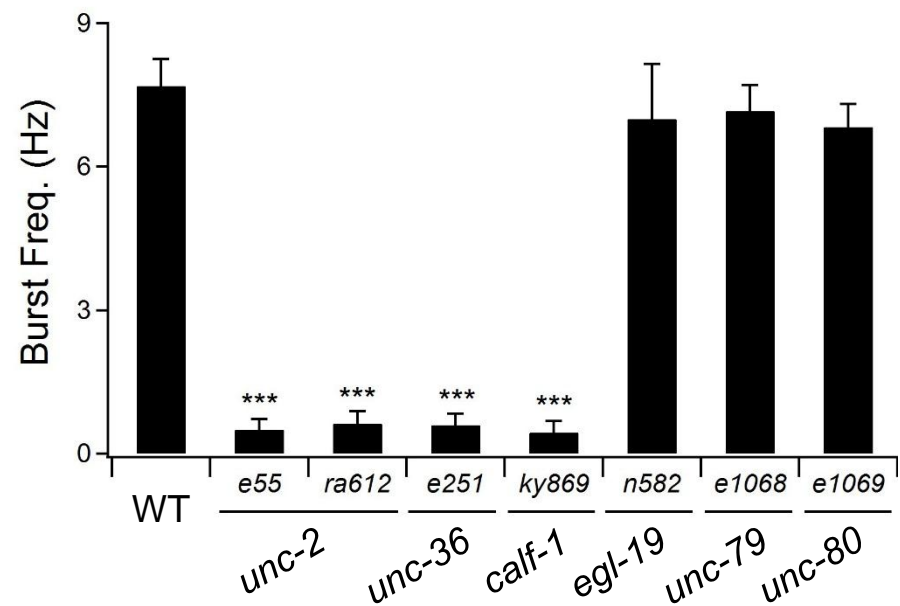
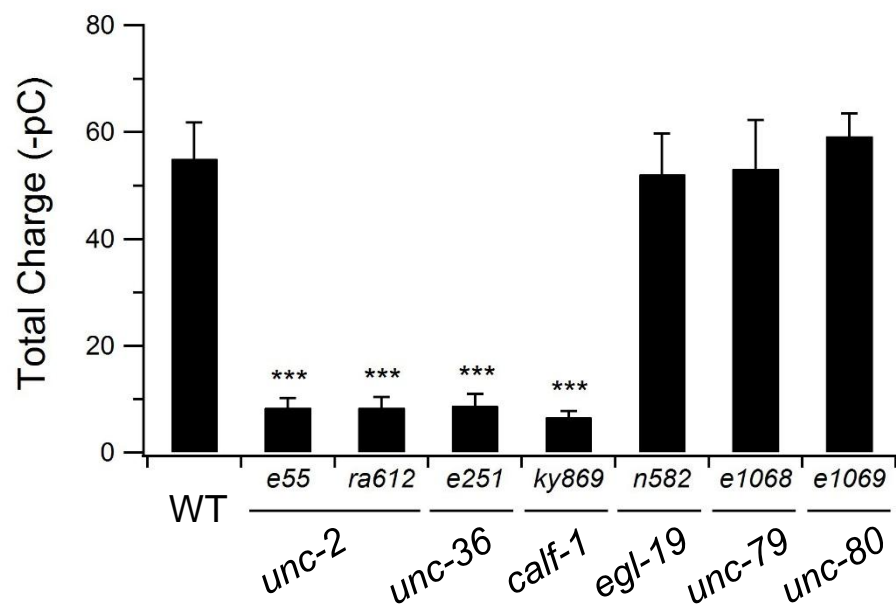
Spontaneous APs (Premotor IN/B MN ablation)

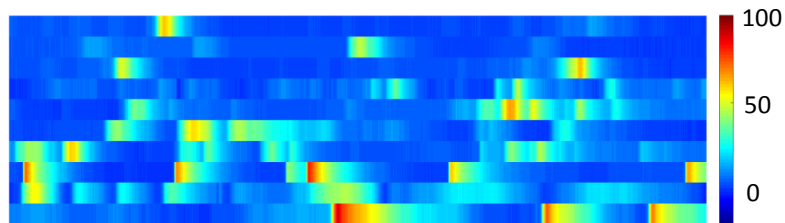
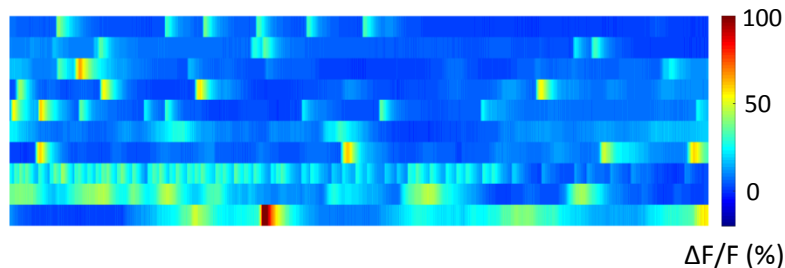
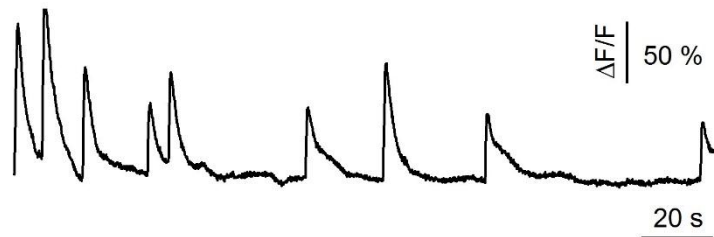
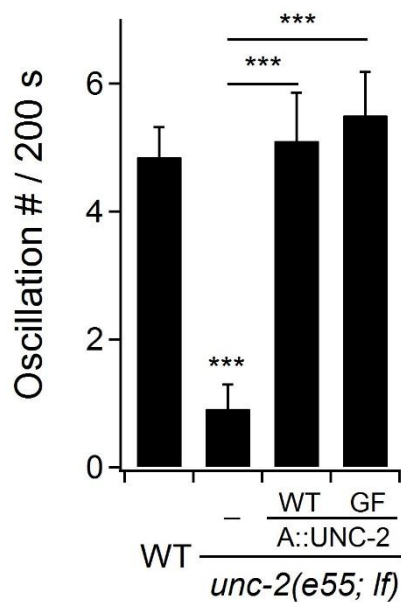
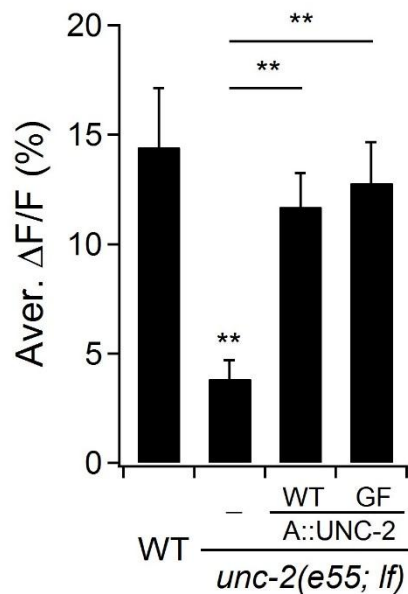
**D****E**

A**B****C****D**

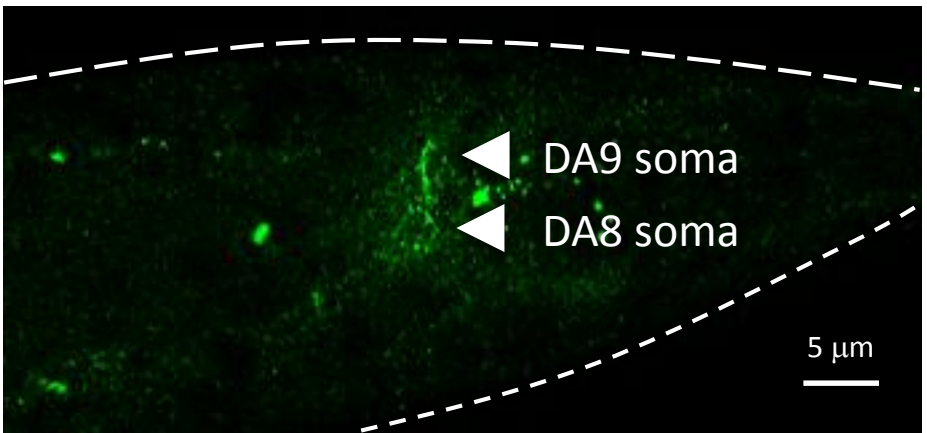
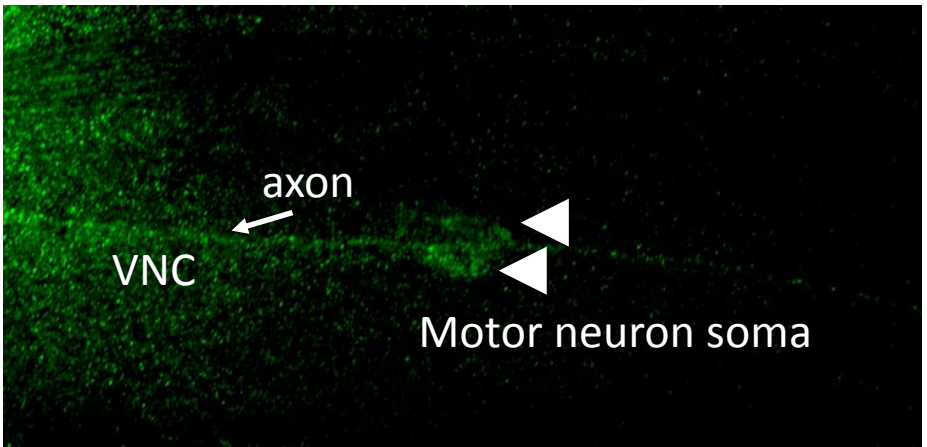
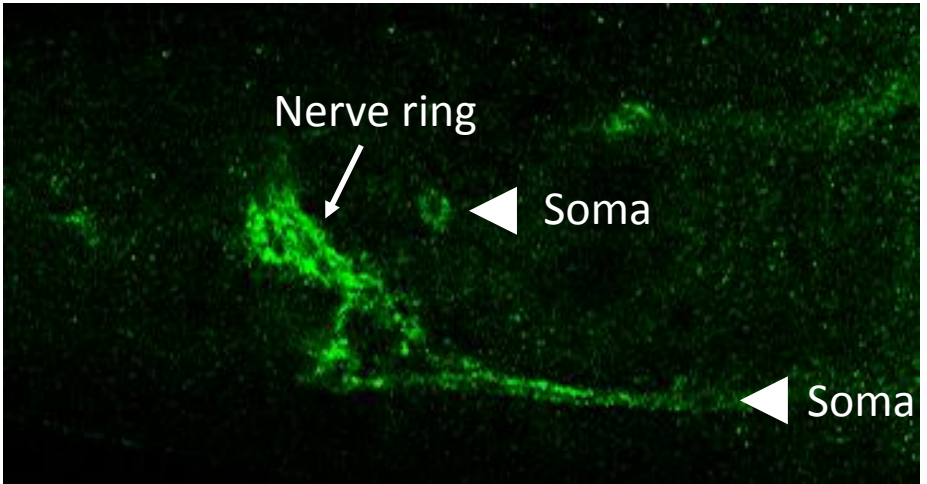
A**B**



A**B****C**

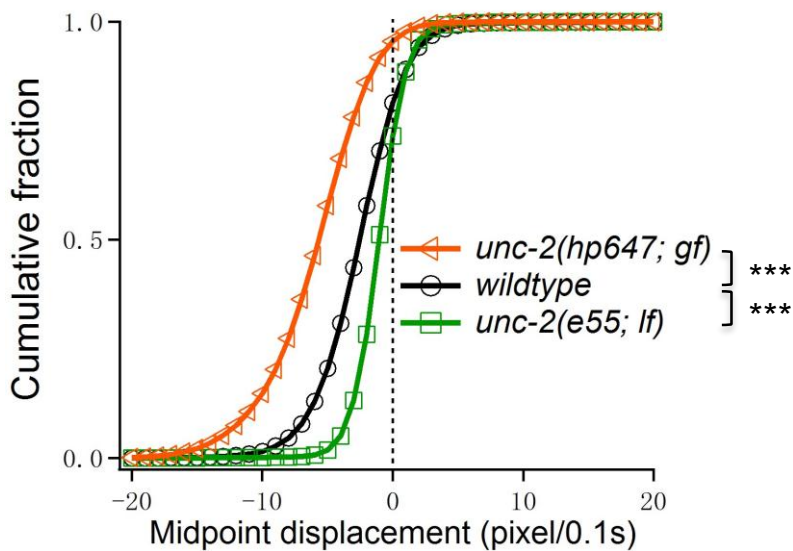
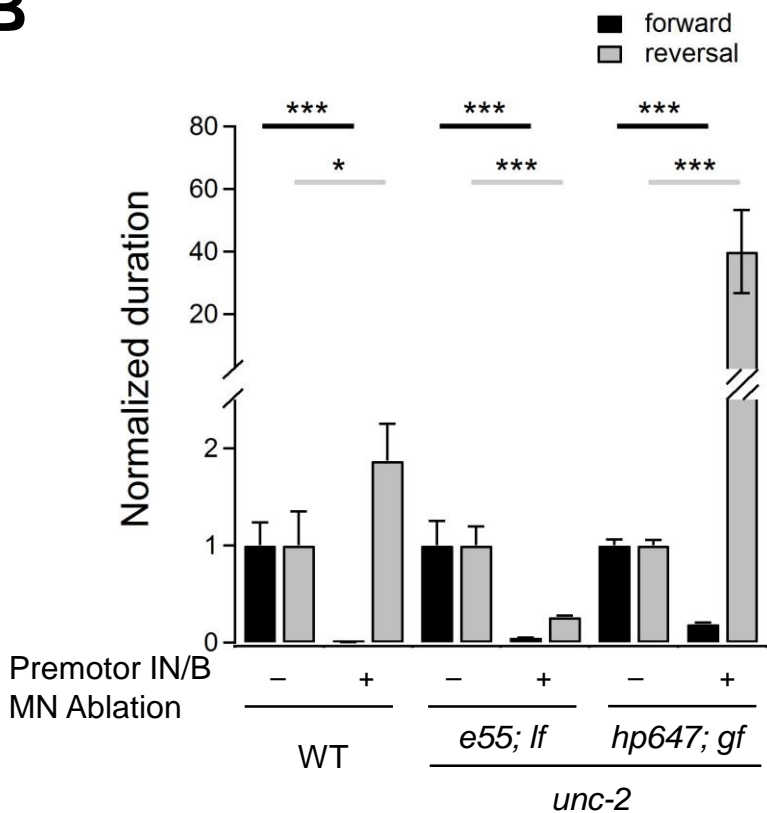
ACa²⁺ oscillation, ablated (+ LED)*unc-2(e55; lf); A::UNC-2(WT)**unc-2(e55; lf); A::UNC-2(GF)***B****C**

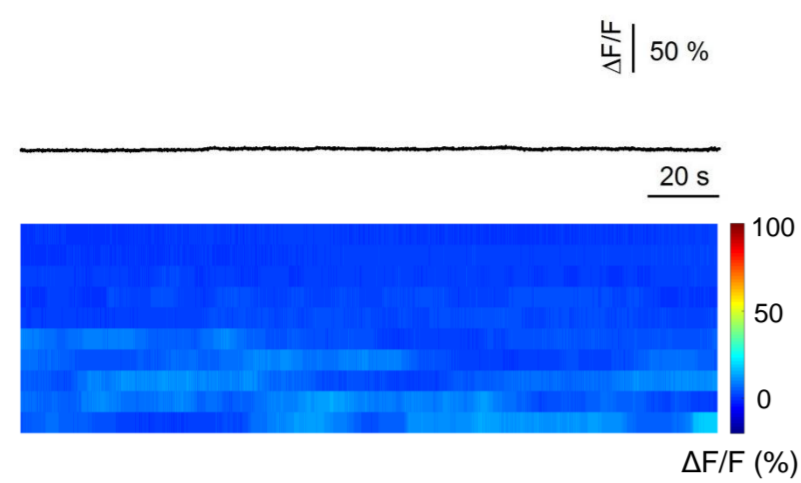
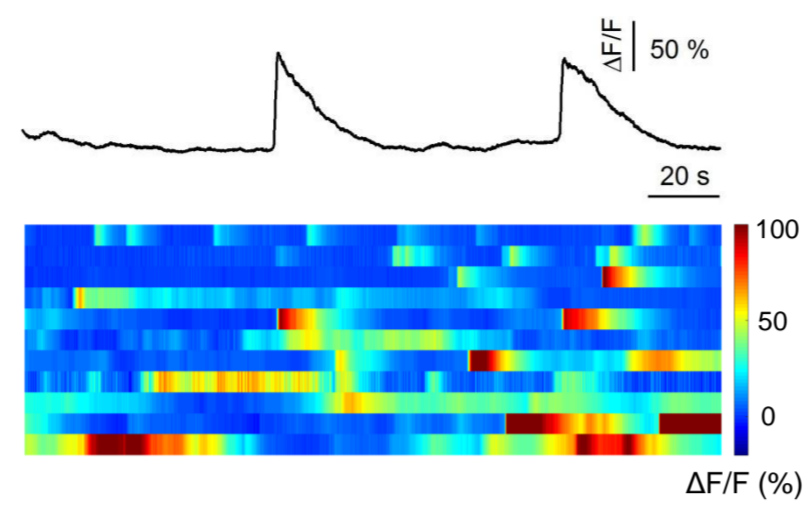
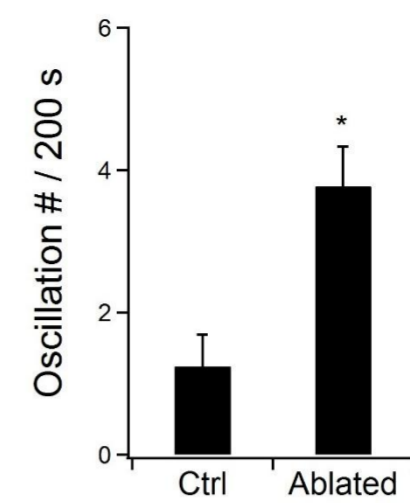
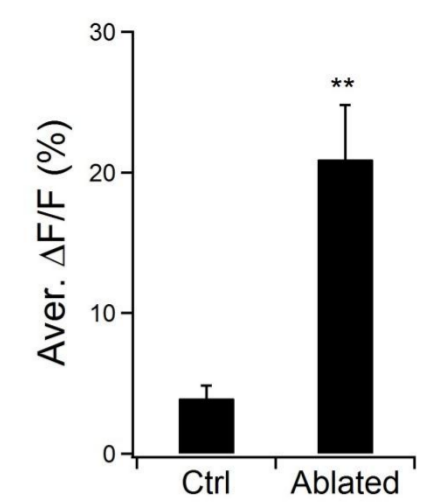
Endogenous GFP::*UNC-2*(*hp858*)



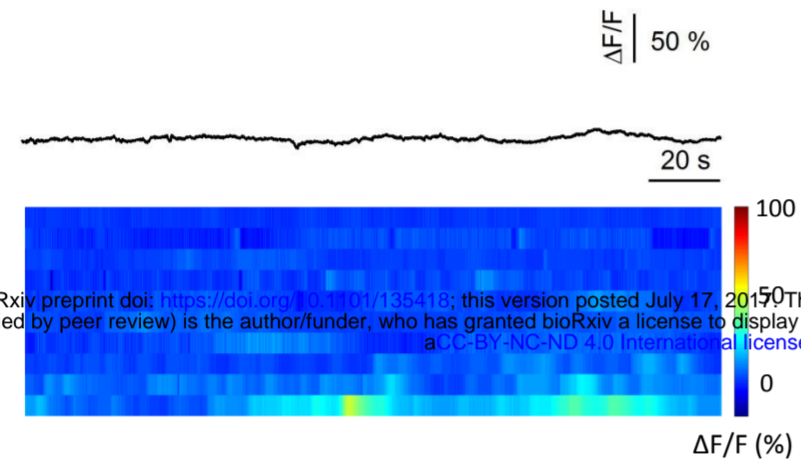
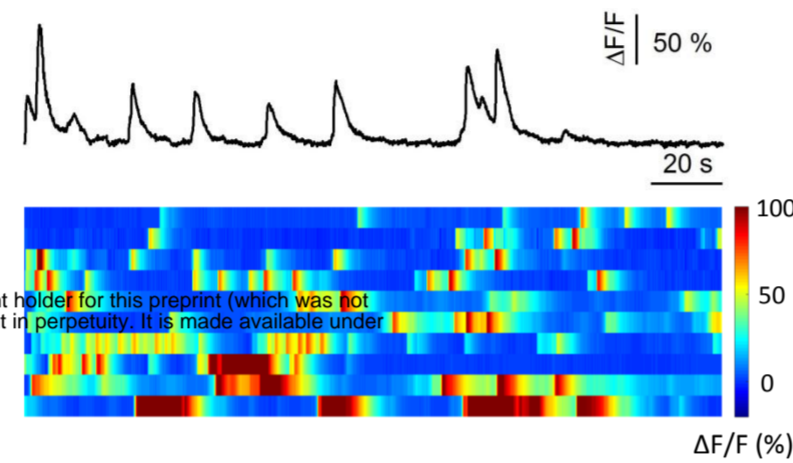
A

Premotor IN/B MN Ablated

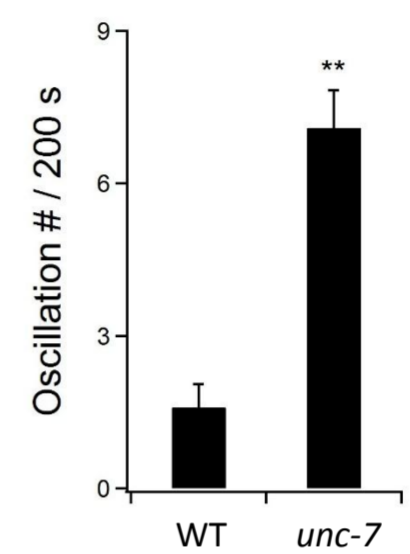
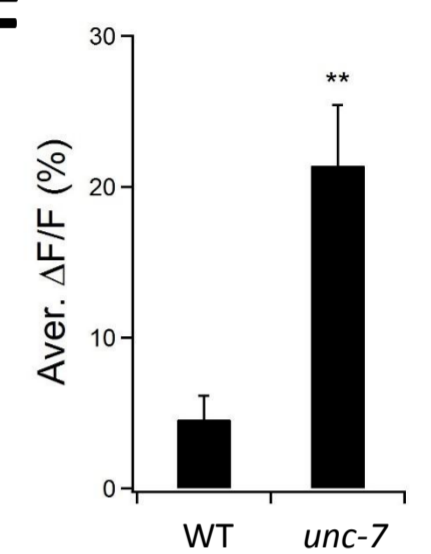
**B**

A*unc-13(s69; lf)*, Control*unc-13(s69; lf)*, Premotor IN / B MN Ablated**B***unc-13(s69; lf)***C***unc-13(s69; lf)***D**

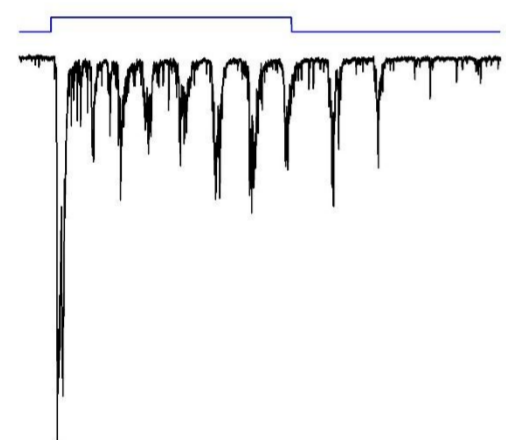
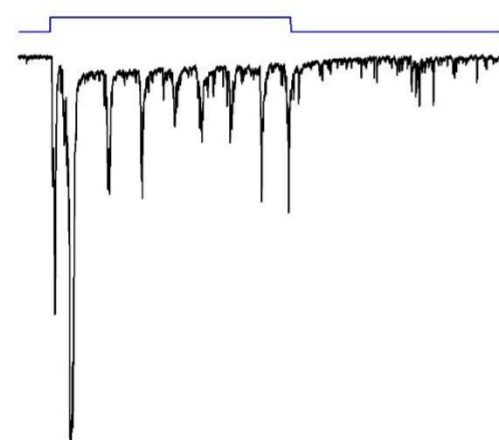
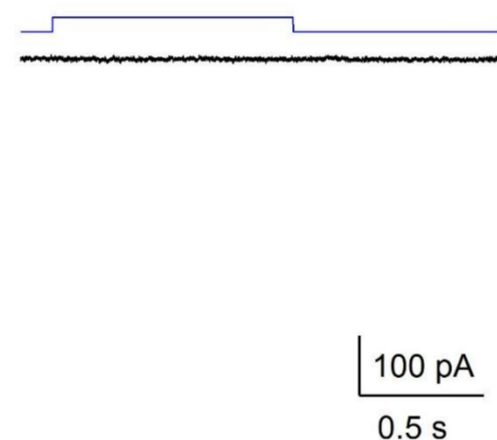
wildtype

*unc-7(e5; lf)*

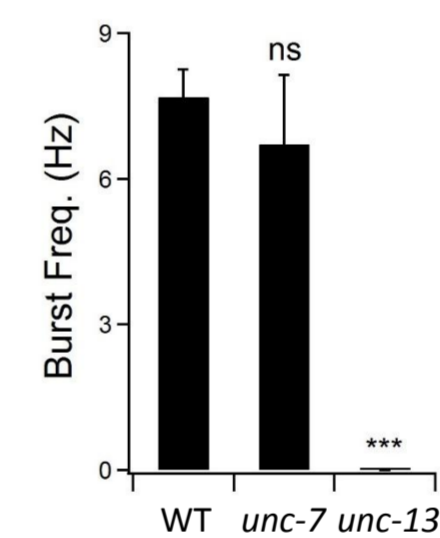
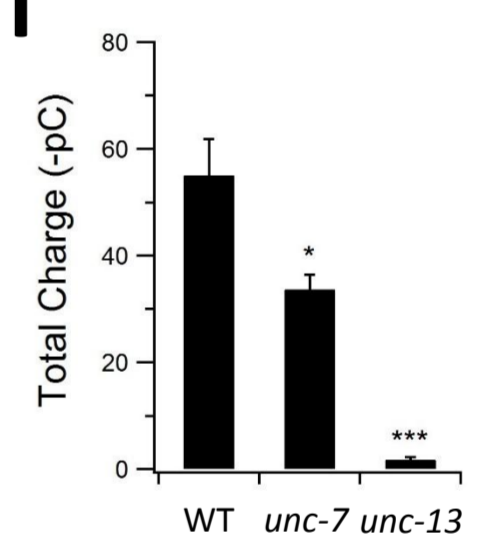
bioRxiv preprint doi: <https://doi.org/10.1101/135418>; this version posted July 17, 2015. The copyright holder for this preprint (which was not certified by peer review) is the author/funder, who has granted bioRxiv a license to display the preprint in perpetuity. It is made available under aCC-BY-NC-ND 4.0 International license.

E**F****G**

wildtype

*unc-7(lf)**unc-13(lf)*

100 pA
0.5 s

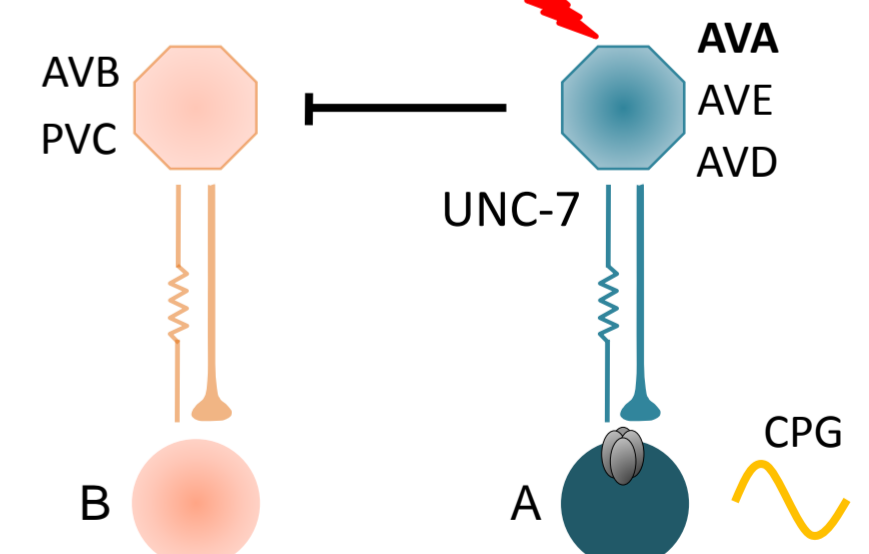
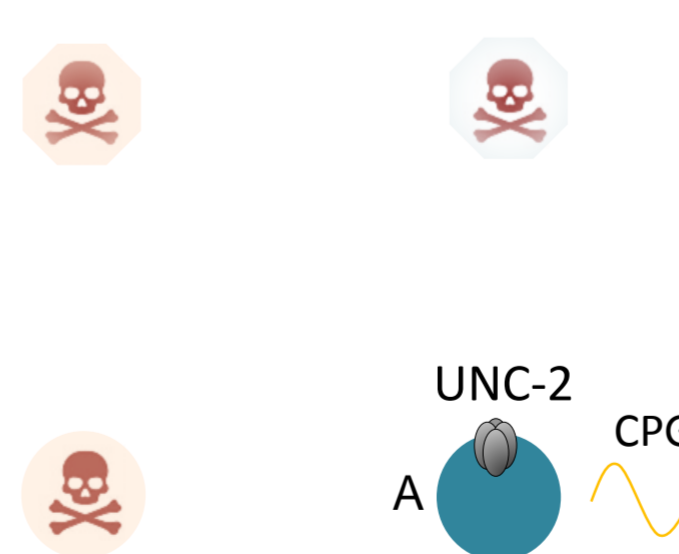
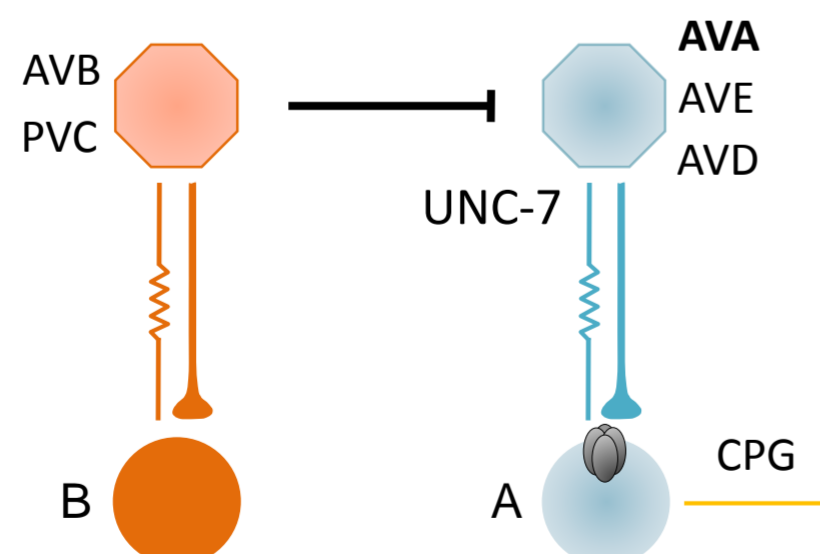
H**I****J**

Reversal CPG attenuated

Reversal CPG released

Reversal CPG potentiated

Premotor INs



Excitatory MNs



forward ←

→ reversal

→ fast, sustained reversal

Motor states

